ISAS - INTERNATIONAL SCHOOL
FOR ADVANCED STUDIES

ATOMIC-SCALE CRYSTALLOGRAPHIC STRUCTURE AND ELECTRONIC DISTRIBUTION IN ALKALI HALIDE COMPOUNDS AND THEIR SOLID SOLUTIONS

Thesis submitted for the title of "Magister Philosophiae"

October 1987

Candidate:

M. Peressi

Supervisor:

A. Baldereschi

TRIESTE

SSA - SCUOLA
ERNAZIONALE
SUPERIORE
UDI AVANZATI
TRIESTE
Strada Costiera 11

ATOMIC-SCALE CRYSTALLOGRAPHIC STRUCTURE AND ELECTRONIC DISTRIBUTION IN ALKALI HALIDE COMPOUNDS AND THEIR SOLID SOLUTIONS

Thesis submitted for the title of "Magister Philosophiae"

October 1987

Candidate:

M. Peressi

Supervisor:

A. Baldereschi

Acknowledgements

I wish to express my gratitude to Professor A. Baldereschi for his precious advice and his helpful suggestions, and to Professor G. Senatore and Professor S. Baroni for their help in clarifying particular points during my work.

ATOMIC-SCALE CRYSTALLOGRAPHIC STRUCTURE AND ELECTRONIC DISTRIBUTION IN ALKALI HALIDE COMPOUNDS AND THEIR SOLID SOLUTIONS

Thesis submitted for the title of "Magister Philosophiae"

October 1987

Candidate:

M. Peressi

Supervisor:

A. Baldereschi

Chapter 1
INTRODUCTION 1

a) Alkali halide compounds and their solid solutions 2
b) Plan of the present work 3

Chapter 2
EXPERIMENTAL DATA
AND EXISTING THEORETICAL MODELS 5

2.1) STRUCTURE AND COHESION OF PURE ALKALI HALIDE COMPOUNDS 6
a) Structure and charge distribution from experimental data 6
b) Cohesion in the Born–Mayer model 8
c) Charge density in the free–ion approximation 10
d) Beyond the free–ion approximation 14

2.2) STRUCTURE AND COHESION OF ALKALI HALIDE SOLID SOLUTIONS 15
a) Structure and cohesion from experimental data 15
b) Theoretical investigations 17

Chapter 3
ATOMIC–SCALE CRYSTALLOGRAPHIC STRUCTURE
OF ALKALI HALIDE SOLID SOLUTIONS 21

3.1) GENERALIZED BORN-MAYER MODEL FOR SOLID SOLUTIONS IN A V.C.A. APPROACH 22
a) Lattice energy in V.C.A. 22
b) Average lattice parameter: deviations from Vegard law 23
c) Limits of the present model 29

3.2) A "SUPERCELL" MODEL 30
a) Simulation of the real alloy 30
b) Lattice energy with a generalized Born-Mayer model 32
c) Structural parameters and heat of mixing 35

Chapter 4
ELECTRONIC CHARGE DISTRIBUTION
OF ALKALI HALIDE COMPOUNDS 39
4.1) TIGHT-BINDING APPROACH TO THE ELECTRONIC CHARGE DENSITY 40
a) Ionic wave functions 40
b) Bloch sums and orthonormalized Bloch functions 47
c) Charge density from the orthonormalized Bloch functions 58
d) Valence electron charge density in alkali halides: application to NaCl . 63
4.2) DEFINITION OF "PSEUDOIONS" AND "ORTHOGONALITY" CHARGE 71
a) Translational symmetry of the charge density 71
b) The pseudoion 71
c) The orthogonality charge 75
4.3) A "CLUSTER" APPROACH WITH THE USE OF SYMMETRY 78
a) Various approaches to the crystal charge density 78
b) Symmetrized orbitals 80
c) Pseudoion and orthogonality charge in terms of symmetrized orbitals . 90

Chapter 5
CONCLUSIONS 93

REFERENCES 96

Chapter 1
INTRODUCTION

a) Alkali halide compounds and their solid solutions

The alkali halides are the simplest and most typical ionic solids. Their structural properties (kind of coordination, lattice constant, heat of formation, bulk modulus) have been largely investigated both experimentally and theoretically. Some informations on the electronic distribution have been deduced from X–ray diffraction [1),2)] and also from nuclear spin resonance measurements [3),4)]. These data indicate that the ions in the crystal are spherical to a high degree, the interstitial charge density is low, and there is a non–negligible shrinkage of the electron density around the anion, if compared with the free ion state.

It has been known for a long time the possibility for the alkali halides to form solid solutions [5)]. Two substancies are said to form a "solid solution" or a "mixed crystal" if the system obtained upon alloying is characterized by a single phase and a single "average" lattice parameter, as measured by X–ray technique. This means that the solid solution has still translational symmetry "on average" in the sense that using X–ray technique many unit cells are simultaneously sampled. The phase diagrams and the thermodynamic parameters of mixed alkali halides have been extensively investigated. Detailed studies [6)] show that two alkali halides AC and BC form a solid solution $A_{1-x}B_xC$ at all compositions x at standard temperature, provided the relative difference $\frac{\Delta a}{a}$ between their lattice parameters is less than 6% (this is for instance the case of KCl–KBr); if $\frac{\Delta a}{a}$ is about between 6% and 13% (i.e. KCl–NaCl, KBr–NaBr, ...) the possibility of mixing increases with temperature and is complete at about 550°C; finally some alkali halides with very different lattice parameters (i.e. KCl–KI) do not form a continuous solid solution at temperature less than the melting point. In general the formation of those solid solutions is characterized by a positive heat of mixing [7)–9)].

An enormous amount of empirical solubility data and very recently informations on the atomic–scale crystallographic structure of alkali halide solid solutions have been collected. X–ray data [10),11)] show that in most of alkali halide solid solutions the average lattice parameter follows the Vegard law [12),13)], i.e. it varies linearly with composition between the values of the two pure compounds. Accurate EXAFS data [14)–16)] show that, although a single average lattice parameter can be assigned to alkali halide solid solutions, the anion–cation bond lengths do not average to a single bond but instead remain close, throughout the composition range, to their respective values in the pure binary compounds.

On the theoretical side, much work has been done to explain the structural, cohesive [17)] and electronic properties [18)–23)] of the pure alkali halides. Most

of the theoretical investigations on the structural and cohesive properties are based on the model proposed by Born and Mayer [17]. In a very simplified picture, a pure alkali halide is described as composed by an equal number of positive and negative ions forming close–packed structures of alternate charges. The electrostatic interactions between the ions give rise to a net binding, and short–range repulsive interactions prevent the structure to collapse; the lattice energy of the crystal is written as a sum of energy terms arising from two–body central interactions between the point–like ions. The parameters required by the models are fitted to available experimental data or deduced from the results of *ab initio* theoretical studies.

The existing models have successfully explained the cohesive properties of pure alkali halides in standard conditions of temperature and pressure, whereas the theoretical investigations on the alkali halide solid solutions is still lacking in spite of the availability of experimental data. The classical theory of ionic crystals has been applied to the problem of isolated impurities [24)–28)]. In this case it gives results in good agreement with experimental data, although strongly dependent on the particular choice of the model pair potential. The validity of the Born–Mayer model for solid solutions over the whole composition range [29),32)] has still to be confirmed. Significant experimental data and existing theoretical models for both pure compounds and their solid solutions are reviewed in Chapter 2.

b) Plan of the present work

The structural, cohesive and electronic properties of the alkali halide solid solutions constitute an interesting and still open problem.

The purpose of this work is to explain both the validity of the Vegard law —and eventual deviations from it— and the bimodal distribution of the nearest neighbour distances; we try also to reproduce the experimental data about the heats of mixing. To this purpose we simulate the alloy with a periodically repeated supercell allowing internal distortions and evaluate the energy within the Born–Mayer model generalized to include ionic polarization. The techniques used and the results obtained are presented in Chapter 3.

As it will be clear in the description of the Born-Mayer model for pure alkali halides, the electrostatic energy arising from the charge–charge interaction between the ions (the Madelung term) is largely the most important one in the description of the cohesive energy of the crystal. The equilibrium configuration

of the crystal is however determined by a delicate balance of this attractive energy with smaller energy correction terms, whose exact knowledge is not important for an approximate evaluation of the cohesive energy but is essential as far as the calculation of the structural parameters is concerned.

A more accurate estimate of these terms than the one given by the Born-Mayer model could play an essential role in our study of the atomic-scale structure of the alkali halide solid solutions; a refinement of the model in this sense could also be useful in studying those phenomena such as pressure-induced phase transitions involving structural changes, where the Born-Mayer model fails [33].

One of the small energy correction terms is certainly the Coulomb energy arising from deviations of the actual electron distribution from the simplified distribution assumed in the evaluation of the Madelung energy. We devote our interest, for a moment, to the pure alkali halides, since first of all a more accurate study of their electronic charge density —beyond both the point–charge picture and the free–ion approximation— is required. Something in this sense has already been done, both within the framework of self–consistent calculations [18)–20)] and within the Hartree–Fock approach to ionic crystals as proposed by Lowdin [34] ; the results, in agreement with experiment, indicate a shrinkage of the electronic charge around the anion.

In Chapter 4 we shall study —although avoiding heavy self–consistent calculations— the charge density of pure alkali halides beyond the free–ion approximation. Our aim is to understand in detail how the ion is modified in the crystal with respect to the free state, which is the physical origin of this modification, and how relevant is the effect of such a modification on the charge density and on the cohesive energy. To this purpose we shall resort to a tight–binding approach based on ionic Hartree–Fock orbitals, similar to the one proposed by Lowdin [34] and recently applied by Gygi [21]. Finally, we shall discuss the advantages of a different scheme in which the "in–crystal" ionic charges are obtained by a cluster approach taking into account the crystal symmetry properties. Preliminary calculations along these lines are also presented. The methods used can be applied in general to any alkali halide compound; in particular the application to NaCl is presented here.

Chapter 2
EXPERIMENTAL DATA AND EXISTING THEORETICAL MODELS

Summary

Experimental data and existing theoretical works are presented in this chapter both for the pure alkali halide compounds and their alloys. In a very simplified picture, the alkali halides are described as an assembly of negative and positive ions, bearing net charges of integer amount. Experimental data and recent self–consistent calculations indicate a shrinkage of the charge density around the anion, in contrast with the widely used rigid–ion scheme.

The crystallographic structure of the alkali halide pseudobinary solid solutions has also been experimentally investigated. X-ray data show that the average lattice parameter varies linearly with composition between the values for the constituent pure compounds, whereas recent EXAFS data indicate a bimodal distribution for the nearest neighbour distances, also varying with composition. Model calculations based on the pioneering work of Born and Mayer have successfully explained the cohesive and structural properties of the pure compounds at standard conditions of temperature and pressure, but the theoretical investigation of the same properties of their solid solutions is still lacking.

2.1
STRUCTURE AND COHESION OF PURE ALKALI HALIDE COMPOUNDS

a) Structure and charge distribution from experimental data

Crystal structures

The typical structures of alkali halides are the rocksalt and the cesium chloride structures, which are both cubic and characterized by one lattice parameter a; with reference to the cubic axes the first one is composed of two FCC sublattices — one for each species of ions — shifted by $a(\frac{1}{2}, \frac{1}{2}, \frac{1}{2})$ relative to one another, whereas the latter is composed of two SC lattices with the same shift. In Fig. 1 we show the cubic cell (a), the elementary FCC cell (b), and the correspondent Wigner-Seitz cell (c) for the NaCl structure, which is the most common for alkali halides.

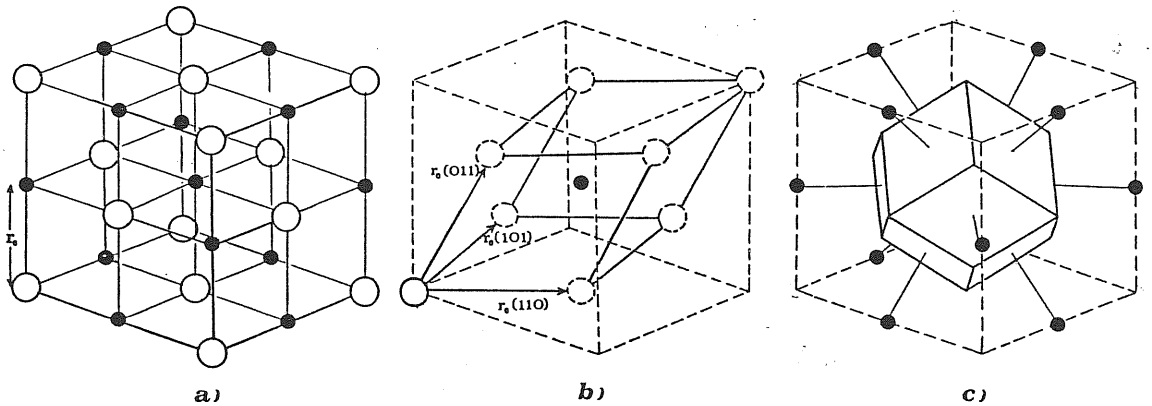

Fig.1: Cubic cell (a), elementary FCC cell (b), and Wigner–Seitz cell (c) for NaCl structure.

One can recognize that each ion is surrounded by the same number of ions of the other species, belonging to other sublattice — 6 in rocksalt and 8 in CsCl —: we use the symbol NN (nearest neighbours in the crystal) to distinguish them from the nearest neighbour ions of the same species and in the same sublattice, indicated with nn (nearest neighbours in the sublattice).

Analogous symbols will be used to indicate the second neighbours in the crystal (NNN) and in the sublattice (nnn).

Charge distribution

Experimental maps of the charge density [1),23)] are usually obtained by means of Fourier synthesis of X–ray structure factors. The experimental map for NaCl reported in Fig. 2 shows that the ions are spherical to a high degree, they do not overlap very much and the interstitial charge density is low. The simplified picture of an ionic crystal as an assembly of rigid ions is thus not very far from reality, and the point-charge Madelung approximation for a first evaluation of the electrostatic energy is justified.

Recently accurate experimental data on the structure factors have been collected for NaF [2)] from X–ray reflection measurements. It is evident a compressional effect of the crystalline field on the wave function: more precisely it is clear that the anion contracts, whereas it cannot be decided from the data available whether the cation is contracted or expanded.

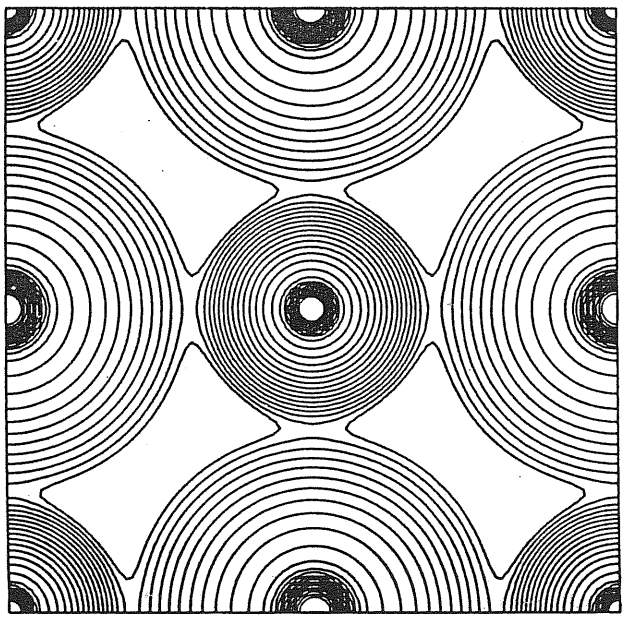

Fig.2: Experimental charge density contours in a (001) plane. The contour levels are in a logarithmic scale; the lowest corresponds to a density of .007 electrons/Å^3 and adjacent contours differ by a factor of $\sqrt{2}$ (from Ref. 23).

b) Cohesion in the Born-Mayer model

Lattice energy

The cohesive energy of an alkali halide is defined as the internal energy of the crystal, relative to the sum of the energies of free ions at infinite distance and at zero temperature. The cohesive energy is the sum of the lattice energy E_L, i.e. the internal energy of the solid with the ions at rest in the correspondent equilibrium positions, and of the internal energy due to ionic vibrations around the equilibrium lattice sites. If the crystal is considered in conditions of zero temperature and pressure — as it is done in the present work — the cohesive energy coincides with the lattice energy, apart from a negligible contribution of the zero–point kinetic energy.

Born-Mayer model

The Born–Mayer model, which has successfully explained the cohesive properties of pure alkali halides [17], describes the lattice energy as a sum of two–body central interactions.

The most relevant contribution to the lattice energy is provided by the two–body electrostatic interactions between ionic charges. In a multipole expansion of the ionic charge one recognizes that the cubic lattice symmetry forces several multipole moments to be zero. The dominant part of the electrostatic energy is thus the one due to interactions between point–like ionic charges $\pm e$, also known as Madelung energy; it is written per couple of ions as

$$E_{coul.} = \frac{1}{2N_p} \sum_{ij}{}' \frac{(\pm)e^2}{r_{ij}} \tag{2.1.1}$$

where $\sum'_{ij}$ runs over all the ions in the crystal except $i = j$, and N_p is the number of ion pairs considered. Since all these two–body interactions scale with the lattice parameter, eq. 2.1.1 can be rewritten in the form:

$$E_{coul.} = -\frac{\alpha_a e^2}{a} \tag{2.1.2}$$

where α_a is a positive adimensional constant (the Madelung constant), depending only on the structure and on the characteristic length used (lattice parameter or nearest neighbour distance, usually); several methods can be used to evaluate it, in particular we remind the Ewald method [17].

In addition to the net binding provided by the Madelung energy, the terms arising from the syncronization of the electronic motions in the ions contributes

to the cohesion of the crystal. This Van der Waals interaction decays rapidly with distance (the dipole–dipole term goes as r^{-6}); it is essential in the cohesion of the solid rare gas, for instance, but it contributes very little in the case of alkali halides and can be neglected in an approximate description.

The attractive forces in the crystal are balanced by the repulsive forces, very relevant at small distances, opposing the interpenetration of the ions. In the Born model the repulsive term collects several small energy terms, some of them attractive and some repulsive, which could be investigated by detailed quantum mechanical calculations. There are electrostatic correction terms to the Madelung energy due to the deviations of the true charge density distribution in the crystal from the simplified point–charge picture assumed; self–interaction energy of each ion and its change from the free–ion state to the condensed phase; exchange effects. The repulsive contribution to the cohesive energy at equilibrium is typically about 10% of the total cohesive energy. Empirical models are generally employed to represent these short–range repulsive forces: in the Born–Mayer model they are described by a unique function of the interionic distance, involving "strength" and "hardness" parameters to be determined from crystal data. The repulsive energy per ion pair in the Born–Mayer model is written as:

$$E_{rep.} = B \exp(-\frac{r}{\rho}) \tag{2.1.3}$$

a form which applies when one considers explicitly only the Born repulsion of the first shell of neighbours in the crystal. Taking into account explicitly the NNN repulsion, one can write:

$$E_{rep.} = M b_{+-} e^{-\frac{r}{\rho}} + \frac{1}{2} M'(b_{++} + b_{--}) e^{-\frac{r'}{\rho}} \tag{2.1.4}$$

where M and M' are the number of NN and of NNN, and r' is the NNN distance. The determination of the parameters is usually done by fitting the analytic expression of the lattice energy to the experimental equilibrium interatomic distance and bulk modulus. Cohesive energy is satisfactorily reproduced.

The simplest form of the Born–Mayer model will be used for calculations in the present work, i.e. :

$$E(a) = -\frac{\alpha_a e^2}{a} + B \exp(-\frac{a}{2\rho}) \tag{2.1.5}$$

if expressed as a function of the lattice parameter $a = 2r_0$ of the unit cell. Fig. 3 shows the total lattice energy, the Madelung and the repulsive terms.

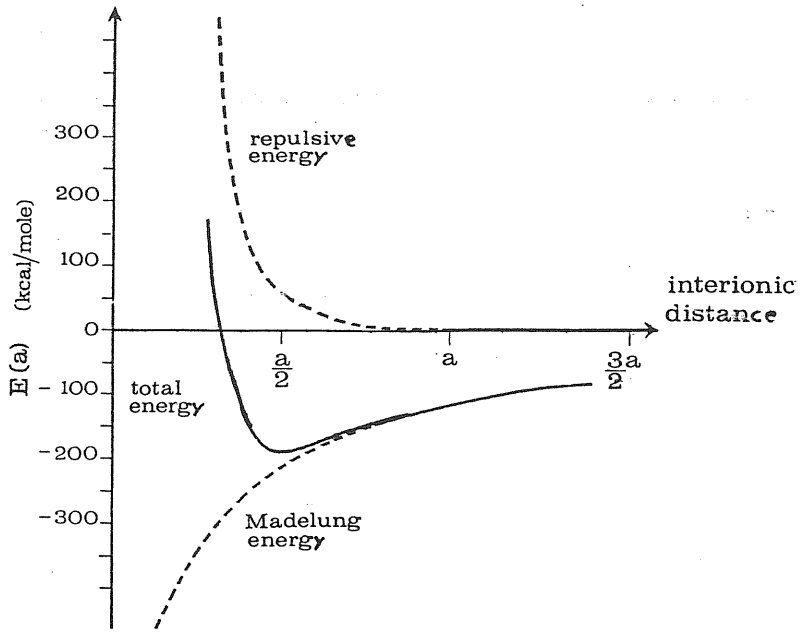

Fig.3: Madelung energy, repulsive energy, and total lattice energy in the Born–Mayer model as a function of the interionic distance.

c) Charge density in the free–ion approximation

The free ion

The simplest approximation to the crystal charge density beyond the point-charge picture is to start from the knowledge of the free-ions, and consider just the sum over the lattice sites of the ionic charge densities , supposed to be froozen:

$$\rho_0(\mathbf{r}) = \sum_{\mathbf{R}_n} \sum_{\mu} \rho_\mu(\mathbf{r} - \mathbf{R}_n - \mathbf{d}_\mu) \qquad (2.1.6)$$

where $\mathbf{R}_n$ runs over the Bravais lattice, μ indicates the kind of ion and $\mathbf{d}_\mu$ its position in the unit cell. The two linear graphs along (100) and (110) directions in Fig. 4 show a core charge very localized on the lattice sites. In Fig. 5,6 are shown the plots of the total and valence charge density of the crystal in the free–ion approximation in the planes [001] and [011].

The charge density ρ_μ for each ion is calculated from the occupied ionic orbitals $\varphi_{\mu\nu}$:

$$\rho_\mu(\mathbf{r}) = \sum_{\nu_{occ.}} |\varphi_{\mu\nu}(\mathbf{r})|^2 \qquad (2.1.7)$$

It is convenient to use the Hartree–Fock approach for the free ion since local density calculations do not describe it well [35]. Let us consider for instance a single electron outside the closed–shell core as in the alkali metals. In the Hartree–Fock scheme there is a perfect cancellation between self–interaction contributions contained in both the electrostatic and the exchange terms. The Hartree–Fock equations as well as physical understanding suggest that the large distance behaviour of the total potential felt by the valence electron should be $-e^2/r$; in local density calculations the electrostatic potential refers to a neutral charge distribution and decays exponentially with distance, and the same behaviour, although smoother, is shown by the local exchange and correlation potential; the resulting total potential at large distances has a magnitude less than e^2/r, and some ad hoc corrections are needed to reproduce correctly the state of the valence electron .

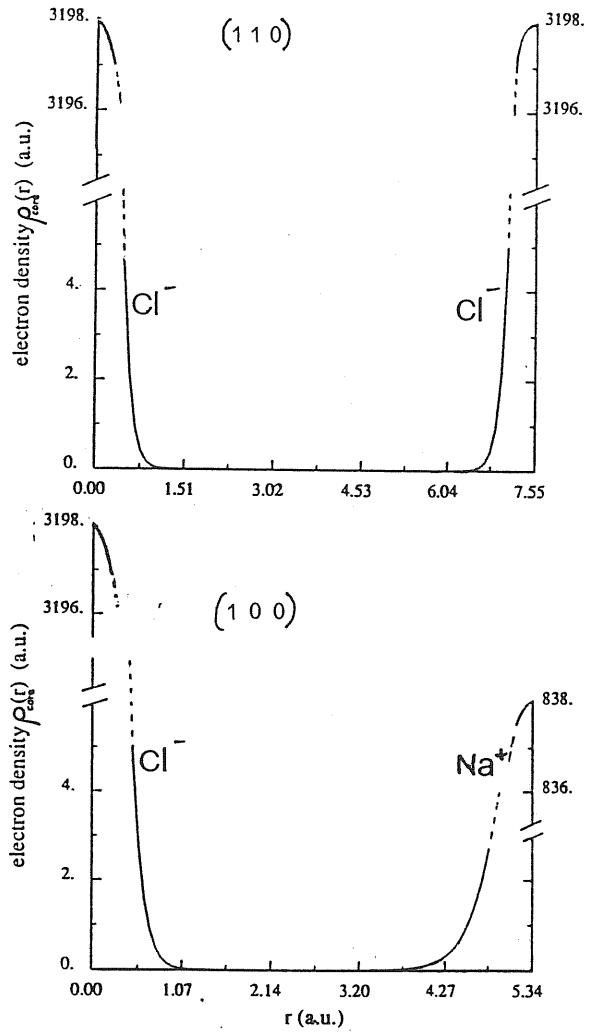

Fig.4: **Core electron density in the free–ion approximation along (100) and (110) directions.**

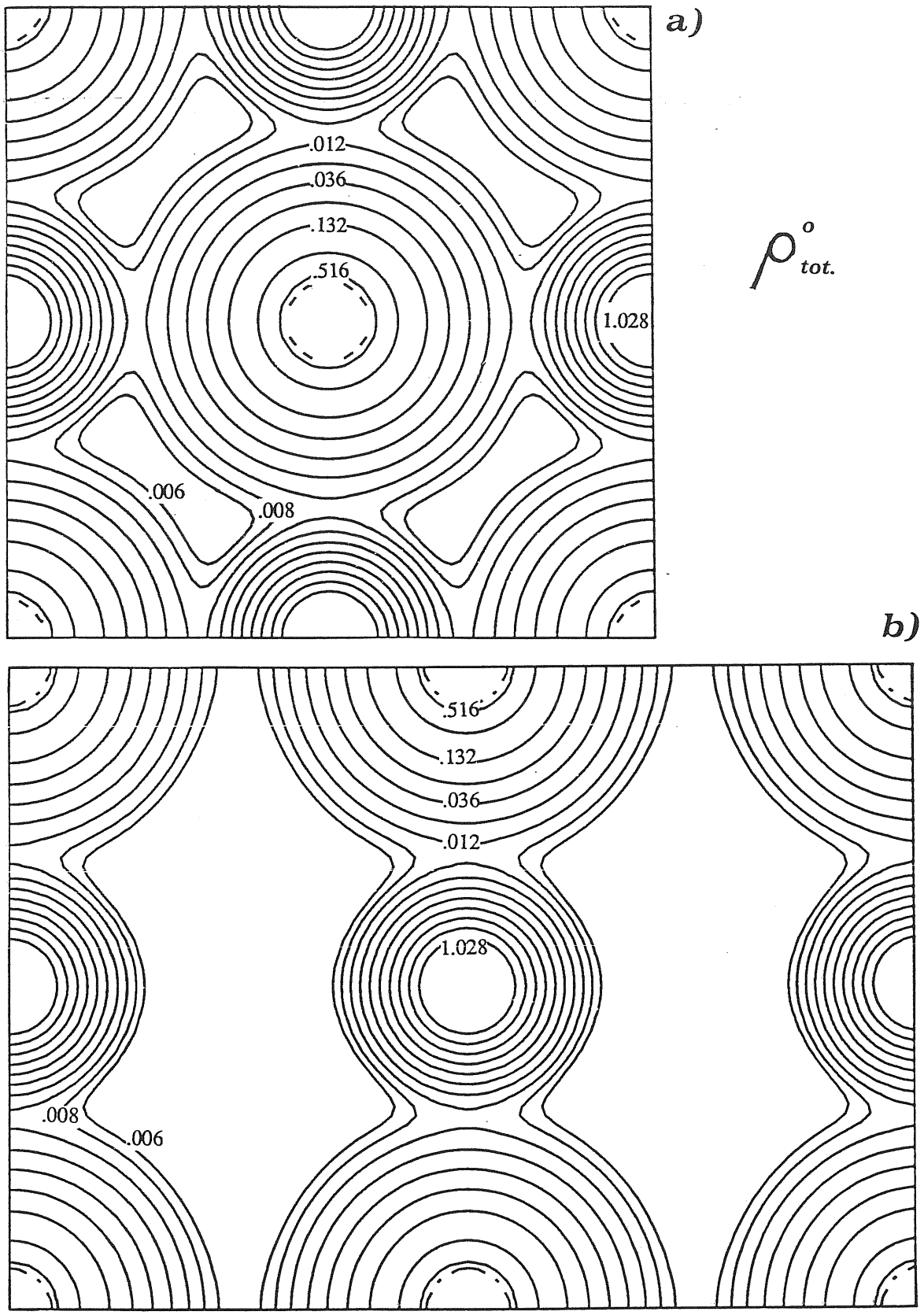

Fig.5: Total electron density in the (001) plane (a) and in the (011) plane (b) in the free–ion approximation. Chlorine ions are at the corners. The lowest level corresponds to .006 electrons/a.u.^{3}, and the interval between the i–level and the $(i-1)$–level is $2^{(i-1)}$..002 electrons/a.u.^{3}.

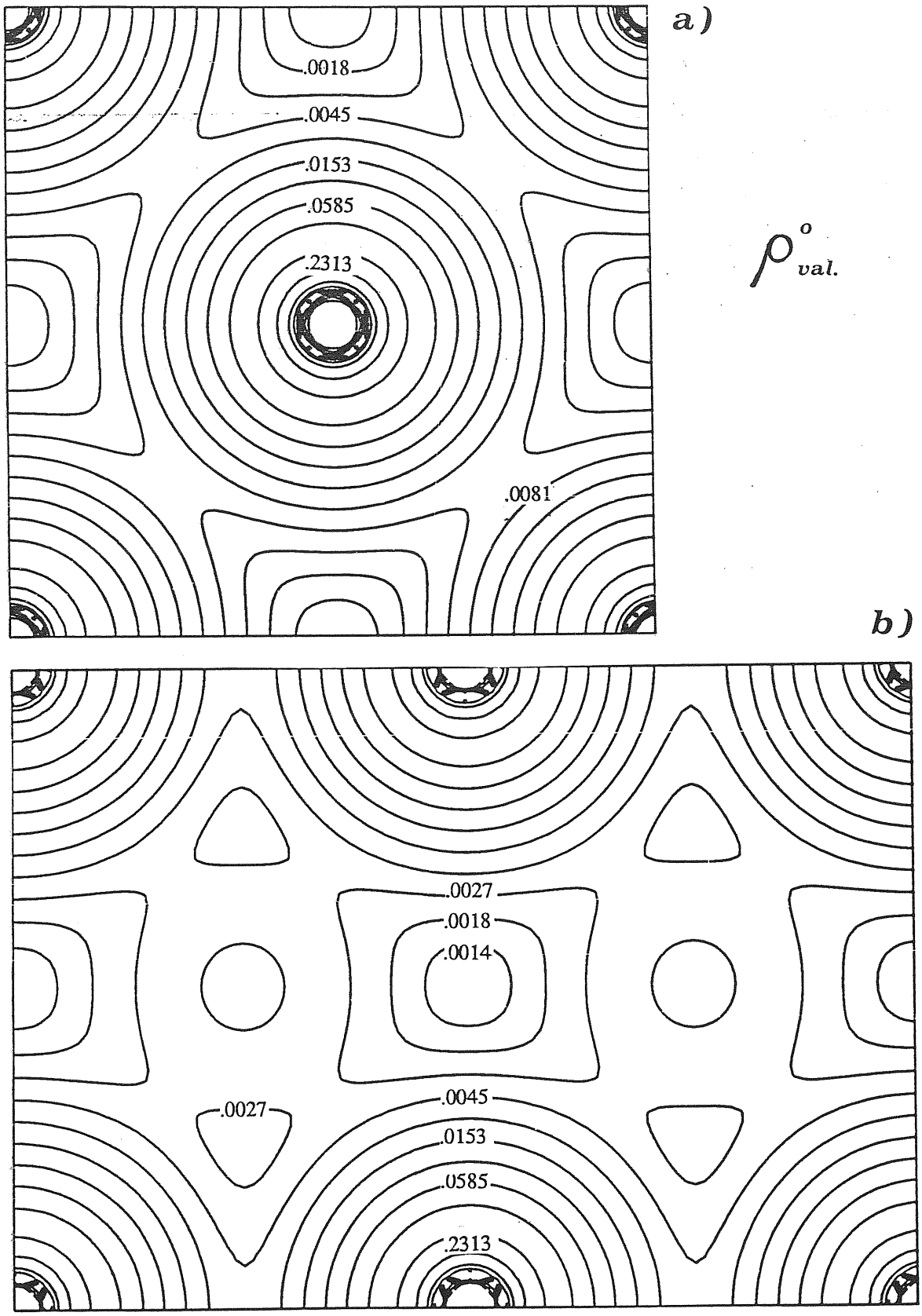

Fig.6: Valence electron density in the (001) plane (a) and in the (011) plane (b) in the free–ion approximation. Chlorine ions are at the corners. The lowest level corresponds to $1.35 \cdot 10^{-3}$ electrons/a.u.^{3}, and the interval between the i–level and the $(i-1)$–level is $2^{(i-1)} \cdot 4.5 \cdot 10^{-4}$ electrons/a.u.^{3}.

Extended rigid–ion approach

An approximate method to investigate the forces between closed-shell systems such as alkaline and halogen ions or inert-gas atoms has been developed by Gordon and Kim [36]. In this method all the energy terms are estimated from the electron charge density: the Coulomb interactions between ions, electrons and ions, and among electrons, as well as the remaining contributions to the interaction energy (i.e. electronic kinetic energy, exchange and correlation effects) which are evaluated approximating locally the electron density with that one of a uniform free-electron gas. The crystal electron density itself is approximated simply by the sum of the free-ion densities obtained in the Hartree-Fock approximation, as already proposed in the previous paragraph.

We stress that within this scheme one calculates all the interactions starting from overlapping but still spherical rigid charge densities: any modification of the ionic charge due to the overlap with the neighbouring ions is excluded from the beginning.

d) Beyond the free-ion approximation

A complete treatment of the electron-electron interactions has been done in tight-binding theory [37], and also self-consistent calculations for the structural properties of alkali halides have been performed [19)–21]. Beyond the free–ion approximation, a more accurate electron charge density has been obtained within the framework of these self–consistent calculations. For NaCl, for instance, the results indicate an essentially spherical charge distribution around the ions, which are not rigid but isotropically deformable, as assumed in the breathing shell model [38),39]. In particular these investigations indicate —in agreement with experiment— a non–negligible shrinkage of the electronic charge density around the anions, the effect being stronger as the interatomic distance becomes smaller. This effect can only be explained when overlaps are taken into account, therefore it cannot within the rigid–ion model or more refined versions of it.

2.2
STRUCTURE AND COHESION OF ALKALI HALIDE SOLID SOLUTIONS

a) Structure and cohesion from experimental data

The lattice parameter

The average lattice parameter a of a solid solution is usually varying with the composition x according to a law of the form:

$$a^n(x) = xa_2^n + (1-x)a_1^n \tag{2.2.1}$$

where a_1 and a_2 are the lattice parameters of the constituents and x is the molar fraction of the second component in the solid solution. The additivity of distances —already known as Vegard law [12]— is expressed by $n = 1$, whereas the value $n = 3$ indicates additivity of volumes, the so-called Retgers law. Different values of n have also been proposed in the past based on both experimental data or theoretical models [13),29)].

The crystallographic structure of pseudobinary solid solutions $A_{1-x}B_xC$ of alkali halides has first been investigated with the X-ray diffraction technique [5)].

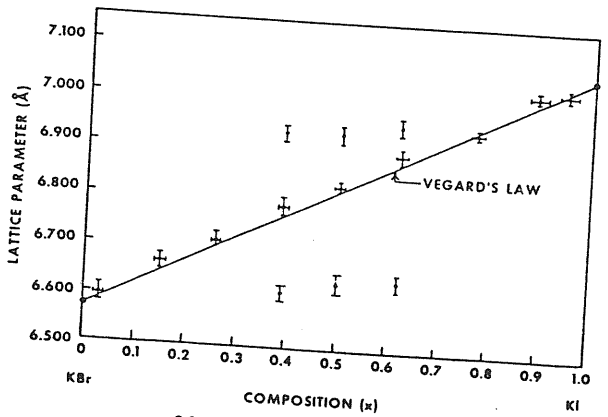

Fig.7: Lattice parameter variation of $KBr_{1-x}I_x$ with composition x (from Ref. 10).

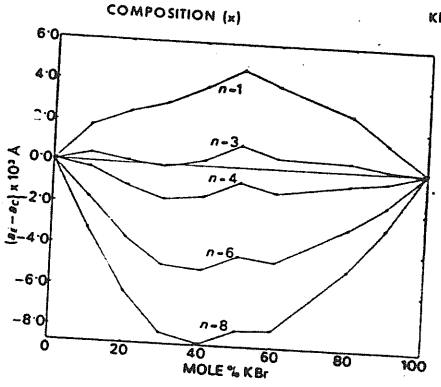

Fig.8: Difference between the experimental values of the lattice parameter for $KCl_{1-x}Br_x$ and the values calculated according to eq. (2.2.1) for different values of n (from Ref. 11).

X-ray data show that in general the average lattice parameter varies linearly with composition between the values for the AC and BC end compounds , i.e. the Vegard law is followed. However there are some non-negligible deviations from it: some accurate measurements indicate positive deviations from Vegard law and hence a closer agreement with Retgers law, as it is shown for instance in Fig. 7 for $KBr_{1-x}I_x$ [10] and in Fig. 8 for $KCl_{1-x}Br_x$ [11] . The largest deviations from the Vegard law occur in solid solutions of alkali halides characterized by very different lattice parameters. When this condition is verified, the sign of the deviation from the Vegard law can also change as a function of composition (S–shape).

Experimental evidencies for lattice distorsions

Accurate EXAFS data [14)–16)] are available for $K_{1-x}Rb_xBr$, $RbBr_{1-x}I_x$, and $KCl_{1-x}Br_x$. They show the existence — at each composition — of two distinct anion–cation nearest neighbour distances $r[A-B]$, $r[B-C]$, differ one from the other and also from the average distance deduced from the lattice parameter value, as it has been already observed in the past for semiconducting alloys [40)–42)]. The two nearest neighbour distances are intermediate between those of the pure compounds and the average Vegard value. In $K_{1-x}Rb_xBr$, for instance, the nearest neighbour distances $r[K-Br]$ and $r[Rb-Br]$ vary linearly with composition and their total variation is about 40% of the difference between nearest neighbour distances in the pure compounds, i.e. the variation is more pronounced than that observed in semiconducting alloys.

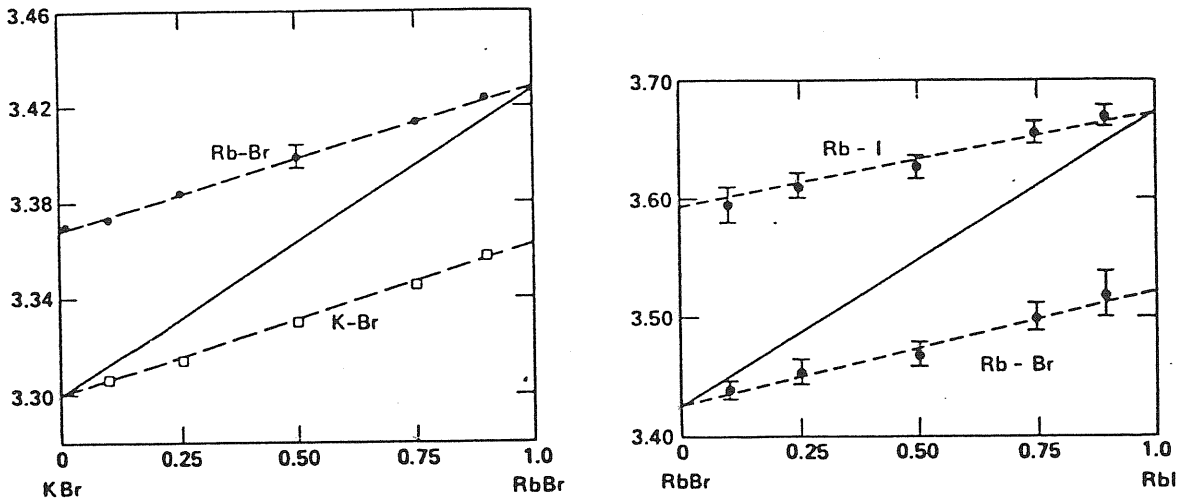

Fig.9: Anion–cation NN distances in $K_{1-x}Rb_xBr$ and $RbBr_{1-x}I_x$ as a function of composition x. The points indicate the experimental EXAFS data; the solid line shows the average anion–cation distance resulting by a linear interpolation of the NN distances in the pure end compounds (from Ref. 14).

Fig.10: Nearest neighbour K–Cl distances in $KCl_{1-x}Br_x$ obtained from EXAFS measurements (from Ref. 15).

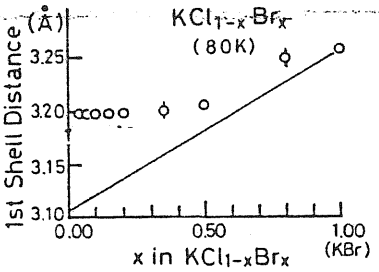

Heats of formation

The heat of formation ΔH_f (or heat of mixing) of a solid solution is defined as the difference of the internal energies of the solid solution and of the separate–phase mixture of the two components:

$$\Delta H_f = U_{A_{1-x}B_xC} - [xU_{BC} + (1-x)U_{AC}] \qquad (2.2.2)$$

If the system is not at zero temperature, the internal energy contains also the thermal energy, but in ΔH_f only deviations of the thermal energy of the solid solution from a weighted average of the two end compounds enter accordind to eq. (2.2.2). It is thus clear that —since also the zero point kinetic energy is a negligible quantity— one can replace for all practical purposes the internal energy by the lattice energy.

The experimental data [7)–9)] indicate positive heats of formation, suggesting that the alkali halide solid solutions are unstable. In a very crude estimate, the deviations of the lattice energy of the solid solutions from a linearly interpolated dependence of the two compounds behaves as $x(1-x)$, reaching their maximum for intermediate values of the composition x.

b) Theoretical investigations

Models without distortions

The alkali halide solid solutions have already received some attention in theoretical investigations in the past, at least for a determination of average structural parameters and for thermodynamic properties such as, for instance, the heat of formation.

Tobolski [6)] assumes the validity of the Vegard law to evaluate the heat of formation of the alkali halide solid solutions, obtaining only a partial agreement with the experimental data [7)–9)]. Wallace [8)] uses a more refined Born–Mayer model to evaluate the lattice energy; he calculates the lattice parameter by

minimizing the lattice energy, and with the value obtained evaluates the heat of mixing. The agreement with experimental data is satisfactory for the lattice parameter, but not for the heats of mixing. In a recent theoretical analysis of the structural phase transitions in mixed alkali halide crystals Shanker et al. [30] perform their calculations within the framework of the VCA using an interionic potential containing an adjustable multiplicative factor for the Van der Waals interactions and the exponential form for the repulsive potential, with parameters determined by fitting the experimental values of the lattice energies of pure end compounds in standard observed structures.
Krishamurty and Murti [32] formulate a scheme to calculate the thermodynamic properties of concentrated alkali halide solid solutions including the change in volume upon alloying and the vibrational contribution. They model the alloy with a regular lattice of "pseudoions" interacting with an average ion–ion potential suitably constructed from the end member interionic potentials. The model is applied to $K_{1-x}Na_xCl$: the results are not very satisfactory, since the relative difference with the experimental data is about 17% for intermediate compositions.
Cox et Sangster [31] calculate the volumes of formation Ω_f for substitutional impurities in alkali halides from the pressure dependence of their energy of formation:

$$\Omega_f = -\frac{1}{3} k_T a \left(\frac{\partial E_f}{\partial a} \right)_{a=a_0} \qquad (2.2.3)$$

They then estimate deviations from the Vegard law over the complete composition range by fitting to the end points $x = 0, 1$ cubic polinomials and their derivatives, given by the calculated Ω_f ; they find for $Na_{1-x}K_xCl$, $NaCl_{1-x}Br_x$, and $K_{1-x}Rb_xCl$ small positive deviations both from Vegard and Retgers law, in good agreement with experimental X–ray data. We must notice however that they perform all their calculations with a fixed set of parameters of the model potential, and in this way, for instance, isothermal compressibilities cannot be well reproduced.

Models for the lattice internal distorsions

Some models have been proposed to explain the internal lattice distorsions around substitutional defects both in case of impurity and of solid solution as prooved by the EXAFS experimental analysis. The local structure of metallic [43] and semiconducting [42),44)–46] pseudobinary alloys has been the subject of several theoretical investigations. These studies however do not apply to ionic solid solutions which are substantially different both in lattice structure and in type of binding.

For ionic materials, only the case of infinite dilution, i.e. the isolated impurity limit, has received some attention in the past [24)-28)]. Harrison et al. [24)] propose a very simple central force model for generic pseudobinary alloys, describing the crystal only through NN harmonic interactions. The validity of the model is however very limited, since it applies only in the case of extreme diluition and allows radial displacements of the ions surrounding the impurity; it predicts the bond length between the impurity atom and its nearest neighbours: the relative deviations of the bond lengths of the solute depend only on the geometrical crystal structure and are 50% in the case of pseudobinary alloys with rocksalt structure.

Hardy [25)] has also proposed a method to calculate the ionic displacements around an impurity and has applied it to the case of K^+ : NaCl . He describes the crystal as containing a large regular superlattice of defects: changes in volume and some short– and long–range internal distorsions are allowed in each supercell. With only NN repulsions included and without any polarization effect the model predicts a contraction of the K–Cl bond length with respect to the pure KCl: the reduction is about 55% of the difference between r[Na–Cl] and r[K–Cl] in the pure compounds; the inclusion of polarizability modifies the result predicting a variation of about 48%.

Fukay [26)] has used two different models (isotropic approximation and the superlattice approximation suggested by Hartree) to calculate the lattice distorsions around impurity monovalent ions. The superlattice approach allows also anisotropic distorsions, but the isotropic approximation gives results closer to the experimental data.

Dick and Das [27)] are also interested in the problem of the lattice relaxation around impurities. Their model allows the ions surrounding the impurity to relax along radial directions and to polarize, while all other ions are fixed and do not polarize. The minimization of the lattice energy gives the values of the distorsions and of the electronic dipoles; the results strongly depend on the values being used for ionic polarizabilities and on the parameters of the Van der Waals interactions, whose estimate is very difficult.

Hess [28)] investigates the effects of an impurity ion in alkali halide crystals, using a deformation–dipole model with single–ion parameter; when applied to KCl:Li^+, the model gives results in qualitative agreement with experiment.

All these models agree in predicting relevant relaxations of the lattice around a substitutional defect. The only theoretical result that can be compared with the recent and accurate EXAFS data is the one given by Fukay [26)] for r[K – Br] in KCl : Br^-: he predicts a radial relaxation of about .065$\AA$ of K^+ NN to Br^-, whereas EXAFS data indicate a displacement of .08$\AA$, i.e. a reduction of the bond length with respect to the pure compound of about 50% of the difference

between the two lattice parameters.

It is evident that several theoretical investigations have been done up to now for the isolated impurity problem; on the other side, other works treating the solid solution over the whole range of composition have been concerned with the thermodynamical aspects [7] or the average structural parameters. Few theoretical models taking into account the lattice relaxation in case of large defect concentration exist: an attempt in this sense has been done by Durham and Hawkins [29]. They use an interaction potential containing Coulomb, Van der Waals and exponential repulsive terms between NN and NNN. They consider the octaedra having ions of two different species at the vertices, and the common ion at the center, which relaxes depending on the kind of ions which occupy the vertices; one must then take into account the probability of each configuration. The idea of a bimodal distribution of the NN distance is correct, but it is not sufficiently developed : the authors simply say that the relaxations are very small and can be neglected in the evaluation of the heat of formation of the solid solutions, for which they obtained theoretical values which are too small by about 30% for $KCl_{.5}Br_{.5}$ and $K_{.5}Rb.5Cl$.

Chapter 3
ATOMIC–SCALE CRYSTALLOGRAPHIC STRUCTURE OF ALKALI HALIDE SOLID SOLUTIONS

Summary

A very simple model of alkali halide solutions is presented in the first part of this chapter, based on the virtual crystal approximation and on the Born–Mayer model for treating ion–ion interactions. The results are poor, since the predicted lattice parameter shows too large deviations from the Vegard law, and the bimodal distribution of the NN distances is of course absent.

In order to take into account the lattice relaxation indicated by EXAFS data, a more accurate model is proposed beyond the virtual crystal approximation. The random system is simulated with a periodically repeated supercell allowing internal distorsions. For a given supercell the symmetry dictates precise criteria for anion and cation distributions as well as for the atomic displacements from the ideal sites of the rocksalt virtual crystal . The lattice energy is evaluated with the Born–Mayer model generalized to include polarization effects. The resulting average lattice parameter and anion–cation distances agree with recent EXAFS data on $K_{1-x}Rb_xBr$, $RbBr_{1-x}I_x$, and $KCl_{1-x}Br_x$. The results show that ionic polarization plays a significant role in the determination of both interatomic distances and heats of formation.

3.1
GENERALIZED BORN–MAYER MODEL FOR SOLID SOLUTIONS IN A V.C.A. APPROACH

a) Lattice energy in the VCA

The virtual crystal approximation

The simplest model for the structure of a pseudobinary alloy $A_{1-x}B_xC$ describes it as an ideal and undistorted lattice; for the systems treated here, it is a rocksalt lattice with one of the two FCC sublattices containing the ions C and the other the ions A and B. The NN distances are thus all equal, being a compromise between the NN distances of the constituents. We start with this assumption, and we investigate if such a crude model gives reason of the approximate validity of the Vegard law and of the deviations from it.

Lattice energy evaluated with the Born–Mayer model

We use the simplest version of the Born–Mayer model, i.e. we neglect all second–neighbour and Van der Waals interactions; the parameters B and ρ are determined for each compound by fitting the analytic expression of the lattice energy to the experimental equilibrium interatomic distance and bulk modulus, and are reported in Tab. 1.

	r_0 (ang)	K_0 $(10^{-12}cm^2/dine)$	ρ (ang)	B $(10^{-8}erg)$	α $(10^4 erg/cm^2)$	β $(10^{12}erg/cm^2)$
KCl	3.147	5.73	.326	2.05	4.943	−5.959
	3.107*		.326*	1.86*		
KBr	3.298	6.75	.336	2.30	4.397	−5.142
	3.260*		.336*	2.10*		
KI	3.530	8.55	.349	2.77	3.719	−4.172
RbBr	3.427	7.69	.342	2.61	4.032	−4.655
RbI	3.671	9.48	.348	3.99	3.485	−3.899

Tab.1: Equilibrium lattice parameter, compressibility, repulsion parameters and harmonic and anharmonic force constants for some alkali halides in standard conditions of temperature and pressure. For KCl and KBr data at zero temperature and pressure* are also reported.

We write the energy of the two pure compounds:

$$E_{AC}(a) = -\frac{\alpha_a e^2}{a} + B_{AC}\exp(-\frac{a}{2\rho_{AC}}) \qquad (3.1.1)$$

$$E_{BC}(a) = -\frac{\alpha_a e^2}{a} + B_{BC}\exp(-\frac{a}{2\rho_{BC}}) \qquad (3.1.2)$$

where a indicates the lattice parameter which is twice the NN distance. If x is the molar fraction of BC in the solid solution, the energy of the mixed crystal within the VCA is:

$$E_x(a) = xE_{BC}(a) + (1-x)E_{AC}(a) \qquad (3.1.3)$$

$$E_x(a) = -\frac{\alpha_a e^2}{a} + xB_{BC}\exp(-\frac{a}{2\rho_{BC}}) + (1-x)B_{AC}\exp(-\frac{a}{2\rho_{AC}}) \qquad (3.1.4)$$

which follows immediately if we consider that the Madelung energy is the same in the pure compounds and in the solution, since the ions of mixed type are isovalent, and if we evaluate the repulsive energy arising only from NN interactions.

b) Average lattice parameter: deviations from Vegard law

Techniques and results

The equilibrium lattice parameter a_0 of the mixed crystal is found by minimizing the lattice energy, i.e. by solving the equation:

$$\left.\frac{dE_x(a)}{da}\right|_{a=a_0} = \frac{\alpha_a e^2}{a_0^2} - x\frac{B_{BC}}{2\rho_{BC}}\exp\left(-\frac{a_0}{2\rho_{BC}}\right) - (1-x)\frac{B_{AC}}{2\rho_{AC}}\exp\left(-\frac{a_0}{2\rho_{AC}}\right) = 0 \qquad (3.1.5)$$

Although an exact analytic solution is not possible, one can easily check that this equation does not express the Vegard law. Numerical solutions have been carried out for $KBr_{1-x}I_x$, $RbBr_{1-x}I_x$, $K_{1-x}Rb_xBr$ and are reported in Tab. 2. The deviations from the Vegard law are always positive and reach the maximum value (about 4–5% of the difference of the lattice parameters of the pure compounds) for $x \cong .5$.

$K\,Br_{1-x}I_x$

x	r	r_{Veg}	δr	E	E_{sep}	ΔH_f	ΔH_f^{exp}
0.0	3.298	3.298	.000	-157·981	-157·980	0	
0.1	3.326	3.321	.005	-156·664	-156·989	324	
0.2	3.354	3.344	.009	-155·443	-155·998	554	
0.3	3.379	3.368	.012	-154·306	-155·006	699	
0.4	3.404	3.391	.013	-153·245	-154·015	769	
0.5	3.427	3.414	.013	-152·250	-153·023	773	390
0.6	3.449	3.472	.012	-151·315	-152·032	716	
0.7	3.471	3.460	.011	-150·434	-151·041	606	
0.8	3.491	3.484	.008	-149·602	-150·049	447	
0.9	3.511	3.507	.004	-148·814	-149·058	244	
1.0	3.530	3.530	.000	-148·066	-148·067	0	

$Rb\,Br_{1-x}I_x$

x	r	r_{Veg}	δr	E	E_{sep}	ΔH_f
0.0	3.427	3.427	.000	-152·348	-152·349	0
0.1	3.458	3.451	.007	-151·078	-151·418	339
0.2	3.488	3.476	.012	-149·911	-150·486	575
0.3	3.515	3.500	.015	-148·834	-149·555	721
0.4	3.541	3.525	.016	-147·835	-148·624	789
0.5	3.565	3.549	.017	-146·904	-147·693	789
0.6	3.589	3.574	.015	-146·034	-146·762	728
0.7	3.611	3.598	.013	-145·218	-145·831	613
0.8	3.632	3.622	.010	-144·449	-144·900	450
0.9	3.652	3.647	.005	-143·724	-143·969	244
1.0	3.671	3.671	.000	-143·038	-143·038	0

$K_{1-x}Rb_x\,Br$

x	r	r_{Veg}	δr	E	E_{sep}	ΔH_f
0.0	3.298	3.298	.000	-157·981	-157·980	0
0.1	3.312	3.311	.002	-157·319	-157·417	97
0.2	3.327	3.324	.003	-156·683	-156·854	170
0.3	3.340	3.337	.004	-156·072	-156·291	219
0.4	3.354	3.349	.004	-155·482	-155·728	245
0.5	3.367	3.362	.004	-154·914	-155·164	250
0.6	3.379	3.375	.004	-154·366	-154·601	235
0.7	3.392	3.388	.003	-153·836	-154·038	202
0.8	3.404	3.401	.003	-153·324	-153·475	151
0.9	3.415	3.414	.001	-152·828	-152·912	83
1.0	3.427	3.427	.000	-152·348	-152·349	0

Tab.2: Deviations from Vegard law and heats of formation calculated within the VCA. Distances are referred to the average anion–cation NN distances; E indicates the lattice energy of the alloy and E_{sep}, the correspondent value of the mixture of the two compounds in the separate phase; ΔH_f is the heat of formation (distances in Å, energies in cal./mole).

In order to find an approximate expression for a_0 we can solve eq. (3.1.5) with respect to x, obtaining:

$$x(a_0) = \frac{1 - \left(\frac{a_0}{a_{BC}}\right)^2 \exp(-\frac{a_0 - a_{BC}}{2\rho_{BC}})}{\left[\left(\frac{a_0}{a_{AC}}\right)^2 \exp(-\frac{a_0 - a_{AC}}{2\rho_{AC}}) - \left(\frac{a_0}{a_{BC}}\right)^2 \exp(-\frac{a_0 - a_{BC}}{2\rho_{BC}})\right]} \tag{3.1.6}$$

where a_{AC} and a_{BC} are the equilibrium lattice parameters of the two systems. We try then to approximate the inverse function $a_0(x)$ with a cubic polynomial fitting the end points $x = 0, 1$ and the correspondent derivatives calculated from $x'(a_0)$. We obtain:

$$a_0(x) \cong a_V(x) + x(1-x)\left[(a_{BC} - a_{AC} - a_0'(1))\, x + (a_{AC} - a_{BC} + a_0'(0))\,(1-x)\right] \tag{3.1.7}$$

where $a_V(x) = xa_{BC} + (1-x)a_{AC}$, as predicted by the Vegard law. The analytic solution is very close to the numerical one, at least for the systems considered here; it has the advantage of being very simple, making evident the Vegard law and the deviations from it, which are proportional to $(a_{BC} - a_{AC})$.

We ask ourselves if the present model indicates additivity of volumes rather than of distances. The Retgers law can be written as:

$$a_R(x) = \left[xa_{BC}^3 + (1-x)a_{AC}^3\right]^{\frac{1}{3}} \tag{3.1.8}$$

Approximating it with a cubic polynomial fitting the end points $x = 0, 1$ and the corresponding derivatives, we obtain:

$$a_0(x) \cong a_V(x) + x(1-x)\,(a_{BC} - a_{AC})^2 \left[\frac{2a_{BC} + a_{AC}}{2a_{BC}^2}x + \frac{a_{BC} + 2a_{AC}}{2a_{AC}^2}(1-x)\right] \tag{3.1.9}$$

with a positive deviation from $a_V(x)$ proportional to $\frac{(a_{BC} - a_{AC})^2}{a_{AC}a_{BC}}$. Looking at the analytic formulation (eq. (3.1.7)) of our results, we can conclude that in the present model neither the Vegard law nor the Retgers law are reproduced, the latter conclusion following from the comparison of the deviations from the Vegard law in eq. (3.1.7) and eq. (3.1.8). Looking in details at the results obtained, we recognize that the Retgers law rather than the Vegard law is followed, but the deviations from both these laws are not at all negligible.

We have also evaluated the heat of formation, i.e. the difference between the lattice energy of the mixed crystal at equilibrium and the corresponding weighted average of the lattice energies of the separated binary compounds. The heats of formation are always positive: it could not be otherwise in this model, as it appears evident from eq. (3.1.3).

Comparison with experimental data

The equilibrium lattice parameter predicted by this model is compared with the experimental data for $KBr_{1-x}I_x$ [11] and $KCl_{1-x}Br_x$ [10] in Fig. 11. The observed positive bowing of $a(x)$ with respect to $a_V(x)$ is reproduced, but the deviations are too large with respect to those experimentally observed.

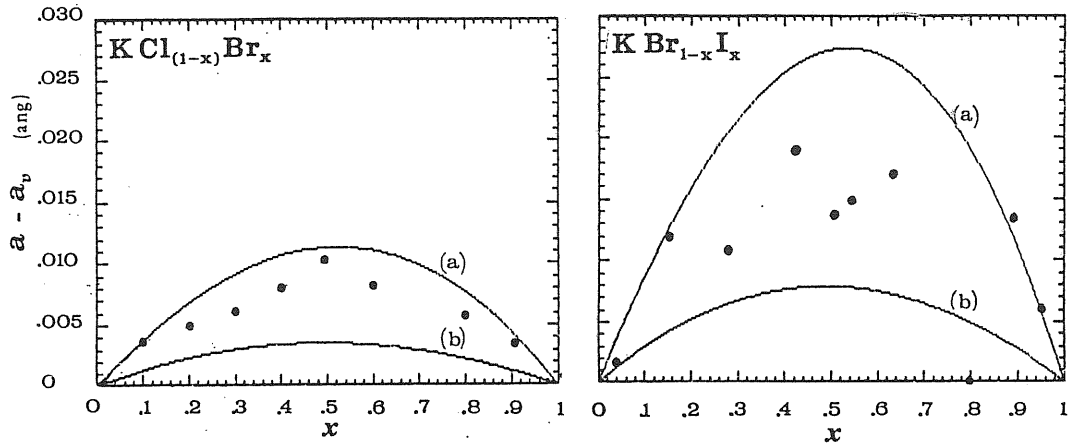

Fig.11: Differences of the equilibrium lattice parameter calculated according to the present model in the VCA (a) and to the Retgers law (b) with respect to the value predicted by the Vegard law. Dots indicate experimental data.

The heats of formation are also too large with respect to the measured quantities, as we have shown for instance in Fig. 12 for $KCl_{1-x}Br_x$, for which several experimental data [7)–9)] have been collected.

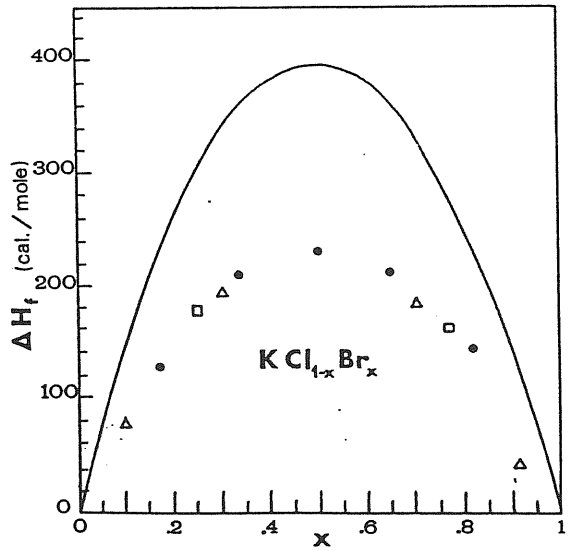

Fig.12: Heats of formation for $KCl_{1-x}Br_x$ at 80°K calculated according to the present VCA model (solid line) and measured (solid circles from Ref. 7, open squares from Ref. 8, and open triangles from Ref. 9)

Harmonic and anharmonic terms

In order to understand the physical origin of the deviations from the Vegard law, we separate the interionic potential near the equilibrium lattice parameter into its harmonic and anharmonic contributions. Considering only terms up to the third order in Δa we can write for the total energy of the two binary compounds AC and BC:

$$E_{AC}(a) \cong E^0_{AC} + \alpha_{AC}(a - a_{AC})^2 + \beta_{AC}(a - a_{AC})^3 \tag{3.1.10}$$

$$E_{BC}(a) \cong E^0_{BC} + \alpha_{BC}(a - a_{BC})^2 + \beta_{BC}(a - a_{BC})^3 \tag{3.1.11}$$

We obtain the equilibrium lattice parameter $a(x)$ of the mixed system $A_{1-x}B_xC$ by inserting eq. (3.1.10) and (3.1.11) in eq. (3.1.3) and minimizing the total energy in third order. For harmonic systems, i.e. $\beta_{AC} = \beta_{BC} = 0$, with a common elastic constant $\alpha_{AC} = \alpha_{BC} \equiv \alpha$ the equilibrium lattice parameter follows perfectly the Vegard law. In general $\alpha_{AC} \neq \alpha_{BC}$, and there are deviations from the Vegard law due to the difference between the elastic constants; further deviations are given by the anharmonic terms. The equilibrium condition gives:

$$x(a) = \frac{\left[2\alpha_{AC} + 3\beta_{AC}(a - a_{AC})\right](a - a_{AC})}{\left[2\alpha_{AC} + 3\beta_{AC}(a - a_{AC})\right](a - a_{AC}) - \left[2\alpha_{BC} + 3\beta_{BC}(a - a_{BC})\right](a - a_{BC})} \tag{3.1.12}$$

or —with the usual approximate form for the inverse relation—:

$$a(x) \cong a_V(x) + x(1-x)(a_{BC} - a_{AC}) \cdot$$
$$\cdot \left\{ (\alpha_{BC} - \alpha_{AC}) \left[\frac{x}{\alpha_{BC}} + \frac{1-x}{\alpha_{AC}} \right] - \frac{3}{2}(a_{BC} - a_{AC}) \left[\frac{\beta_{AC}}{\alpha_{BC}} x + \frac{\beta_{BC}}{\alpha_{AC}}(1-x) \right] \right\} \tag{3.1.13}$$

If we use the simplest Born–Mayer model for an alkali halide and approximate the energy around the equilibrium lattice parameter a_0 in terms of harmonic and anharmonic contributions, the force constants in terms of repulsive parameters are:

$$\alpha = \frac{\alpha_a e^2}{a_0^2} \left(\frac{1}{4\rho} - \frac{1}{a_0} \right) \tag{3.1.14}$$

$$\beta = \frac{\alpha_a e^2}{a_0^2} \left(\frac{1}{a_0^2} - \frac{1}{24\rho^2} \right) \tag{3.1.15}$$

After having determined the force constants for the alkali halides constituting the alloy (see Tab. 1), we can use eq. 3.1.13 to evaluate the equilibrium lattice parameter. Fig. 13 shows the results for $Na_{1-x}K_xCl$, where the lattice parameters of the end members are very different. One recognizes that:

1) the deviations from the Vegard law due to harmonic terms are negative;
2) including also the third–order anharmonic terms, the deviations become positive and are close to those calculated in the full "VCA—Born-Mayer" model as discussed above.

These simple computations show the importance of anharmonic forces in alkali halide solid solutions. It is therefore important to check if the anharmonic terms are well reproduced by the Born–Mayer model, since the determination of the repulsive parameters is done from experimental data which do not include anharmonic force constants. Comparing the third derivative with respect to the lattice parameter of the lattice energy obtained from the Born–Mayer model with that obtained from experimental data on the derivative of the bulk modulus with respect to pressure, we obtain an agreement of about 25% in the case of NaCl, which is enough for our purposes.

We can approximate the deviations from the Vegard law with a cubic polynomial:

$$\Delta a(x) = x(1-x)\left[b_2 x + b_1(1-x)\right] \tag{3.1.16}$$

If $b_1 \cdot b_2 > 0$ the deviations $\Delta a(x)$ have the same sign —i.e. the common sign of b_1 and b_2— in the whole interval (0,1); otherwise if $b_1 \cdot b_2 < 0$ the deviations change sign as a function of composition x, becoming zero when $x = \left(1 - \frac{b_2}{b_1}\right)^{-1}$. If the cohesive energy is developed up to third order anharmonic terms only, the quantities b_1 and b_2 are always positive for the alkali halides, so that in this approximation positive deviations from the Vegard law are predicted for all alkali halide solid solutions. This result remains valid when anharmonic terms of all orders are included.

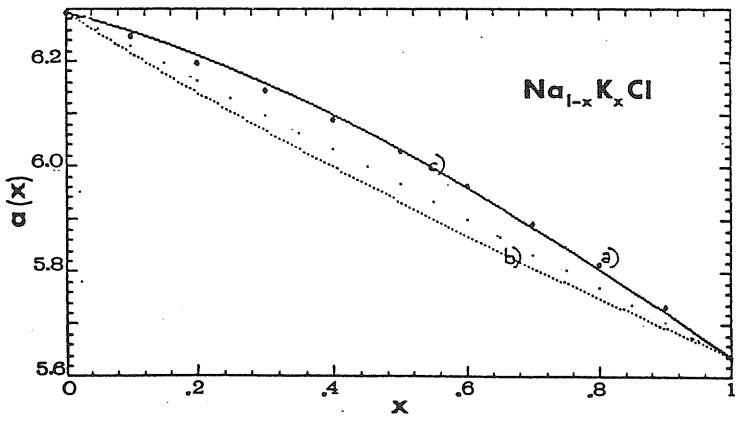

Fig.13: Average lattice parameter of $Na_{1-x}K_xCl$ as a function of the composition x, predicted within the present model including all anharmonic terms (points), only the harmonic (dotted line), and the harmonic and anharmonic terms up to third order.

c) Limits of the present model

Limits of the virtual crystal approximation

The fundamental limit of the model presented in this chapter is that it assumes an ideal undistorted lattice for the structure of the alloy, and hence it does not allow a bimodal distribution of the NN distances, which is the fundamental result of the EXAFS spectroscopy [14)-16)].

Looking at the results for the lattice parameters, we recognize a qualitative agreement with experimental data [10),11)], but in general the deviations from the Vegard law are much larger than those observed.

The model discussed in this chapter necessarily predicts positive heats of mixing for all alkali halide solid solutions: this trend is evident also from experimental data available [7)-9)], but the predicted values are too large with respect to those measured.

Beyond the VCA

We can easily recognize that the crystallographic structure of solid solutions as assumed in the VCA is not stable. Let us discuss here not about the general stability of the alloy, whose equilibrium configuration corresponds to the minimum of the total cohesive energy, but about the relative stability of the structure under internal distorsions, for a fixed volume. Looking at the forces acting on each ion, we see that at each ideal site of the undistorted lattice the resulting electrostatic force is zero, but this is not true for the short range repulsive forces, except when A and B ions, nearest neighbours to C, are symmetrically placed around C. The total force acting in genegal on C ions is thus not zero; the short range repulsive forces, whose intensity depends on the ion pair involved, tend to produce a relaxation of the lattice from the virtual crystal configuration, whereas the Coulomb forces oppose to the distortions. The final configuration depends on the balance of these two effects.

It becomes necessary now to introduce a model allowing lattice internal distorsions: this is the subject of the next chapter.

3.2
A "SUPERCELL" MODEL

a) Simulation of the real alloy

Definition of the supercell

Although the experimental data do not show any order in the distribution of A and B ions in the homogeneous $A_{1-x}B_xC$ solid solution, we simulate here the alloy with a periodically repeated supercell, large enough to contain a number of A and B ions as indicated by the molar fractions x and $1-x$.

Since the macroscopic symmetry of the real alloy is cubic we choose a cubic supercell: SC, FCC or BCC. We can construct the smallest cubic supercells, one for each kind of lattice. Starting from them, we can obtain bigger cells by multiplying by an integer number N the length of the basis vectors of the smallest cells. Correspondingly the number N of ions contained in the cell increases as N^3. The following Table 3 indicates the basic vectors for the smallest unit cell of each superlattice; r_0 indicates the NN distance.

kind of supercell	*number of ions per cell*	*basis vectors*	*compositions allowed*
$FCC_{N=1}$	2	$r_0(110)$ $r_0(101)$ $r_0(011)$	$0, 1$
$SC_{N=1}$	8	$2r_0(100)$ $2r_0(010)$ $2r_0(001)$	$0, \frac{1}{4}, \frac{3}{4}, 1$
$BCC_{N=1}$	32	$2r_0(\bar{1}11)$ $2r_0(1\bar{1}1)$ $2r_0(11\bar{1})$	

Tab.3: Different supercells describing the rocksalt sructure. Atomic displacements are not possible within these small supercells, but in the bigger ones obtained by multiplying by an integer N the length of the basis vectors.

Symmetry–restricted filling of the supercell

Once the type of supercell has been choosen, one can consider as unit cell the corresponding Wigner–Seitz cell. The important point is that the cubic symmetry with respect to the center of the cell must be recovered when one distributes anions and cations. The ions within the supercell can be grouped into shells of symmetry–equivalent sites; we point out that each site must be considered with an effective weight, which is 1 if it is really within the supercell, and a fraction less than 1 if it is on a surface, or at a side or a vertex, since it belongs simultaneously to several cells.

Each shell can contain only one kind of ions, so that each supercell allows only for certain compositions x^*. The smallest supercell simulating an alloy with composition x different from 0 and 1 is the SC supercell which can describe a solid solution with $x = \frac{1}{4}$ or the complementary concentration $x = \frac{3}{4}$.

Symmetry–restricted distorsions

The cubic symmetry of the superlattice gives precise criteria also for the ionic displacements from the sites of the undistorted lattice. Moreover, several displacements for the ions at a surface, a side or a vertex of the considered Wigner–Seitz cell are forbidden by translational symmetry. The smallest cubic supercell which allows for atomic distortions is the $\mathrm{FCC}_{N=2}$ unit cell with 16 ions (Fig. 14). The ions within the supercell can be grouped into shells of symmetry-equivalent ions. The sublattice centered at the origin contains three shells with 1, 6, and 1 ions, respectively, while the other sublattice contains two shells with 6 and 2 ions, respectively. According to our filling criteria — i.e. each shell can contain only one kind of ions — this supercell allows only for the compositions $x = 1/8$, $x = 1/4$, and the complementary concentrations $x = 7/8$ and $x = 3/4$. The fillings with compositions $x = 1/4$ and $x = 3/4$ will not be considered any further since in this case the supercell reduces to twice the SC cell with 8 ions, and all atomic displacements from ideal sites are symmetry forbidden. For the compositions $x = 1/8$ and $x = 7/8$ only the six ions which are octahedrally coordinated to the central one can have a common radial relaxation δ so that the crystallographic structure is fully described by the lattice constant $a = 4r_0$ and the internal distortion parameter $\epsilon = \delta/a$.

In the present work calculations have been performed for this simple cell, but the programs implemented can be easily generalized to apply the model to larger supercells.

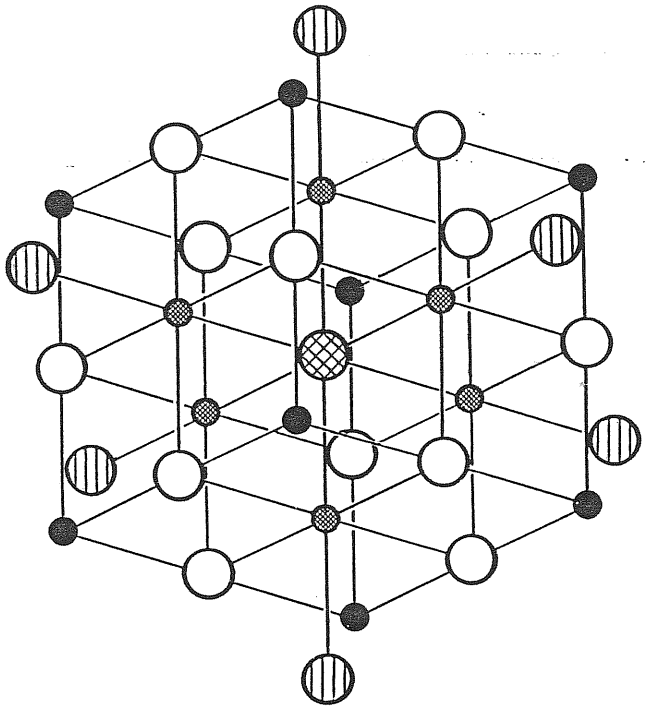

Fig.14: Wigner-Seitz unit cell of the FCC superlattice considered in the present work. The unit cell contains 16 atoms. Non-equivalent atomic sites are indicated with different symbols.

b) Lattice energy with a generalized Born-Mayer model

Distorsion dependent Madelung energy

We intend now to verify if the Born-Mayer model [16] can be applied to the atomic-scale structure of alkali-halide solid solutions and their heat of mixing. As in the previous chapter, we use the simplest version of the model, i.e. we neglect all second-neighbour and Van der Waals interactions, but we include the effects of ionic polarization, which have been found to be important in analogous circumstances of low atomic-site symmetry as for example in the presence of isolated defects or impurities, lattice vibrations [47], crystal surfaces [48], cohesion of alkali-halide molecules [49].

The point–charge Coulomb interactions in the mixed crystal are the same which are present in the pure compounds, since the ions of the mixed type are isovalent, so that the Madelung energy does not depend on the particular alloy considered but only on the geometry of the lattice structure, i.e. on the lattice constant and the distorsion parameter.

The Madelung energy per unit supercell can be written as:

$$E_{coul.}(a,\epsilon) = -\frac{e^2\alpha_a(\epsilon)}{a}, \tag{3.2.1}$$

where $\alpha_a(\epsilon)$ is a distortion-dependent Madelung function (Fig. 15) which for $\epsilon = 0$ has the value $\alpha_a(0) = 55.922$ which corresponds to the well known Madelung constant properly scaled to the dimension of our supercell. It has been computed for several values of ϵ with the Ewald method; it is convenient to introduce the following analytic approximate expression, valid for $|\epsilon| < .005$:

$$\alpha_a(\epsilon) \cong 55.922 - 693.08\epsilon^2 \tag{3.2.2}$$

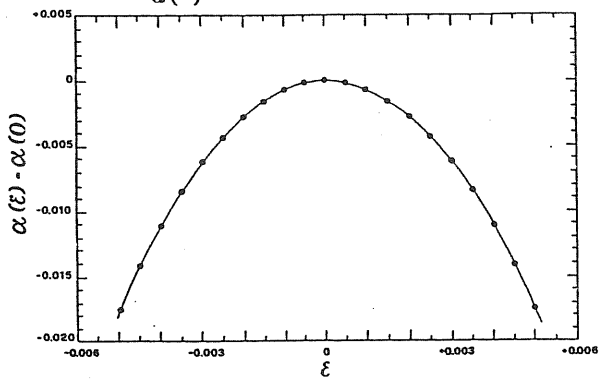

Fig.15: Madelung constant $\alpha(\epsilon)$ as a function of the internal distortion parameter. Dots indicate the results of computations while the full line represents the quadratic approximation given in the text.

Repulsive energy

In the Born–Mayer model the repulsive energy can be seen as the potential energy due to the repulsion between one ion and its NN. In the rocksalt structure for each A(B) ion there are six AC(BC) bonds, each of them with a repulsive energy equal to $\frac{1}{6}B\exp(-\frac{r}{\rho})$. For a given supercell we consider each bond separately with its proper repulsive energy, depending on the ionic pair considered, and then we sum up over all the bonds.

For the small FCC supercell used in the present work we can give easily an analytic expression for the repulsive energy per unit supercell. For $x = 1/8$ it can be written:

$$E_{rep.}(a,\epsilon) = B_{BC}\exp\left(-a(\frac{1}{4}+\epsilon)/\rho_{BC}\right) + B_{AC}\left[2\exp\left(-a/4\rho_{AC}\right)\right.$$
$$\left. + 4\exp\left(-a\sqrt{\frac{1}{16}+\epsilon^2}/\rho_{AC}\right) + \exp\left(-a(\frac{1}{4}-\epsilon)/\rho_{AC}\right)\right] \tag{3.2.3}$$

and a similar expression obtained by exchanging the A and B indices holds for $x = 7/8$. The parameters $B_{AC}, B_{BC}, \rho_{AC}$, and ρ_{BC} are listed in Tab. 1 of the previous chapter, adjusted to reproduce the lattice constant and bulk modulus of the pure AC and BC compounds.

Polarization energy

The local electric field **E** acting on a given ion is no longer zero when the ion is displaced from its ideal virtual crystal site. The distortion of the lattice induces an ionic dipole moment proportional to the local electric field, and — if we consider only charge–dipole interactions — the polarization energy of the ion is:

$$W = -\alpha_{pol.}|\mathbf{E}|^2 \tag{3.2.4}$$

where $\alpha_{pol.}$ is the ionic polarizability. The polarization energy per unit supercell is then found by summing the charge–dipole interactions for each polarized ion belonging to the supercell. Notice that the ionic polarization gives always a negative contribution to the lattice energy, and thus tend to enhance the lattice distortions.

The crystalline field has been evaluated with the Ewald method, taking into account that the vector $\mathbf{E}(\mathbf{r})$ is the opposite of the gradient of the potential at the same position, and the electrostatic potential enters directly in the evaluation of the Madelung constant. In the FCC supercell used here only the six C ions surrounding the center of the cell can polarize; E_{pol} can be written as:

$$E_{pol.}(a, \epsilon) = -\frac{\alpha_c e^2 f(\epsilon)}{a^4}, \tag{3.2.5}$$

where α_C is the polarizability of the C ions, whose value is reported in Tab.4, and $f(\epsilon)$ is a distortion dependent structural sum which must vanish for an undistorted lattice, i.e. $f(0) = 0$. Also for $f(\epsilon)$ it is convenient to use the following analytic approximate expression, valid for $|\epsilon| < .005$:

$$f(\epsilon) \cong 1.028 * 10^7 \, \epsilon^2 \tag{3.2.6}$$

	α		
Li^+	0.029	F^-	0.644
Na^+	0.408	Cl^-	2.960
K^+	1.334	Br^-	4.158
Rb^+	1.979	I^-	6.431
Cs^+	3.335		

Tab.4: Polarizabilities of the ions in the crystal (from Ref.50) in ang.^{3}.

c) Structural parameters and heat of mixing

Techniques and results

The lattice energy per unit supercell is thus the sum of the three terms

$$E(a,\epsilon) = E_{coul.}(a,\epsilon) + E_{rep.}(a,\epsilon) + E_{pol.}(a,\epsilon). \qquad (3.2.7)$$

The equilibrium values of the lattice constant $a(x)$ and of the internal distortion parameter $\epsilon(x)$ of $K_{1-x}Rb_xBr$, $RbBr_{1-x}I_x$ and $KCl_{1-x}Br_x$ have been computed for $x = 1/8$ and $x = 7/8$ by minimizing the total lattice energy with respect to a and ϵ simultaneously.

In order to understand the relevance of the ionic polarization we have also computed the equilibrium values of $a(x)$ and $\epsilon(x)$ by neglecting the polarization contribution. The resulting values of $a(x)$ and $\epsilon(x)$ are given in Fig. 16 and compared with experiment. The calculated values of the heat of mixing are given in Fig. 17.

Lattice parameter and NN distances

From Fig. 16 we see that the average NN distances calculated with the present model and neglecting the ionic polarization follow quite closely the Vegard law: the value is always greater than that predicted by the Vegard law, but the deviations are significantly reduced (by about 50%) with respect to those obtained with the VCA model. The lattice distortions play therefore an important role for the validity of the Vegard law, with a better agreement with the experimental data. The ionic polarization further reduces the equilibrium value of the lattice constant improoving the agreement with experimental data, although the differences between the results obtained by including or neglecting the polarization effects are not very relevant.

Looking at the distortions predicted here, we see that the lattice relaxes from the virtual crystal configuration increasing the bond length which would be larger in the corresponding pure compound and decreasing the other. However the variation of the bond length is not grater than 2%. In the present model we have different lengths also for bonds of the same kind, but the essential quantities are the two average bond lengths r[A-C] and r[B-C].

For the systems studied here we obtain A-C and B-C average equilibrium distances which are closer to the respective distances in the pure compounds than to the virtual crystal NN distances, as predicted by EXAFS data. The agreement is very good for $K_{1-x}Rb_xBr$, whereas for $RbBr_{1-x}I_x$ and $KCl_{1-x}Br_x$ the calculated internal distortions are smaller than those observed; moreover in all these systems the inclusion of polarization effects improves the agreement with the experimental data.

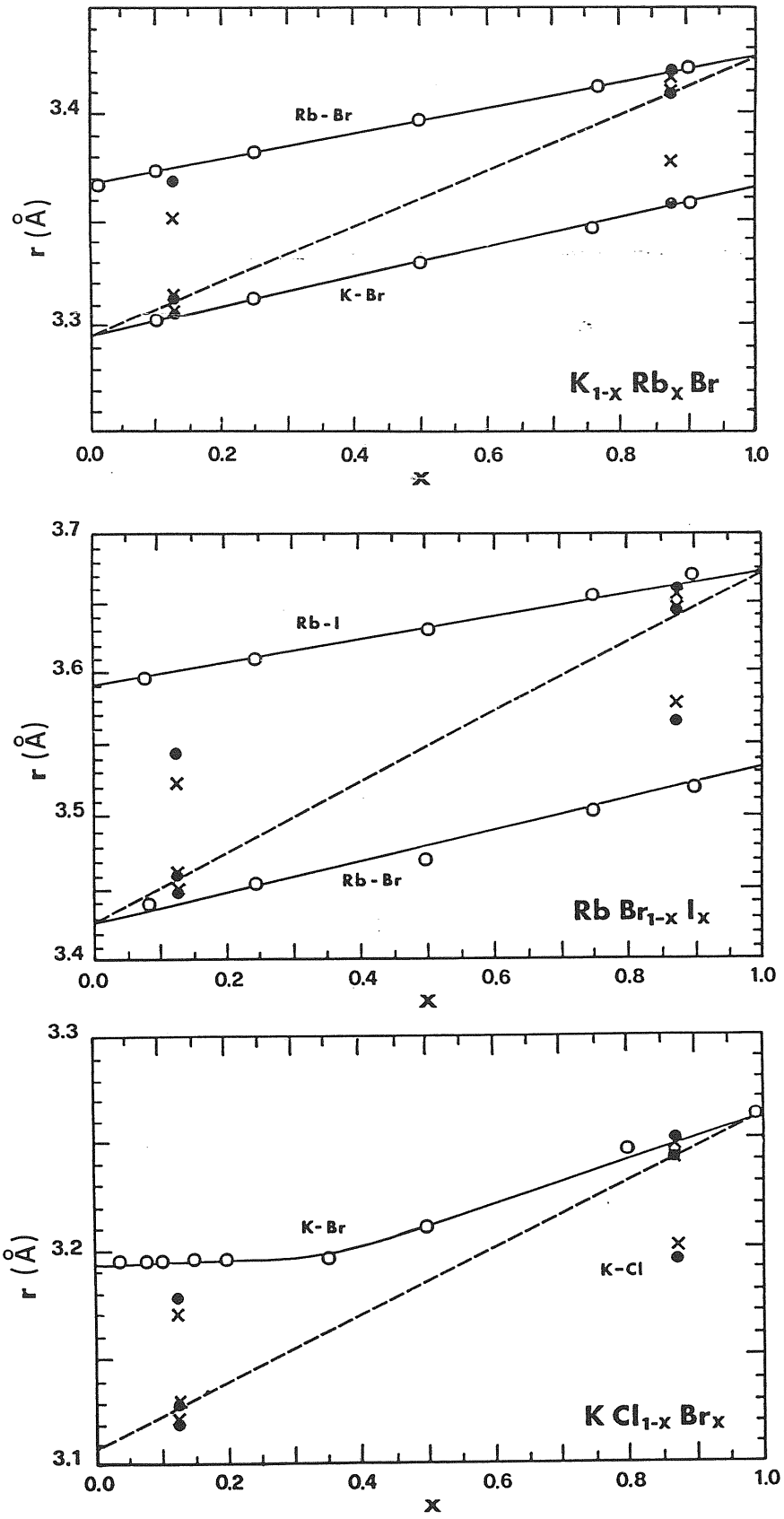

Fig.16: Anion-cation nearest-neighbour distances (in Å) calculated in this work for $K_{1-x}Rb_xBr$, $RbBr_{1-x}I_x$, and $KCl_{1-x}Br_x$ at x=1/8 and x=7/8. Distances calculated with/without polarization effects are represented by dots/crosses. EXAFS data (open circles) are also indicated for comparison. Data for $K_{1-x}Rb_xBr$ and $RbBr_{1-x}I_x$ are from Ref. 16 while those for $KCl_{1-x}Br_x$ are from Ref. 15.

Heats of mixing

Theoretical values of the heats of formation (see Fig. 17) calculated with the supercell tecnique are still positive for all the systems treated here, although smaller than the corresponding values obtained in the VCA. They can be compared with experiment only for $KCl_{1-x}Br_x$ and in this case good agreement is obtained.

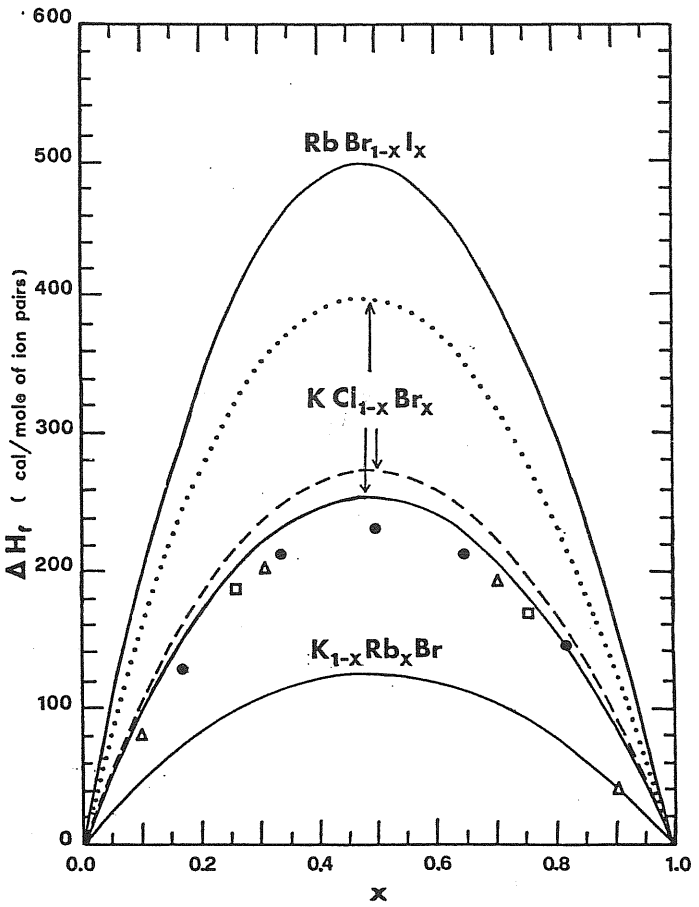

Fig.17:

Predicted heats of solution (in cal./mole of ion pairs) as a function of composition for the systems $K_{1-x}Rb_xBr$, $RbBr_{1-x}I_x$, and $KCl_{1-x}Br_x$. The points indicate the experimental values for $KCl_{1-x}Br_x$ quoted in Ref. 7 (solid circles), Ref. 8 (open squares), and Ref. 9 (open triangles). For the latter system the predictions obtained by neglecting simultaneously polarization effects and internal distortions (dotted curve) and neglecting only polarization effects (broken curve) are also represented.

Importance of polarization terms

The calculations performed neglecting the charge-dipole interaction energy in eq. 3.2.7 show that polarization effects cannot be neglected for an accurate determination of the internal lattice distortion and hence for the evaluation of the NN distances. As already stressed, the charge–dipole energy is negative and behaves as ϵ^2 for small ϵ; it tends thus to increase the distortions.

Polarization effects are specially important in the alloys having a common anion. In this case the displaced ions are the anions, which in general are more polarizable than the cations. This is, for instance, the case of $K_{1-x}Rb_xBr$ where the agreement with EXAFS data is very good. Common cation alloys polarize less and the inclusion of charge-dipole interactions is not sufficient to reproduce the experimental data.

Ionic polarization is also significant for the heats of formation. The calculated values can only be compared with experiment for $KCl_{1-x}Br_x$: in this case the polarization effects reduce their values and improve the agreement with the observation.

Conclusions

The supercell used in this work is the smallest cubic cell allowing internal distortions. Its A-B sublattice however cannot distort and only a fraction of C ions are allowed by symmetry to move offsite. Nevertheless with this simple supercell and a simple version of the Born-Mayer model we have obtained good agreement with experimental data. The encouraging results obtained here suggest that the local structure of alkali halide solid solutions could be satisfactory explained using a refined version of the present model: first, using bigger supercells which allow several compositions x and a more complete relaxation of the lattice, giving a better simulation of the real disordered systems.

A refinement of the Born–Mayer model should also be very important. We should text the importance of the second-neighbour repulsions and Van der Waals interactions. Moreover we should also try to go beyond the completely phenomenological treatment of the short range repulsive interactions as done in the Born–Mayer model, and take into account inter–ionic interactions with microscopic quantum mechanical computations. For instance, an explicit evaluation of the correction to the Madelung energy due to the effective charge distribution in the crystal is in order. A theoretical investigation in this sense is done in the next chapter.

Chapter 4
ELECTRONIC CHARGE DISTRIBUTION OF ALKALI HALIDE COMPOUNDS

Summary

The charge density of the alkali halides can be calculated in terms of Bloch functions constructed with the tight-binding method. Hartree-Fock ionic wave functions are used here as the basis expansion set for the Bloch functions. Throughout the first part of the chapter will be clear how the charge density can be obtained from these tight-binding Bloch functions; the various approximations involved are explained, and the application to the particular case of NaCl is shown.

The crystal charge density has the periodicity of the Bravais lattice and can be expressed in terms of some localized charge densities centered on the lattice sites. The crystal charge density previously calculated with the tight-binding approach is rewritten as a sum of the charge density of some "pseudoions" and of "orthogonality charges"; these picture allows a more direct comparison with the free-ion approximation, and makes easier the investigation of the physical effects appearing when the ions join to form the crystal.

An alternative approach to the study of the charge density is finally described: it includes from the beginning its symmetry properties with respect to the punctual group of the Bravais lattice. The localized charge densities are expressed in terms of symmetrized orbitals, which are particular LCAO orbitals of well defined symmetry constructed for each shell of neighbours for a reference lattice site.

4.1
TIGHT-BINDING APPROACH TO THE ELECTRONIC CHARGE DENSITY

a) Ionic wave functions

Analytic Hartree-Fock wave functions

In the present work we construct the crystal wave functions starting from the free-ion Hartree-Fock wave functions [52]. For our purpose we neglect the spin functions. The orbitals are assumed to be orthogonal to each other. They are characterized by three indices n, l, α which indicate respectively the principal quantum number, the symmetry species (i.e. the quantum number of the angular momentum), and the "subspecies" respectively. The orbital $\varphi_{nl\alpha}$ is expanded in terms of basis functions according to:

$$\varphi_{nl\alpha} = \sum_p c_{nlp}\chi_{pl\alpha} \tag{4.1.1}$$

The basis functions χ are Slater-type orbitals with integer quantum numbers:

$$\chi_{pl\alpha}(r,\theta,\phi) = R_{lp}(r)Y_{l\alpha}(\theta,\phi) \tag{4.1.2}$$

where

$$R_{lp}(r) = [(2n_{lp})!]^{-\frac{1}{2}}\,(2\xi_{lp})^{n_{lp}+\frac{1}{2}}r^{n_{lp}-1}e^{-\xi_{lp}r} \tag{4.1.3}$$

The $Y_{00}(\theta,\phi)$ are normalized spherical harmonics

$$Y_{0,0}(\theta,\phi) = \frac{1}{\sqrt{4\pi}} \tag{4.1.4}$$

$$Y_{1,0}(\theta,\phi) = \sqrt{\frac{3}{4\pi}}\cos\theta \tag{4.1.5}$$

$$Y_{1,\pm1}(\theta,\phi) = \mp\sqrt{\frac{3}{8\pi}}\sin\theta e^{\pm i\phi} \tag{4.1.6}$$

Fig.17: Radial part of s and p orbitals of the outer occupied shell for Cl^- and Na^+, considered at distances equal to nn and NNN equilibrium distances in the crystal.

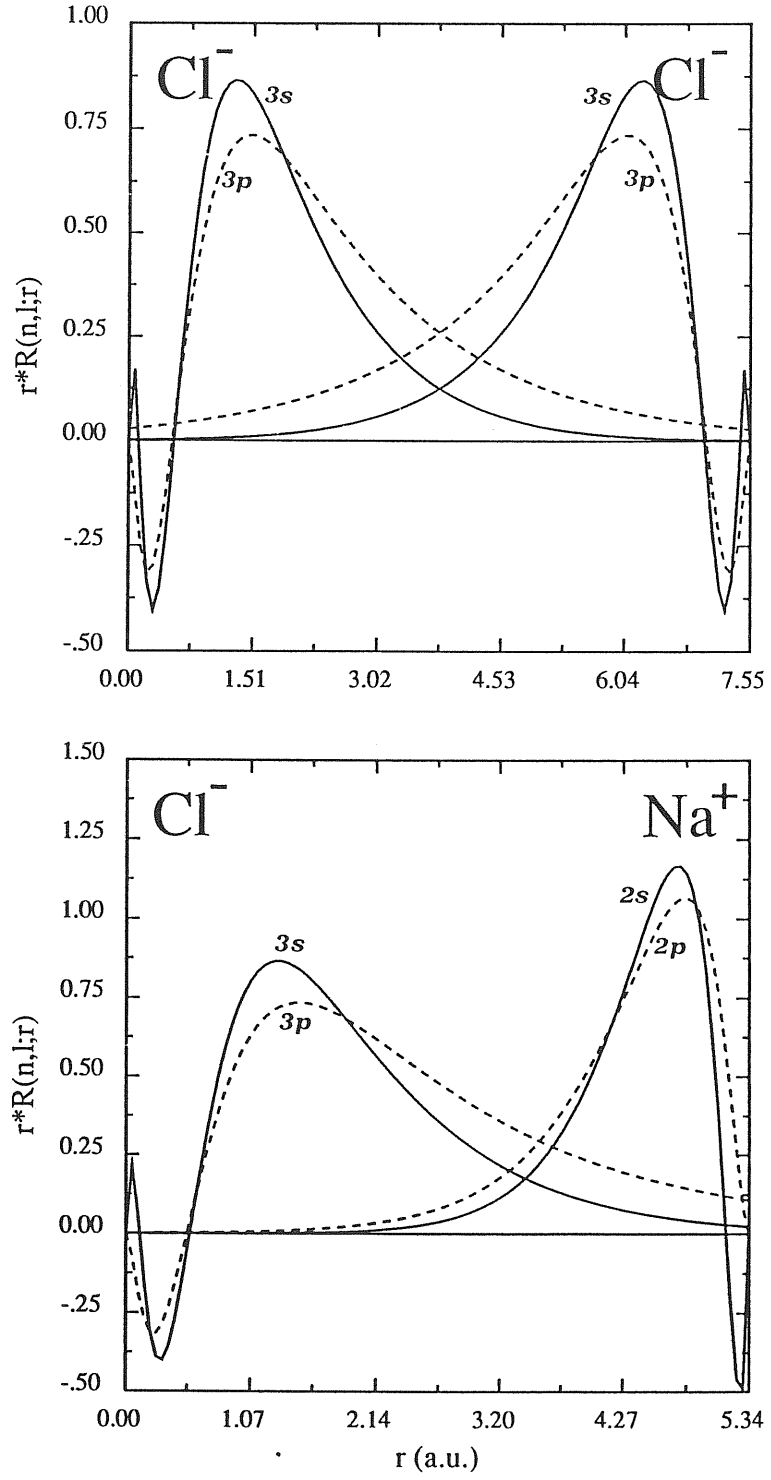

In order to work with real ionic orbitals we define s and p states with angular part given by linear combinations of spherical harmonics :

$$state \longleftrightarrow angular \ \ part \qquad ()$$

$$s \longleftrightarrow Y_{0,0} = \frac{1}{\sqrt{4\pi}} \qquad (4.1.7)$$

$$p_x \longleftrightarrow \frac{1}{\sqrt{2}}(-Y_{1,1} + Y_{1,-1}) = \sqrt{\frac{3}{4\pi}}\,\frac{x}{r} \qquad (4.1.8)$$

$$p_y \longleftrightarrow \frac{i}{\sqrt{2}}(Y_{1,1} + Y_{1,-1}) = \sqrt{\frac{3}{4\pi}}\,\frac{y}{r} \qquad (4.1.9)$$

$$p_z \longleftrightarrow Y_{1,0} = \sqrt{\frac{3}{4\pi}}\,\frac{x}{r} \qquad (4.1.10)$$

The radial part of s and p orbitals of the outer shell for Na^+ and Cl^- are shown in Fig. 17.

Overlap integrals

From Fig.17 we can see that the Na^+ and Cl^- ions overlap a little when they are put together to form the crystal, which is characterized by a nearest neighbour distance of 5.34 *a.u.* . The overlap effects play an important role in our case when ionic orbitals are used for expanding the crystal wave functions, so we implemented a very general procedure to calculate the overlap integrals between two ionic orbitals. The integrals on the same center are zero or one because of the properties of ionic orbitals. The non trivial quantities are the two-center integrals of the type

$$\int \phi^*_{\mu' n' l' m'}(\mathrm{r})\phi_{\mu n l m}\,(\mathrm{r}-\mathrm{R})d\mathrm{r} \qquad (4.1.11)$$

where R is the relative distance between the centers, μ and μ' refer to the type of ion, and $n'l'm', nlm$ are the quantum numbers of the orbitals.

Let us first consider the case where R is along the quantization axis. Because of symmetry properties, the integral is non-zero only if $m = m'$, and do not depend on the sign of m. The independent integrals are labelled with the symbols σ, π corresponding to the values $m = 0, \pm 1$ (we are not interested here in states with higher angular momenta). The overlap integrals between s and p functions are thus expressed in terms of the independent integrals $(ss\sigma)$, $(sp\sigma)$, $(pp\sigma)$, and $(pp\pi)$[53].

In the general case in which the vector R has direction cosines l_x, l_y, l_z with respect to the axis x, y, z the two-centers integralscan be also expressed in terms

of the independent integrals. The expressions of the overlap integrals between real wave functions involving s and p_x, p_y, p_z orbitals are :

$$< s \mid s > = (ss\sigma) \tag{4.1.12}$$

$$< s \mid p_x > = l_x(sp\sigma) \tag{4.1.13}$$

$$< p_x \mid p_x > = l_x^2(pp\sigma) + (1 - l_x^2)(pp\pi) \tag{4.1.14}$$

$$< p_x \mid p_y > = l_x l_y(pp\sigma) - l_x l_y(pp\pi) \tag{4.1.15}$$

Using these expressions, the overlap integrals between ionic wave functions of Na^+ and Cl^- centered on two arbitrary points can all be expressed in terms of few independent integrals.

The starting point in our work is the calculation of the overlap integral between two Slater-type atomic orbitals of arbitrary quantum numbers at a given distance along the common quantization axis. We use the exact general formula derived in Ref. 54. The integrals $(ss\sigma)$, $(sp\sigma)$, $(pp\sigma)$, and $(pp\pi)$ are then computed in terms of these Slater-type orbitals integrals. Fig. 19 and 20 show the independent integrals $(ss\sigma)$, $(sp\sigma)$, $(pp\sigma)$, and $(pp\pi)$ for Cl^-–Cl^- and Cl^-–Na^+ as a function of the distance between the centers. The values of these integrals at the distances corresponding to the shells of neighbouring ions in the crystal are reported in Tab. 5; Fig. 18 makes evident the comparison.

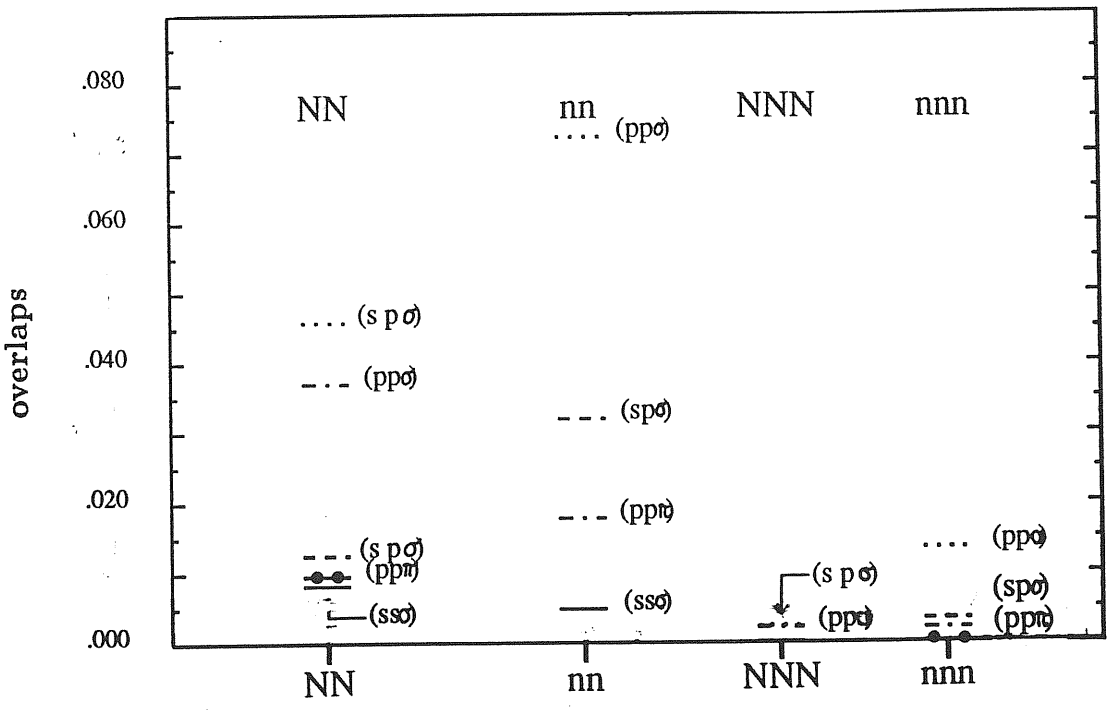

Fig.18: Independent overlap integrals for Cl^--Cl^- and Cl^--Na^+ at distances corresponding to nn, nnn, NN, and NNN equilibrium distances in the crystal.

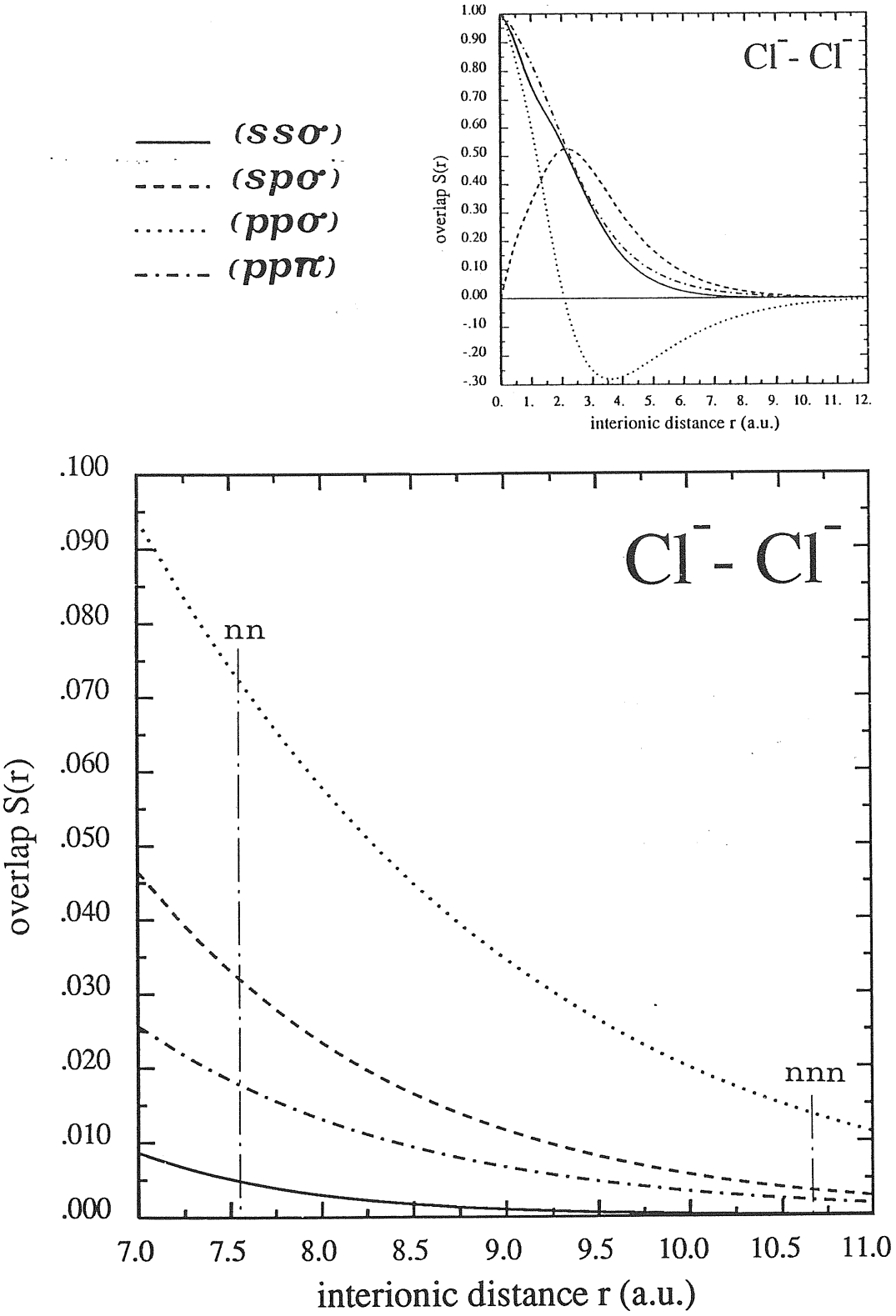

Fig.19: Independent overlap integrals between two chlorine ions as a function of the interionic distance, with the proper sign in (a), and with their modulus in (b), where nn and nnn equilibrium distances are indicated.

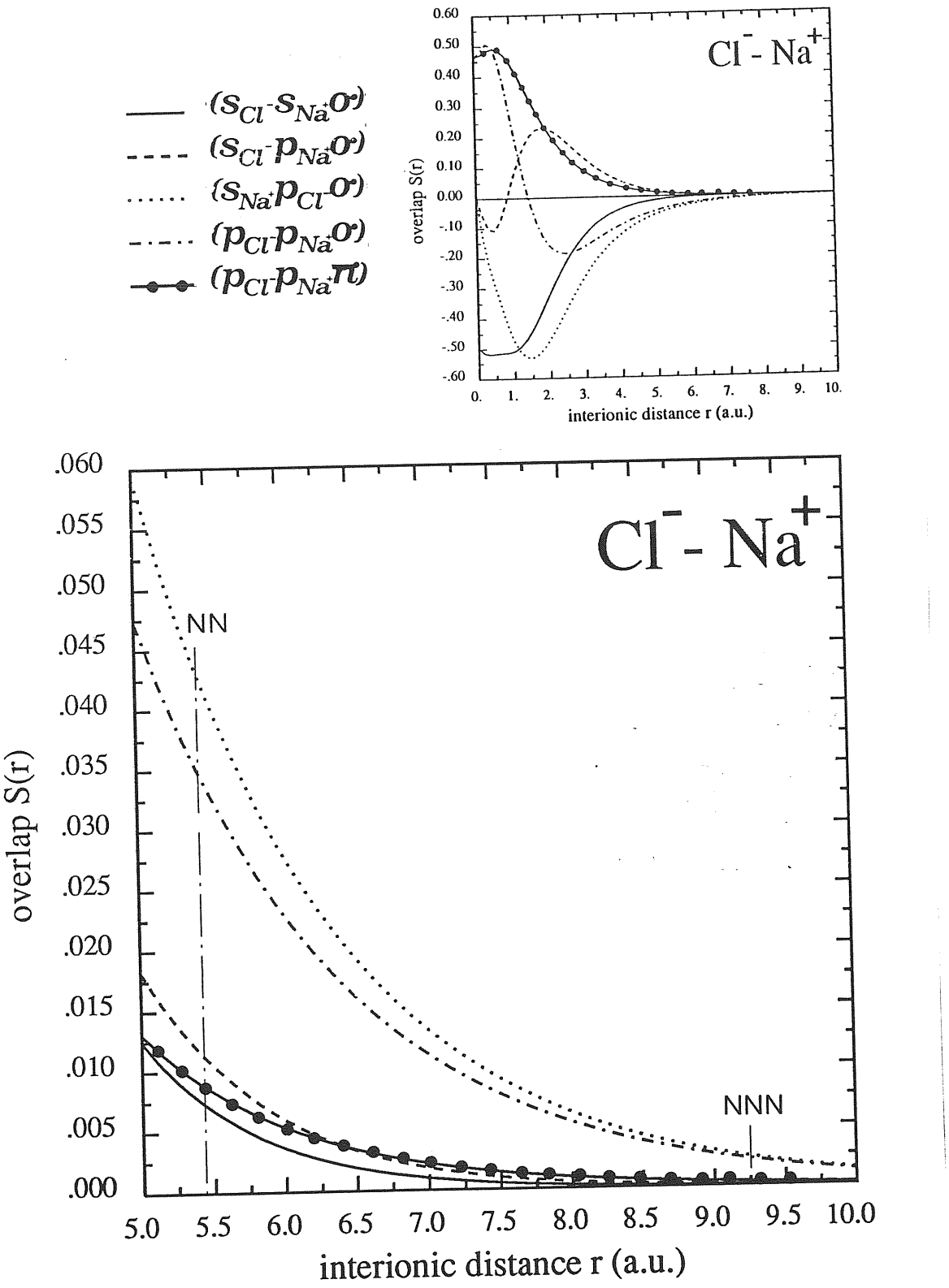

Fig.20: Independent overlap integrals between Cl^- and Na^+ ions as a function of the interionic distance, with the proper sign in (a), and with their modulus in (b), where NN and NNN equilibrium distances are indicated.

$Cl^- - Cl^-$ overlaps

interionic distance (a.u.)	$(ss\sigma)$	$(sp\sigma)$	$(pp\sigma)$	$(pp\pi)$
0.000000	1.00000	0.00000	1.00000	1.00000
7.553220	0.00481	0.03197	−0.07232	0.01775
10.681818	0.00014	0.00334	−0.01347	0.00204
13.082450	0.00001	0.00051	−0.00310	0.00036
15.106334	0.00000	0.00010	−0.00082	0.00008
16.889450	0.00000	0.00002	−0.00024	0.00002
18.501443	0.00000	0.00000	−0.00008	0.00001
19.983866	0.00000	0.00000	−0.00003	0.00000
21.363636	0.00000	0.00000	−0.00001	0.00000

$Cl^- - Na^+$ overlaps

interionic distance (a.u.)	$(s_{Cl}\text{-}s_{Na}+\sigma)$	$(s_{Cl}\text{-}p_{Na}+\sigma)$	$(s_{Na}+p_{Cl}\text{-}\sigma)$	$(p_{Cl}\text{-}p_{Na}+\sigma)$	$(p_{Cl}\text{-}p_{Na}+\pi)$
5.340909	−0.00822	0.01256	−0.04588	−0.03706	0.00960
9.250775	−0.00005	0.00011	−0.00238	−0.00218	0.00030
11.942593	−0.00000	0.00000	−0.00027	−0.00027	0.00003
16.022727	0.00000	0.00000	−0.00001	−0.00001	0.00000

Tab.5: Independent overlap integrals for Cl^--Cl^- and Cl^--Na^+ at distances corresponding to the first shells of neighbour ions in the crystal.

b) Bloch sums and orthonormalized Bloch functions

Bloch sums and normalization

The orbitals of the ions Na^+ and Cl^- inside the unit cell of the crystal are used to construct the crystal wave functions. Let us indicate the ionic orbital with $\varphi_{\mu\nu}$, where μ is the type of ion and the index ν summarizes the quantum numbers n, l, m of the orbital. The vector $\mathbf{d}_\mu$ is the position of the ion in the unit cell.

In the tight-binding method[55] the crystal wave function is expressed by the Bloch sum:

$$\Psi_{\mu\nu}(\mathbf{k},\mathbf{r}) = \sum_{\mathbf{R}_n} e^{i\mathbf{k}\cdot\mathbf{R}_n}\varphi_{\mu\nu}(\mathbf{r}-\mathbf{d}_\mu-\mathbf{R}_n) \qquad (4.1.16)$$

where $\mathbf{R}_n$ indicates a translation vector of the crystal lattice, which is in our case a FCC lattice with lattice constant $a = 10.681818$ *a.u.*. We can set up such Bloch sums corresponding to each atomic orbital of an ion, and corresponding to each ion in the unit cell of the crystal. The Bloch sums corresponding to different wave vectors are orthogonal to each other, whereas in general two Bloch sums with different quantum numbers but with the same k vector are not orthogonal .

However, the first problem that one has to solve is the normalization of these Bloch sums. We can write them in a normalized form:

$$\Psi_{\mu\nu}(\mathbf{k},\mathbf{r}) = A(\mathbf{k})\sum_{\mathbf{R}_n} e^{i\mathbf{k}\cdot\mathbf{R}_n}\varphi_{\mu\nu}(\mathbf{r}-\mathbf{d}_\mu-\mathbf{R}_n) \qquad (4.1.17)$$

where $A(\mathbf{k})$ is the normalizing factor which depends on the vector $\mathbf{k}$. If we impose that the Bloch sums are normalized to one over the unit cell, the factor $A(\mathbf{k})$ is given by the condition:

$$< \Psi_{\mu\nu}(\mathbf{k},\mathbf{r})|\Psi_{\mu\nu}(\mathbf{k},\mathbf{r}) >_\Omega = 1 \qquad (4.1.18)$$

that is, after a little of algebra:

$$1 = |A(\mathbf{k})|^2 \sum_{\mathbf{R}_n} e^{i\mathbf{k}\cdot\mathbf{R}_n} \int_{space} \varphi_{\mu\nu}(\mathbf{r})\varphi_{\mu\nu}(\mathbf{r}-\mathbf{R}_n)d\mathbf{r} \qquad (4.1.19)$$

Since the ionic functions are localized, the overlap between them decreases sharply with increasing distance, and one can limit the sum in the eq. (4.1.19) to a given order of neighbours.

We express the overlap integrals in terms of the independent integrals as explained in the previous section. Once we have these independent integrals,

the calculation can be carried out analytically for the first shells of neighbouring ions in the FCC sublattice . Taking into account the contribution of *nn* and of *nnn* ions for each sublattice (positions like $\frac{a}{2}(110)$ and $a(100)$), the formulas for the *s*-type and p_x-type Bloch sums are :

$$\begin{aligned} A_s^2(\mathbf{K}) &= 1 + 4(ss\sigma)_1(\cos\xi\cos\eta + \cos\xi\cos\varsigma + \cos\varsigma\cos\eta) \\ &\quad + 2(ss\sigma)_2(\cos 2\xi + \cos 2\eta + \cos 2\varsigma) \qquad (4.1.20) \\ A_{p_x}^2(\mathbf{K}) &= 1 + 2\Big\{(pp\sigma)_1[\cos\xi\cos\eta + \cos\xi\cos\varsigma] + \\ &\quad + (pp\pi)_1[\cos\xi\cos\eta + \cos\xi\cos\varsigma + 2\cos\varsigma\cos\eta]\Big\} \\ &\quad + 2\{(pp\sigma)_2\cos 2\xi + (pp\pi)_2[\cos 2\eta + \cos 2\varsigma]\} \qquad (4.1.21) \end{aligned}$$

where we use the quantities

$$\xi = \frac{ak_x}{2}, \quad \eta = \frac{ak_y}{2}, \quad \varsigma = \frac{ak_z}{2} \qquad (4.1.22)$$

The label put on the independent integrals indicate the corresponding distance: 1 for *nn* and 2 for *nnn* shell in each sublattice. The second formula with an obvious permutation of indices holds for p_y and p_z functions.

			$\Gamma = \frac{2\pi}{a}(0,0,0)$	$X = \frac{2\pi}{a}(1,0,0)$	$L = \frac{2\pi}{a}(\frac{1}{2},\frac{1}{2},\frac{1}{2})$
Cl^-	Ψ_{3s}	$\emptyset$	1.0000	1.0000	1.0000
		nn	0.9723	1.0098	1.0000
		nnn	0.9719	1.0094	1.0004
	Ψ_{3p_x}	$\emptyset$	1.0000	1.0000	1.0000
		nn	1.0829	0.8807	1.0000
		nnn	1.0950	0.8872	0.9907
Na^+	Ψ_{2s}	$\emptyset$	1.0000	1.0000	1.0000
		nn	1.0000	1.0000	1.0000
		nnn	1.0000	1.0000	1.0000
	Ψ_{2p_x}	$\emptyset$	1.0000	1.0000	1.0000
		nn	1.0000	1.0000	1.0000
		nnn	-0.9998	1.0002	1.0000

Tab.6: Normalization coefficients A(k) at Γ, X, L for the Bloch sums constructed from s and p orbitals of Cl^- and Na^+. The contributions due to the overlap of the nn and of the nnn shell are evident.

The quantity $A(\mathrm{k})$ is always of the order of unity, since the overlaps between orbitals centered on different sites are smaller than the overlap of one orbital with itself and hence are corrections to it. In Tab. 6 we report the coefficients $A(\mathrm{k})$ at $\Gamma, \mathrm{X}, \mathrm{L}$ for the Bloch sums constructed from s and p orbitals of Cl^- and Na^+ , specifying the contributions of the first two shells of ions in the anion or cation sublattices respectively. The most important overlap effects can be seen for the p-like Bloch sums of Cl^- where, for instance, the correction to $A_{p_x}(\mathrm{X})$ arising from the nn anions is of the order of 12%; also for Cl^- , however, the contribution to $A(\mathrm{k})$ arising from the nnn shell is never higher than 1%. As far Na^+ is concerned, since the ionic orbitals are very localized we can neglect the overlap of the neighbouring ions in the normalization of the corresponding Bloch sums , as it appears evident from the Table.

Orthogonalization of Bloch functions

We point out that the non trivial problem is to set up a system of orthogonal Bloch functions for any k vector. Let us consider the subspace spanned by a certain family $\{\Psi_n(\mathrm{k})\}$ $(n = 1, 2, ..., N)$ of Bloch sums. From this family we can construct a basis set of orthogonal Bloch functions $\{\Phi_n\}$ which are linear combinations of all the Bloch sums Ψ_n. For each k we consider the $N \times N$ overlap matrix $\mathrm{O}(\mathrm{k})$ between these Bloch sums. The element (n, m) is:

$$O_{n,m}(\mathrm{k}) = < \Psi_n(\mathrm{k}, \mathrm{r}) | \Psi_m(\mathrm{k}, \mathrm{r}) >_\Omega \tag{4.1.23}$$

Let us indicate with $\lambda_n(\mathrm{k})$ the eigenvalues and with $\mathrm{v}_n(\mathrm{k})$ the array representing the eigenvector corresponding to $\lambda_n(\mathrm{k})$ and normalized to one. In formulas:

$$\mathrm{O} \cdot \mathrm{v}_n = \lambda_n \mathrm{v}_n \qquad i.e. \qquad \sum_{i=1}^{N} O_{j,i} v_{i,n} = \lambda_n v_{j,n} \tag{4.1.24}$$

$$\mathrm{v}_n^T \cdot \mathrm{v}_{n'} = \delta_{nn'} \qquad i.e. \qquad \sum_{i=1}^{N} v_{i,n} v_{i,n'} = \delta_{nn'} \tag{4.1.25}$$

The important result is that we can construct the basis set $\{\Phi_n\}$ making linear combinations of the Ψ_n with coefficients given by the components of the eigenvectors of O, whereas the eigenvalues are related to the normalization factor:

$$\Phi_n(\mathrm{k}, \mathrm{r}) = \lambda_n^{-\frac{1}{2}}(\mathrm{k}) \cdot \sum_{j=1}^{N} v_{j,n}(\mathrm{k}) \Psi_j(\mathrm{k}, \mathrm{r}) \tag{4.1.26}$$

Using eqs. 4.1.24 and 4.1.25 one can easily proove the orthonormalization:

$$< \Phi_n(\mathrm{k}, \mathrm{r}) | \Phi_{n'}(\mathrm{k}, \mathrm{r}) >_\Omega = \delta_{nn'} \tag{4.1.27}$$

The overlap matrix

The electronic configurations of Cl^- and of Na^+ are:

$$\begin{array}{lccccc} Cl^- : & 1s^2 & 2s^2 & 2p^6 & 3s^2 & 3p^6 \\ Na^+ : & 1s^2 & 2s^2 & 2p^6 & & \end{array}$$

In principle we should orthogonalize the Bloch sums coming from all the orbitals of both Cl^- and Na^+ , and thus consider a complete overlap matrix with rank $N = 14$. Since the lowest energy ionic orbitals of Na^+ $(1s, 2s)$ and those of Cl^- $(1s, 2s, 2p)$ are very localized, a good approximation is to consider the corresponding Bloch sums already normalized and orthogonal each other and with respect to all those arising from the remaining ionic orbitals. Our effort is thus limited to the orthonormalization of the wave functions constructed from the valence band of Cl^- and from the highest core states of Na^+ only . We thus consider the following Bloch sums:

$$\Psi_{Cl^-,3s}, \quad \Psi_{Cl^-,3p_x}, \quad \Psi_{Cl^-,3p_y}, \quad \Psi_{Cl^-,3p_z}$$

$$\Psi_{Na^+,2s}, \quad \Psi_{Na^+,2p_x}, \quad \Psi_{Na^+,2p_y}, \quad \Psi_{Na^+,2p_z}$$

and the corresponding 8×8 overlap matrix. Within the accuracy of our calculations we can also neglect the overlaps between $2s$ and $2p$ orbitals of Na^+ and consider the corresponding Bloch sums as already normalized and orthogonal each other. We work thus with an overlap matrix with these structure:

	$Cl^-_{val.}$	$Na^+_{\substack{ext. \\ core}}$
$Cl^-_{val.}$	A	B
$Na^+_{\substack{ext. \\ core}}$	$B^\dagger$	1

The non-normalized Bloch sums were defined through the expression:

$$\Psi_{\mu\nu}(\mathbf{k},\mathbf{r}) = \sum_{\mathbf{R}_n} e^{i\mathbf{k}\cdot\mathbf{R}_n} \varphi_{\mu\nu}(\mathbf{r} - \mathbf{d}_\mu - \mathbf{R}_n) \qquad (4.1.28)$$

It is convenient to introduce a suitable phase factor and modify the definition of the Bloch sums as in the following:

$$\Psi_{\mu\nu}(\mathbf{k},\mathbf{r}) = i^{l_\nu} \sum_{\mathbf{R}_n} e^{i\mathbf{k}\cdot(\mathbf{d}_\mu+\mathbf{R}_n)} \varphi_{\mu\nu}(\mathbf{r}-\mathbf{d}_\mu-\mathbf{R}_n) \qquad (4.1.28a)$$

With these definitions the overlap matrix is real and symmetric, and the generic element $\mathbf{O}_{\mu\nu,\mu'\nu'}(\mathbf{k})$ is given by:

$$< \Psi_{\mu\nu}(\mathbf{k},\mathbf{r}) | \Psi_{\mu'\nu'}(\mathbf{k},\mathbf{r}) >_\Omega =$$

$$i^{l_{\nu'}-l_\nu} e^{i\mathbf{k}\cdot(\mathbf{d}_{\mu'}-\mathbf{d}_\mu)} \cdot \sum_{\mathbf{R}_n} e^{i\mathbf{k}\cdot\mathbf{R}_n} \int_{space} \varphi_{\mu\nu}(\mathbf{r}-\mathbf{d}_\mu)\varphi_{\mu'\nu'}(\mathbf{r}-\mathbf{d}_{\mu'}-\mathbf{R}_n)d\mathbf{r} \qquad (4.1.29)$$

It is convenient to rearrange the terms and to change the integration variable, so that the overlap integral can be written in the form

$$\mathbf{O}_{\mu\nu,\mu'\nu'}(\mathbf{k}) = i^{l_{\nu'}-l_\nu} \cdot \sum_{\tau_n} e^{i\mathbf{k}\cdot\tau_n} \cdot \int_{space} \varphi_{\mu\nu}(\mathbf{r})\varphi_{\mu'\nu'}(\mathbf{r}-\tau_n)d\mathbf{r} \qquad (4.1.30)$$

where now the sum $\sum_{\tau_n}$ runs over the vectors of one of the two FCC sublattices of the crystal (one centered at the origin and coinciding with the FCC Bravais lattice, the other shifted by $\frac{a}{2}(110)$), depending on the fact that $\mu = \mu'$ or $\mu \neq \mu'$. The vectors τ_n can be grouped into shells of symmetry-equivalent sites. In Fig. 14 the ionic sites corresponding to different sublattices and different shells are indicated with different symbols. Grouping the sum $\sum_{\tau_n}$ into sums over shells and using the expressions of the overlap integrals in terms of the independent quantities $(ss\sigma)$, $(sp\sigma)$, $(pp\sigma)$, and $(pp\pi)$, one can write explicit expressions for the elements of $\mathbf{O}(\mathbf{k})$. We list the formulas for the four different kinds of elements of $\mathbf{O}(\mathbf{k})$:

$$< \Psi_s | \Psi_s > = \sum_{shells} \left[\sum_{\tau_i} e^{i\mathbf{k}\cdot\tau_i} \right] (ss\sigma)_n \qquad (4.1.31)$$

$$< \Psi_s | \Psi_{p_x} > = \sum_{shells} \left[\sum_{\tau_i} i l_{x_i} e^{i\mathbf{k}\cdot\tau_i} \right] (sp\sigma)_n \qquad (4.1.32)$$

$$< \Psi_{p_x} | \Psi_{p_x} > = \sum_{shells} \left\{ \left[\sum_{\tau_i} l_{x_i}^2 e^{i\mathbf{k}\cdot\tau_i} \right] (pp\sigma)_n + \left[\sum_{\tau_i} (1-l_{x_i}^2) e^{i\mathbf{k}\cdot\tau_i} \right] (pp\pi)_n \right\} \qquad (4.1.33)$$

$$< \Psi_{p_x} | \Psi_{p_y} > = \sum_{shells} \left\{ \left[\sum_{\tau_i} l_{x_i} l_{y_i} e^{i\mathbf{k}\cdot\tau_i} \right] (pp\sigma)_n - \left[\sum_{\tau_i} l_{x_i} l_{y_i} e^{i\mathbf{k}\cdot\tau_i} \right] (pp\pi)_n \right\} \qquad (4.1.34)$$

The internal sum is done within a given shell, and the external runs over different shells. The quantities in square brackets are structure factors that can be computed once forever for the two FCC sublattices. For the cubic symmetry of the crystal in the sums $\sum_{\tau_i}$ at each vector τ_i corresponds also the vector $-\tau_i$, so that the structure factors here considered are real quantities; we can understand now the choice of the phase factor of the Bloch sums to have a real symmetric overlap matrix.

Overlap matrix at high symmetry points

We have implemented very general programs to construct orthonormalized Bloch functions at each k vector of the Brillouin zone, but as we will see later only few points are needed to evaluate approximately the charge density and in particular some high symmetry points can be used. We report in Tables 7-9 the overlap matrices and its eigenvectors in the points

$$\Gamma = \frac{2\pi}{a}(0,0,0), \quad X = \frac{2\pi}{a}(1,0,0), \quad L = \frac{2\pi}{a}(\frac{1}{2},\frac{1}{2},\frac{1}{2})$$

These and other high symmetry points of the Brillouin zone for the FCC structure are represented in Fig. 21.

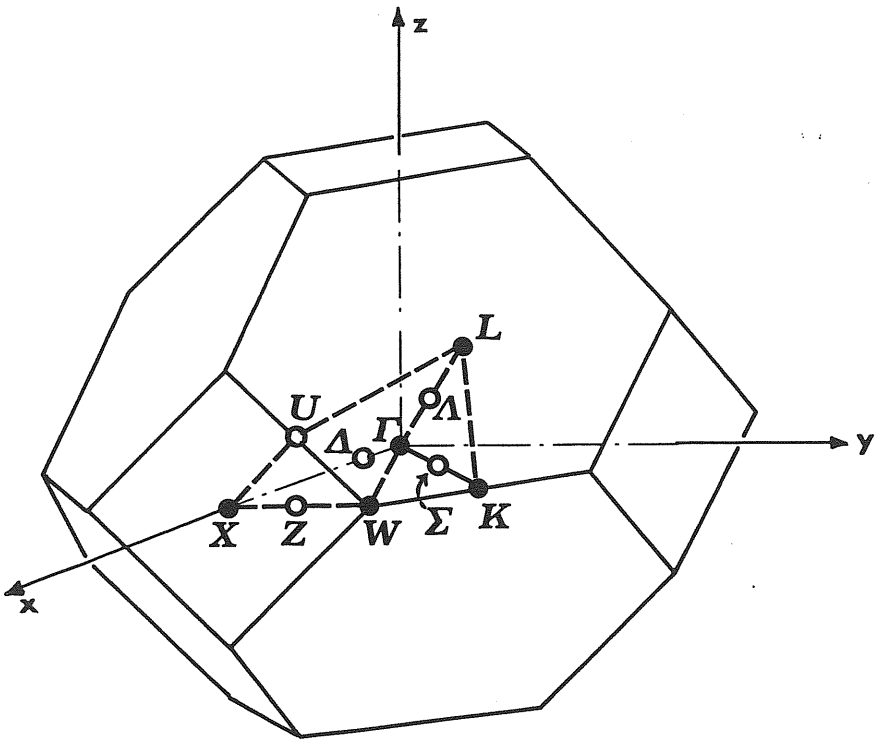

Fig.21: Brillouin zone for the FCC structure. High symmetry points are indicated.

Γ	$\Psi_{Cl^-,3s}$	$\Psi_{Cl^-,3p_x}$	$\Psi_{Cl^-,3p_y}$	$\Psi_{Cl^-,3p_z}$	$\Psi_{Na^+,2s}$	$\Psi_{Na^+,2p_x}$	$\Psi_{Na^+,2p_y}$	$\Psi_{Na^+,2p_z}$
$\Psi_{Cl^-,3s}$	1.059	0.000	0.000	0.000	−0.050	0.000	0.000	0.000
$\Psi_{Cl^-,3p_x}$	0.000	0.810	0.000	0.000	0.000	−0.042	0.000	0.000
$\Psi_{Cl^-,3p_y}$	0.000	0.000	0.810	0.000	0.000	0.000	−0.042	0.000
$\Psi_{Cl^-,3p_z}$	0.000	0.000	0.000	0.810	0.000	0.000	0.000	−0.042
$\Psi_{Na^+,2s}$	−0.050	0.000	0.000	0.000	1.000	0.000	0.000	0.000
$\Psi_{Na^+,2p_x}$	0.000	−0.042	0.000	0.000	0.000	1.000	0.000	0.000
$\Psi_{Na^+,2p_y}$	0.000	0.000	−0.042	0.000	0.000	0.000	1.000	0.000
$\Psi_{Na^+,2p_z}$	0.000	0.000	0.000	−0.042	0.000	0.000	0.000	1.000

0.801	0.801	0.801	0.972	1.009	1.009	1.009	1.087

1.003	0.000	0.000	0.000	0.000	0.025	0.025	0.025
0.000	1.041	−0.148	−0.148	−0.068	0.000	0.000	0.000
0.000	−0.148	1.041	−0.148	−0.068	0.000	0.000	0.000
0.000	−0.148	−0.148	1.041	−0.068	0.000	0.000	0.000
0.000	−0.068	−0.068	−0.068	1.018	0.000	0.000	0.000
0.025	0.000	0.000	0.000	0.000	1.001	0.001	0.001
0.025	0.000	0.000	0.000	0.000	0.001	1.001	0.001
0.025	0.000	0.000	0.000	0.000	0.001	0.001	1.001

Tab.7: Overlap matrix between Bloch sums constructed from s and p orbitals of Na^+ and Cl^- at Γ; eigenvalues and inverse matrix are also reported.

X	$\Psi_{Cl^-,3s}$	$\Psi_{Cl^-,3p_x}$	$\Psi_{Cl^-,3p_y}$	$\Psi_{Cl^-,3p_z}$	$\Psi_{Na^+,2s}$	$\Psi_{Na^+,2p_x}$	$\Psi_{Na^+,2p_y}$	$\Psi_{Na^+,2p_z}$
$\Psi_{Cl^-,3s}$	0.982	0.000	0.000	0.000	−0.016	0.000	0.000	0.000
$\Psi_{Cl^-,3p_x}$	0.000	1.258	0.000	0.000	0.000	0.115	0.000	0.000
$\Psi_{Cl^-,3p_y}$	0.000	0.000	0.923	0.000	0.000	0.000	−0.070	0.000
$\Psi_{Cl^-,3p_z}$	0.000	0.000	0.000	0.923	0.000	0.000	0.000	−0.070
$\Psi_{Na^+,2s}$	−0.016	0.000	0.000	0.000	1.000	0.000	0.000	0.000
$\Psi_{Na^+,2p_x}$	0.000	0.115	0.000	0.000	0.000	1.000	0.000	0.000
$\Psi_{Na^+,2p_y}$	0.000	0.000	−0.070	0.000	0.000	0.000	1.000	0.000
$\Psi_{Na^+,2p_z}$	0.000	0.000	0.000	−0.070	0.000	0.000	0.000	1.000

0.881	0.881	0.956	0.972	1.009	1.042	1.042	1.302

1.019	0.000	0.000	0.000	0.016	0.000	0.000	0.000
0.000	0.804	0.000	0.000	0.000	−0.093	0.000	0.000
0.000	0.000	1.089	0.000	0.000	0.000	0.076	0.000
0.000	0.000	0.000	1.089	0.000	0.000	0.000	0.076
0.016	0.000	0.000	0.000	1.000	0.000	0.000	0.000
0.000	−0.093	0.000	0.000	0.000	1.011	0.000	0.000
0.000	0.000	0.076	0.000	0.000	0.000	1.005	0.000
0.000	0.000	0.000	0.076	0.000	0.000	0.000	1.005

Tab.8: Overlap matrix between Bloch sums constructed from s and p orbitals of Na^+ and Cl^- at X; eigenvalues and inverse matrix are also reported.

L	$\Psi_{Cl^-,3s}$	$\Psi_{Cl^-,3p_x}$	$\Psi_{Cl^-,3p_y}$	$\Psi_{Cl^-,3p_z}$	$\Psi_{Na^+,2s}$	$\Psi_{Na^+,2p_x}$	$\Psi_{Na^+,2p_y}$	$\Psi_{Na^+,2p_z}$
$\Psi_{Cl^-,3s}$	0.999	0.000	0.000	0.000	0.000	−0.025	−0.025	−0.025
$\Psi_{Cl^-,3p_x}$	0.000	1.016	0.175	0.175	0.091	0.000	0.000	0.000
$\Psi_{Cl^-,3p_y}$	0.000	0.175	1.016	0.175	0.091	0.000	0.000	0.000
$\Psi_{Cl^-,3p_z}$	0.000	0.175	0.175	1.016	0.091	0.000	0.000	0.000
$\Psi_{Na^+,2s}$	0.000	0.091	0.091	0.091	1.000	0.000	0.000	0.000
$\Psi_{Na^+,2p_x}$	−0.025	0.000	0.000	0.000	0.000	1.000	0.000	0.000
$\Psi_{Na^+,2p_y}$	−0.025	0.000	0.000	0.000	0.000	0.000	1.000	0.000
$\Psi_{Na^+,2p_z}$	−0.025	0.000	0.000	0.000	0.000	0.000	0.000	1.000

0.841	0.841	0.942	0.956	1.000	1.000	1.043	1.425

0.947	0.000	0.000	0.000	0.047	0.000	0.000	0.000
0.000	1.237	0.000	0.000	0.000	0.052	0.000	0.000
0.000	0.000	1.237	0.000	0.000	0.000	0.052	0.000
0.000	0.000	0.000	1.237	0.000	0.000	0.000	0.052
0.047	0.000	0.000	0.000	1.002	0.000	0.000	0.000
0.000	0.052	0.000	0.000	0.000	1.002	0.000	0.000
0.000	0.000	0.052	0.000	0.000	0.000	1.002	0.000
0.000	0.000	0.000	0.052	0.000	0.000	0.000	1.002

Tab.9: Overlap matrix between Bloch sums constructed from s and p orbitals of Na^+ and Cl^- at L; eigenvalues and inverse matrix are also reported.

Although we have implemented a very general procedure to construct the basis set $\{\Phi_n\}$ it is instructive to derive the same result from symmetry properties where it is possible. Let us consider the point groups corresponding to the high symmetry points $\Gamma, \mathbf{X}, \mathbf{L}$. For each group we can list the irreducible representations[51] and the basis set for each of them, as reported in Tab. 10; commas separate the different rows within a certain representation.

group	*representation*	*bases*
$\Gamma = \frac{2\pi}{a}(0,0,0)$	Γ_1^+	1
	Γ_4^-	$x,\ y,\ z$
$\mathbf{X} = \frac{2\pi}{a}(1,0,0)$	X_1	1
	X_4	x
	X_5	$y,\ z$
$\mathbf{L} = \frac{2\pi}{a}(\frac{1}{2},\frac{1}{2},\frac{1}{2})$	L_1	1
	L_2	$x+y+z$
	L_3	$y-z,\ 2x-y-z$

Tab.10: Some irreducible representations for the groups of Γ, X, L. Only those representations that can be described by s–like or p–like basis function are listed.

A correspondence can be established between basis functions and crystal wave functions at these symmetry points. The symbols used for the basis of the irreducible representations are 1 for s-like functions, x, y, z for p_x, p_y, p_z-like functions. Basis functions belonging to different representations or to different rows of a certain representation do not combine wich each other, in particular they have zero overlap. The coefficients of the linear combinations of x, y, z-like functions in the basis predicts how these functions overlap with each other.

All these considerations are really shown by the overlap matrices: for instance at Γ and $\mathbf{X}$ only $< s \mid s >$ and $< p_\alpha \mid p_\alpha >$ elements are non zero; at $\mathbf{L}$ we can recognize that Ψ_{p_x}, Ψ_{p_y} and Ψ_{p_z} Bloch sums of Cl^- have the same overlap one to each other, and the same occures for the s state of one ion

with respect to the p states of the other. Within the subspace corresponding to one kind of ion one could choose as basis set at high symmetry points the linear combinations of the Bloch sums as indicated for the basis of the various representations. At Γ and $\mathbf{X}$ the tight-binding Bloch sums themselves can be considered as the basis set (only the normalization is needed) whereas at $\mathbf{L}$ one could choose for instance :

$$\Phi_1 = \alpha\ \Psi_s \tag{4.1.35}$$

$$\Phi_2 = \beta\ (\Psi_{p_x} + \Psi_{p_y} + \Psi_{p_z}) \tag{4.1.36}$$

$$\Phi_3 = \gamma\ (\Psi_{p_y} - \Psi_{p_z}) \tag{4.1.37}$$

$$\Phi_4 = \delta\ (2\Psi_{p_x} - \Psi_{p_y} - \Psi_{p_z}) \tag{4.1.38}$$

where $\alpha, \beta, \gamma, \delta$ are the normalization coefficients:

$$\alpha = \quad A_s(L) \tag{4.1.39}$$

$$\beta = \frac{1}{\sqrt{3}} A_p(L) \tag{4.1.40}$$

$$\gamma = \frac{1}{\sqrt{2}} A_p(L) \tag{4.1.41}$$

$$\delta = \frac{1}{\sqrt{6}} A_p(L) \tag{4.1.42}$$

with

$$A_s(L) = 1.0004\ , \qquad A_p(L) = 0.9919 \tag{4.1.43}$$

Now the problem that cannot be solved just using symmetry is imposing the orthogonality between Bloch sums arising from orbitals of the same kind but of different ions . Looking at the overlap matrices, we recognize that this is again very easy at Γ and $\mathbf{X}$ where the non-neglibible overlaps are only between functions of the same type (s with s, p_x with p_x, etc.) also for ions of different kinds. In this case it would be sufficient to consider (remembering that $A_{Na^+}(\mathbf{k})$ is practically 1) :

$$\frac{A_{Cl^-,3s}(\mathbf{k})\Psi_{Cl^-,3s} \pm \Psi_{Na^+,2s}}{\sqrt{2}} \tag{4.1.44}$$

and similar combinations also for the other states. One should also carry on an analogous reasoning for $\mathbf{L}$, but at this point the use of symmetry is no longer convenient with respect to the numerical effort required to diagonalize a 8×8 matrix.

c) Charge density from the orthonormalized Bloch functions

Exact crystal states and tight-binding Bloch functions

Within the one-electron approximation and the band approximation the crystal states can be chosen simultaneously to be eigenfunctions of the one-electron hamiltonian H_e and of all the translation operators; thus they are Bloch-type functions characterized by a particular vector k and satisfying the Schrœdinger equation:

$$\left[-\frac{\hbar^2\nabla^2}{2m}+V(\mathrm{r})\right]\Psi_n^{Schr.}(\mathrm{k},\mathrm{r})=E_n(\mathrm{k})\Psi_n^{Schr.}(\mathrm{k},\mathrm{r}) \qquad (4.1.45)$$

where V(r) is the periodic crystal potential. Some of the crystal states are occupied and some are free, according to Fermi statistics. If they are normalized we can correctly write the crystal charge density as

$$\rho(\mathrm{r})=2\frac{\Omega}{(2\pi)^3}\sum_{\mathrm{k}}\sum_{n_{occ.}}|\Psi_n^{Schr.}(\mathrm{k},\mathrm{r})|^2 \qquad (4.1.46)$$

We could expand the crystal states $\Psi_n^{Schr.}$ on a complete set of Bloch-type functions known, in particular of Bloch sums Ψ_m constructed as linear combinations of atomic orbitals, as suggested in the tight-binding method :

$$\Psi_n^{Schr.}(\mathrm{k},\mathrm{r})=\sum_m C_{mn}(\mathrm{k})\Psi_m(\mathrm{k},\mathrm{r}) \qquad (4.1.47)$$

The coefficients of the expansion must then be found by requiring that the crystal states satisfy the appropriate Schrœdinger equation.

The procedure is particularly convenient when only few terms in the expansion are important. This is the case of the inner or "core" crystal states: atomic orbitals of low energy are very localized near the nucleus and are expected to change very little when ions (or atoms) are joined together to form the crystal. To each inner atomic orbital correspond a very narrow energy band $E_n(\mathrm{k})$[56] and crystal eigenfunctions which are nearly equal to linear combinations of degenerate free-ion functions. This is the reason why we can ignore the mixing of Bloch sums derived from core ionic orbitals with the others.

Moreover in the alkali halides there is a large gap of about $10eV$ between the valence and the conduction band, so that one can also ignore the mixing between Bloch sums constructed from the valence atomic states and those arising from higher energy atomic states. We can thus consider that the set of the Bloch sums $\{\Psi_n\}$ constructed from the occupied atomic orbitals spans the same Hilbert subspace corresponding to the occupied crystal states $\{\Psi_{n_{occ.}}^{Schr.}\}$.

Since the quantity $(\Psi_1^{Schr.}, ..., \Psi_{N_{occ.}}^{Schr.})$ can be seen as a vector in this abstract Hilbert subspace and the charge density as its "length", one can show that it is invariant for a unitary transformation (rotation) of the basis set $\{\Psi_n^{Schr.}\}$. As far as the charge density is concerned, we do not worry about finding the exact solution of the Schrœdinger equation but we just construct in this subspace a basis set of orthonormal Bloch functions $\{\Phi_n\}$ from the occupied ionic orbitals; the charge density can be calculated as:

$$\rho(\mathrm{r}) = 2\frac{\Omega}{(2\pi)^3}\sum_{\mathrm{k}}\sum_{n_{occ.}} |\Phi_n(\mathrm{k},\mathrm{r})|^2 \tag{4.1.48}$$

The orthonormalized Bloch functions can be constructed from the Bloch sums with the method outlined in section b) :

$$\Phi_n(\mathrm{k},\mathrm{r}) = \lambda_n^{-\frac{1}{2}}(\mathrm{k}) \cdot \sum_{j=1}^{N} v_{j,n}(\mathrm{k})\Psi_j(\mathrm{k},\mathrm{r}) \tag{4.1.49}$$

Putting this expression in the formula for the crystal charge density we find:

$$\rho(\mathrm{r}) = 2\frac{\Omega}{(2\pi)^3}\sum_{\mathrm{k}}\sum_{n_{occ.}}\sum_{j_{occ.}}\sum_{j'_{occ.}} \lambda_n^{-1}(\mathrm{k})v_{j,n}(\mathrm{k})v_{j',n}(\mathrm{k})\Psi_j^*(\mathrm{k},\mathrm{r})\Psi_{j'}(\mathrm{k},\mathrm{r}) \tag{4.1.50}$$

One can show that:

$$\sum_{n_{occ.}} \lambda_n^{-1}(\mathrm{k})v_{j,n}(\mathrm{k})v_{j',n}(\mathrm{k}) = \left(O^{-1}(\mathrm{k})\right)_{jj'} \tag{4.1.51}$$

where $O(\mathrm{k})$ is the $n_{occ.} \times n_{occ.}$ overlap matrix between the Bloch sums involved in the formula. Using this relationship we can write finally the following expression relating the crystal charge density to the Bloch sums:

$$\rho(\mathrm{r}) = 2\frac{\Omega}{(2\pi)^3}\sum_{\mathrm{k}}\sum_{n_{occ.}}\sum_{n'_{occ.}} \Psi_n^*(\mathrm{k},\mathrm{r})\left(O^{-1}(\mathrm{k})\right)_{nn'}\Psi_{n'}(\mathrm{k},\mathrm{r}) \tag{4.1.52}$$

Symmetry of the crystal charge density

From the previous equation we can consider the crystal charge density as the integral over the first Brillouin zone of a periodic charge density, say $\rho(\mathrm{k},\mathrm{r})$, wich is a function of the vector k:

$$\rho(\mathrm{k},\mathrm{r}) = 2\sum_{n_{occ.}}\sum_{n'_{occ.}} \Psi_n^*(\mathrm{k},\mathrm{r})\left(O^{-1}(\mathrm{k})\right)_{nn'}\Psi_{n'}(\mathrm{k},\mathrm{r}) \tag{4.1.53}$$

It has the periodicity of the crystal, but not the same symmetry with respect to the operations of the cubic punctual group.

From this charge density $\rho(\mathrm{k},\mathrm{r})$ we can construct a charge density – indicated with $\rho_{\mathrm{k}}(\mathrm{r})$ – wich has the complete symmetry of the lattice:

$$\rho_{\mathrm{k}}(\mathrm{r}) = \frac{1}{n_T}\sum_i \rho(T_i\mathrm{k},\mathrm{r}) \tag{4.1.54}$$

where the T_i's range over all the operations of the cubic punctual group (the group of the lattice) which originate different k vectors within the star of symmetry–equivalent vectors, and n_T is the number of such operations. This symmetrized charge density $\rho_{\mathrm{k}}(\mathrm{r})$ is no longer a function of a particular vector k , but it is determined by any representative vector of the star. The total number of operations in the cubic punctual group is 48, but for instance the star of X contains only 6 different vectors, and that of L contains 8. A further reduction in the number of essential rotations occures since it is easily shown that

$$\rho(-\mathrm{k},\mathrm{r}) = \rho(\mathrm{k},\mathrm{r}) \tag{4.1.55}$$

Moreover one can proove that:

$$\rho(T\mathrm{k},\mathrm{r}) = \rho(\mathrm{k},T^{-1}\mathrm{r}) \tag{4.1.56}$$

This result avoidsthe computation of different overlap matrices and the construction of different Bloch sums (one for each vector Tk in the star). The conclusion is that the symmetrized charge density in a given k is:

$$\rho_{\mathrm{k}}(\mathrm{r}) = \frac{1}{n_T}\sum_i \rho(\mathrm{k},T_i\mathrm{r}) \tag{4.1.57}$$

Brillouin zone integration

To calculate the crystal charge density we must integrate over the Brillouin zone the k–dependent charge density $\rho_{\mathrm{k}}(\mathrm{r})$. In principle we should calculate $\rho_{\mathrm{k}}(\mathrm{r})$ (i.e. the Bloch sums and the overlap matrix) at each point in the Brillouin zone. In practice the knowledge of $\rho_{\mathrm{k}}(\mathrm{r})$ over a set of points k is required if one uses standard techniques[57)–60)] to calculate the average $< f >$ over the Brillouin zone of a periodic function of wave vector:

$$< f >= \frac{\Omega}{(2\pi)^3}\int_{B.z.} f(\mathrm{k})d\mathrm{k} \tag{4.1.58}$$

There are basically two techniques: a method due to Kleinman and Phillips[57] based on a procedure for successive approximations, and a mean value representative points technique introduced by Baldereschi[58] and generalized by Chadi and Cohen[59].

In the Kleinman– Phillips method[57] the reciprocal space is divided into equal volumes similar to the first Brillouin zone. The first division uses the Brillouin zone about each reciprocal lattice point $\mathbf{G}_\nu$. Successive approximations refine this subdivisions: at the second step one introduces the new "sub–reciprocal –lattice points" $\frac{\mathbf{G}_\nu}{2}$; about each point of the new sublattice one draws a subzone, similar to the first Brillouin zone but with a volume reduced by a factor 2^3. For the FCC structure of $NaCl$, for instance, the first approximation uses the Γ point of the Brillouin zone; the second one uses 8 points: Γ, X (3 equivalent points), L (4 equivalent points); the third one 64 points that can be grouped into Γ, X, L, $\Lambda, \Delta, \mathbf{C}_1$ where $\mathbf{C}_1 = \frac{2\pi}{a}(\frac{3}{4}, \frac{1}{4}, \frac{1}{4})$.

The other technique [58)–59)] to perform the Brillouin zone integration uses another set of representative points. A mean-value point is defined as the point such that the value which $f(\mathbf{k})$ assumes at this point approximates for the best its average over the Brillouin zone. If $f(\mathbf{k})$ has the complete symmetry of the crystal point group we can decompose it into symmetrized linear combinations of plane waves of symmetry Γ_1, as follows:

$$f(\mathbf{k}) = f_0 + \sum_{m=1}^{\infty} f_m G_m(\mathbf{k}) \tag{4.1.59}$$

where

$$G_m(\mathbf{k}) = \sum_{\mathbf{R} \in star} e^{i\mathbf{k}\cdot\mathbf{R}} \tag{4.1.60}$$

and the star is that of the equivalent lattice vectors related to each other through the operations of the cubic punctual group. Since

$$\frac{\Omega}{(2\pi)^3} \int_{B.z.} G_m(\mathbf{k}) d\mathbf{k} \equiv 0 \qquad for\ m = 1, 2, \ldots \infty \tag{4.1.61}$$

we have that:

$$< f >= \frac{\Omega}{(2\pi)^3} \int_{B.z.} f(\mathbf{k}) d\mathbf{k} = f_0 \tag{4.1.62}$$

If it would exist a point $\mathbf{k}^*$ such that

$$G_m(\mathbf{k}^*) = 0 \qquad for\ m = 1, 2, \ldots \infty \tag{4.1.63}$$

we would immediately have

$$f_0 = f(\mathbf{k}^*) \tag{4.1.64}$$

Such a point does not exist, but we can find a point that satisfies eq. (4.1.63) for $m = 1, 2, \ldots$ up to a certain finite N. Baldereschi[58] has found for the FCC structure $\mathrm{k}^* = \frac{2\pi}{a}(0.6223, 0.2953, 0)$ with $N = 2$. To satisfy the eq. (4.1.63) for higher N a generalization is necessary. Many points must be used, say a certain set $(\mathrm{k}_1^*, \mathrm{k}_2^*, \ldots \mathrm{k}_n^*)$; the conditions:

$$\sum_{i=1}^{n} \alpha_i G_m(\mathrm{k}^*) = 0 \qquad for\ m = 1, 2, \ldots N \tag{4.1.65}$$

must be imposed, where α_i are the weighting factors corresponding to the special poins of the set and such that:

$$\sum_{i=1}^{n} \alpha_i = 1 \tag{4.1.66}$$

Within this scheme a good approximation to the average $< f >$ is given by

$$< f > \approx \sum_{i=1}^{n} \alpha_i f_m(\mathrm{k}^*) \tag{4.1.67}$$

The first approximation is thus the single mean-value point; the second step requires the use of the two mean-value points of Chadi and Cohen[59] which are for the FCC structure $\mathrm{C_1} = \frac{2\pi}{a}(\frac{3}{4}, \frac{1}{4}, \frac{1}{4})$ and $\mathrm{C_2} = \frac{2\pi}{a}(\frac{1}{4}, \frac{1}{4}, \frac{1}{4})$ with weighting factors $\alpha_1 = \frac{3}{4}, \alpha_2 = \frac{1}{4}$. A further step requires 10 points, whose coordinates and weights are:

$$\begin{array}{llll}
\mathrm{k}_1 = (\frac{7}{8}, \frac{3}{8}, \frac{1}{8}), & \alpha_1 = \frac{3}{16}; & \mathrm{k}_2 = (\frac{7}{8}, \frac{1}{8}, \frac{1}{8}), & \alpha_2 = \frac{3}{32}; \\
\mathrm{k}_3 = (\frac{5}{8}, \frac{5}{8}, \frac{1}{8}), & \alpha_3 = \frac{3}{32}; & \mathrm{k}_4 = (\frac{5}{8}, \frac{3}{8}, \frac{3}{8}), & \alpha_4 = \frac{3}{32}; \\
\mathrm{k}_5 = (\frac{5}{8}, \frac{3}{8}, \frac{1}{8}), & \alpha_5 = \frac{3}{16}; & \mathrm{k}_6 = (\frac{5}{8}, \frac{1}{8}, \frac{1}{8}), & \alpha_6 = \frac{3}{32}; \\
\mathrm{k}_7 = (\frac{3}{8}, \frac{3}{8}, \frac{3}{8}), & \alpha_7 = \frac{1}{32}; & \mathrm{k}_8 = (\frac{3}{8}, \frac{3}{8}, \frac{1}{8}), & \alpha_8 = \frac{3}{32}; \\
\mathrm{k}_9 = (\frac{3}{8}, \frac{1}{8}, \frac{1}{8}), & \alpha_9 = \frac{3}{32}; & \mathrm{k}_{10} = (\frac{1}{8}, \frac{1}{8}, \frac{1}{8}), & \alpha_{10} = \frac{1}{32}.
\end{array}$$

In conclusion the crystal charge density $\rho(\mathrm{r})$ can be calculated with a good approximation using the weighted average of the symmetrized charge density $\rho_{\mathrm{k}}(\mathrm{r})$ at some representative points of the Brillouin zone:

$$\rho(\mathrm{r}) \approx \sum_{i=1}^{n} \alpha_i \rho_{\mathrm{k}_i^*}(\mathrm{r}). \tag{4.1.68}$$

d) Valence electron charge density in alkali halides: application to NaCl

Core and valence charge

If we consider in the preceding formulas all the occupied crystal states, the resulting $\rho(\mathbf{r})$ is the total crystal charge. It is convenient to separate it into a "core" and a "valence" part. Since the overlap between Bloch sums arising from core atomic states and from valence atomic states cannot be completely neglected , the subspaces spanned by these two sets of Bloch sums are not orthogonal, and they do not correspond exactly to the subspaces of core and valence true crystal states.

The core crystal charge should be calculated properly from the true core crystal states, whereas we assume that the contributions to the core crystal charge density come only from all the core states of the anion and of the cation. Since the corresponding Bloch sums are already normalized and orthogonal each other, it is equivalent to calculate the core crystal charge by summing up directly the ionic core charges:

$$\rho_{core}(\mathbf{r}) = \sum_{\mathbf{R}_n} \left[\rho_{core,Na^+}(\mathbf{r} - \mathbf{d}_{Na^+} - \mathbf{R}_n) + \rho_{core,Cl^-}(\mathbf{r} - \mathbf{d}_{Cl^-} - \mathbf{R}_n)\right] \tag{4.1.69}$$

This part of the crystal charge is thus unchanged with respect to the free–ion approximation.

We consider the mixing of the Bloch sums arising from core atomic states and from valence atomic states in the definition of the valence crystal charge. We orthogonalize the Bloch sums constructed from the valence orbitals of the anion with those constructed from the orbitals of the outer shell of the cation ($2s$, $2p$ for Na^+): the charge density calculated from this set of orthonormalized Bloch functions contains also a part of the core crystal charge which must be subtracted, otherwise it would be calculated twice in the evaluation of the total crystal charge. The valence crystal charge density of $NaCl$, for instance, is given by:

$$\rho_{val.}(\mathbf{r}) = 2\frac{\Omega}{(2\pi)^3} \sum_{\mathbf{k}} \sum_{n=1}^{N} |\Phi_n(\mathbf{k},\mathbf{r})|^2 - \sum_{\mathbf{R}_n} \rho_{\substack{Na^+ \\ external\ core}}(\mathbf{r} - \mathbf{d}_{Na^+} - \mathbf{R}_n) \tag{4.1.70}$$

or

$$\rho_{val.}(\mathrm{r}) = 2\frac{\Omega}{(2\pi)^3}\sum_{\mathrm{k}}\sum_{n,n'=1}^{N}\Psi_n^*(\mathrm{k},\mathrm{r})\left(O^{1-}(\mathrm{k})\right)_{nn'}\Psi_{n'}(\mathrm{k},\mathrm{r}) -$$

$$-\sum_{\mathrm{R}_n}\rho_{\substack{Na+\\ external\ core}}(\mathrm{r}-\mathrm{d}_{Na+}-\mathrm{R}_n) \qquad (4.1.71)$$

where the indices n and n' run over the Bloch sums constructed from the valence band of Cl^- and from $2s$ and $2p$ orbitals of Na^+.

We are interested expecially in the valence crystal charge density which contains the effects of the overlaps between ions.

Techniques and accuracies

We have calculated the valence part of the electronic crystal charge density using both the techniques for the Brillouin zone integration presented before, each of them at the first two levels of approximation. Tab. 11 summarizes the various approximations to $\rho(\mathrm{r})$ used.

	Kleinman – Phillips method	*mean – value points method*
1^{st} *level*	$\rho_{\Gamma}(\mathrm{r})$	$\rho_{\mathrm{B}}(\mathrm{r})$
2^{nd} *level*	$\rho_{\Gamma\mathrm{XL}}(\mathrm{r}) = \frac{1}{8}\rho_{\Gamma}(\mathrm{r}) + \frac{3}{8}\rho_{\mathrm{X}}(\mathrm{r}) + \frac{1}{2}\rho_{\mathrm{L}}(\mathrm{r})$	$\rho_{\mathrm{CC}}(\mathrm{r}) = \frac{3}{4}\rho_{\mathrm{C_1}}(\mathrm{r}) + \frac{1}{4}\rho_{\mathrm{C_2}}(\mathrm{r})$

Tab.11: The first and the second level of approximation in the Kleinmann– Phillips method and in the mean–value points method for the Brillouin zone integration.

The Γ point is not a good representative point; a better approximation is obtained using the mean-value point or a weighted sum of the charge densities at Γ, X, and L; a further improvement is reached using the two mean-value points of Chadi and Cohen.

In the calculation of the overlap matrix elements we have included 10 shells of neighbouring ions in the case of Cl^-–Cl^- overlap and 6 shells in the case of Na^+–Cl^- to have an accuracy of 10^{-5}. We are thus sure that approximations introduced by truncating the infinite sums over the lattice at a given order do not cover the physical effect that we are investigating.

Deviations from the free-ion approximation

We have calculated the valence charge density by taking into account the orthogonalization of Cl^-–Cl^- only, and also of Cl^-–Cl^- and Na^+–Cl^- . The main result of this tight-binding approach to the correct charge density of the crystal is evident in both cases and at each step of approximation for the Brillouin zone integration: the correct electron charge density is more localized around the anion with respect to the free-ions approximation.

A part from the Γ point which cannot be considered a good approximation from a quantitative point of view, the effects are of the same order of magnitude at each step of approximation and in particular the results appear to be already in convergence using the two mean-value points of Chadi-Cohen; the results reported and discussed here refer to this case, exceptions being specified.

We reported in Fig. 22 and 23 the plots for the total and the valence charge densities (ρ_{tot} and ρ_{val}) in the planes [001] and [011], with the same scale used for the corresponding plots in the free-ion approximation ($\rho_{0,tot}$ and $\rho_{0,val}$) For a direct comparison we have also plotted in the same planes the difference $\Delta\rho = \rho - \rho_0$ (see Fig. 24); the curves of $\rho_{0,val}$ (solid line) and of ρ_{val} (dashed line) are shown along the directions (100), (110), (111) in Fig. 25.

In order to understand the physical origin of the shrinkage of the anion we performed our calculations both including and neglecting the anion– cation overlap. Taking into account just the anion-anion overlaps there is an increasing of the order of 2% for the electron charge density at a distance of about 1 a.u. from a Cl^- site, where it reaches its relative maximum value; it is compensated by a lack of electrons in the outer region, with an effect of the order of 10–20% at distances of 3–4 a.u. . Adding the anion-cation orthogonalization there is also a non-negligible valence electron density localized around the cation sites; however the main result does not change, and we can confirm that the localization of the charge density around the anion in the crystal is essentially determined by the anion-anion overlap as already suggested in Ref. 22. The anion-cation overlaps emphasize the shrinkage of the anion in particular along the direction of the chemical bonding where the valence charge density reaches a well defined minimum of 10^{-4} electrons/a.u.^{3} at about 4.2 a.u. from the anion site, with a reduction of the order of 85% with respect to the free-ion approximation.

Our choice of using just two mean-value points for the Brillouin zone approximation is justified if we look at these quantities: the results obtained with the single mean-value point and with two points differ of few % of the deviations from the free-ion approximation.

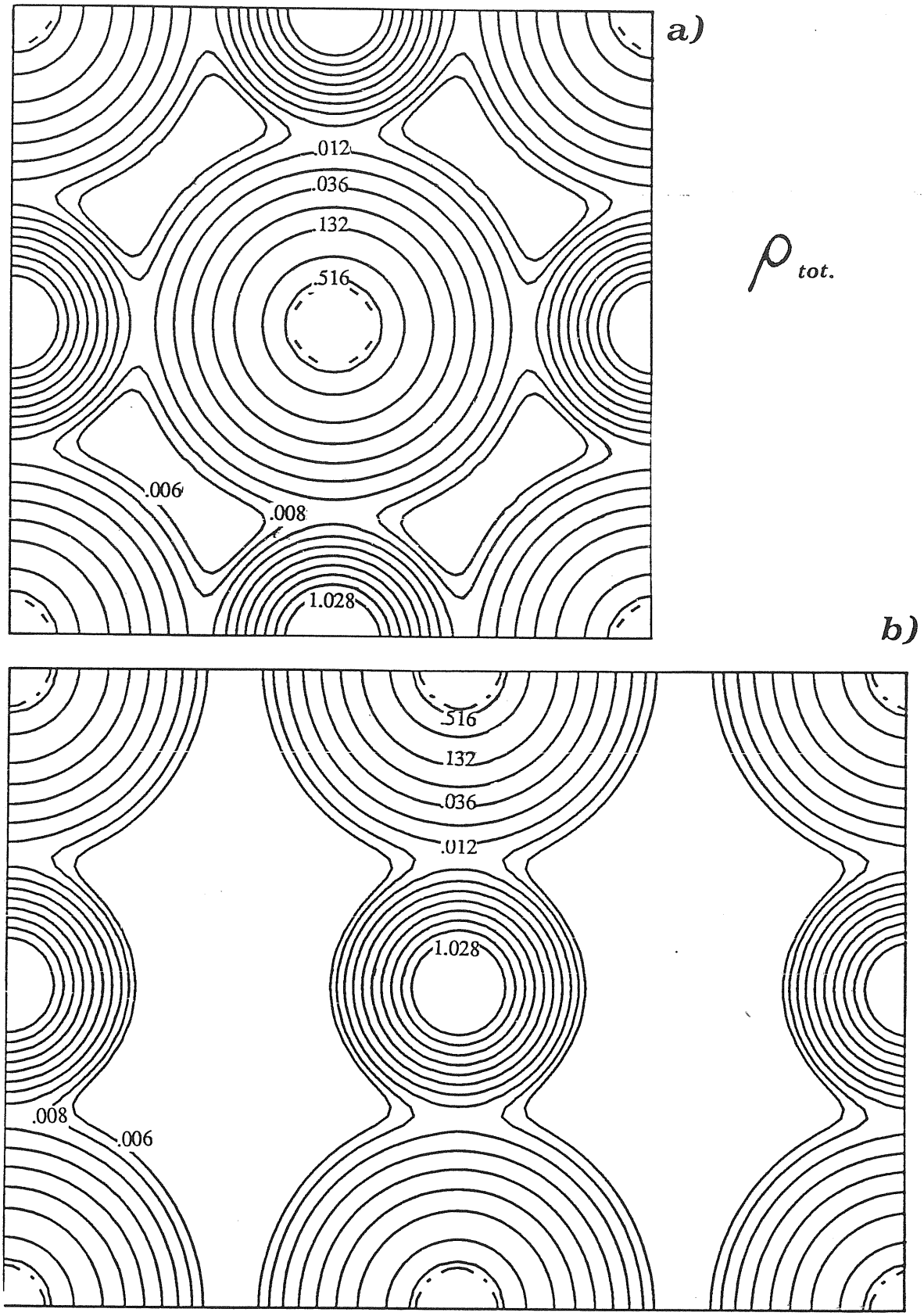

Fig.22: Total electron density in the (001) plane (a) and in the (011) plane (b) in the present approximation. Chlorine ions are at the corners. The lowest level corresponds to .006 electrons/a.u.^{3}, and the interval between the i-level and the $(i-1)$-level is $2^{(i-1)}$.002 electrons/a.u.^{3}.

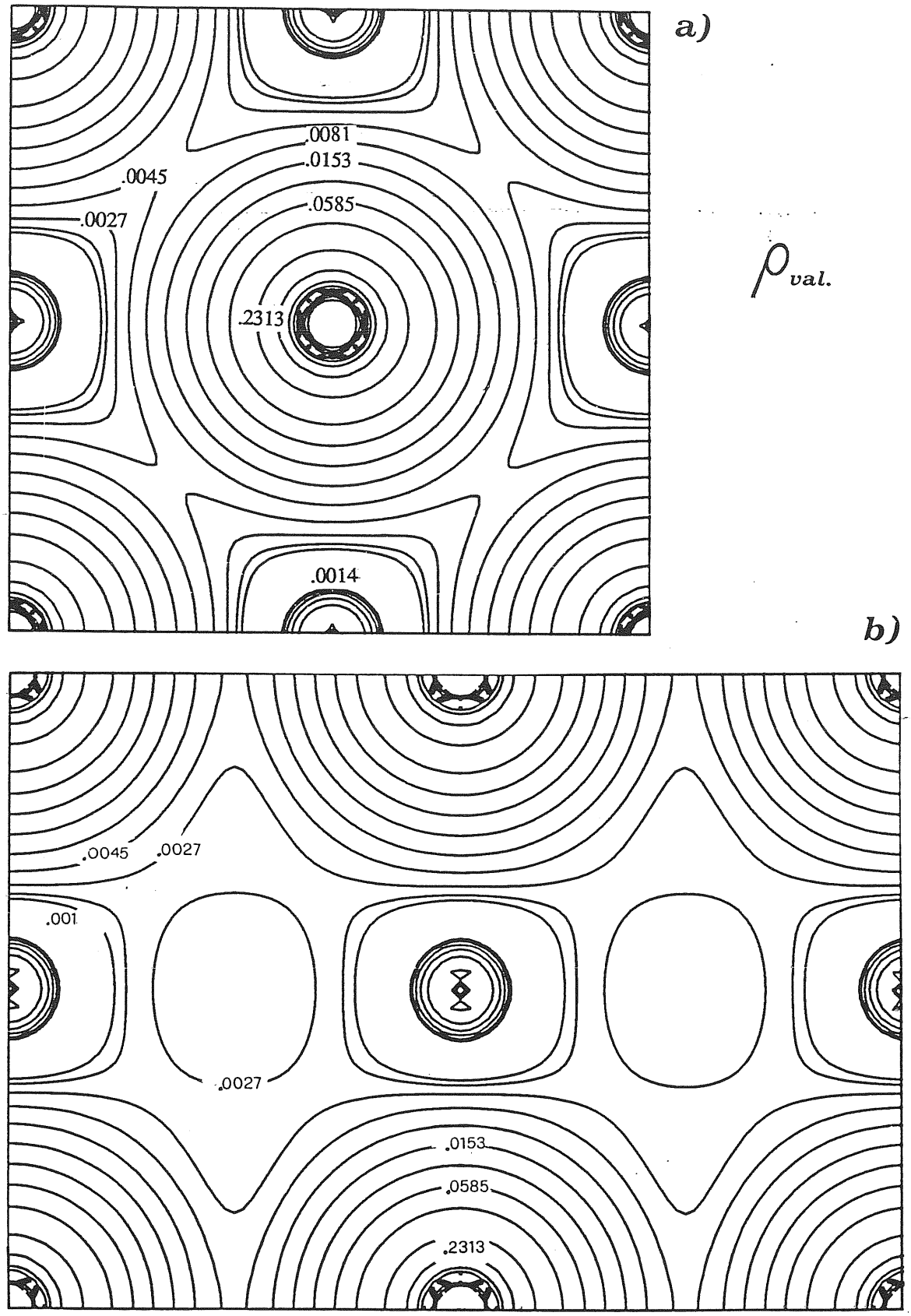

Fig.23: Valence electron density in the (001) plane (a) and in the (011) plane (b) in the present approximation. Chlorine ions are at the corners. The lowest level corresponds to $1.35 \cdot 10^{-3}$ electrons/a.u.^{3}, and the interval between the i-level and the $(i-1)$-level is $2^{(i-1)} \cdot 4.5 \cdot 10^{-4}$ electrons/a.u.^{3}.

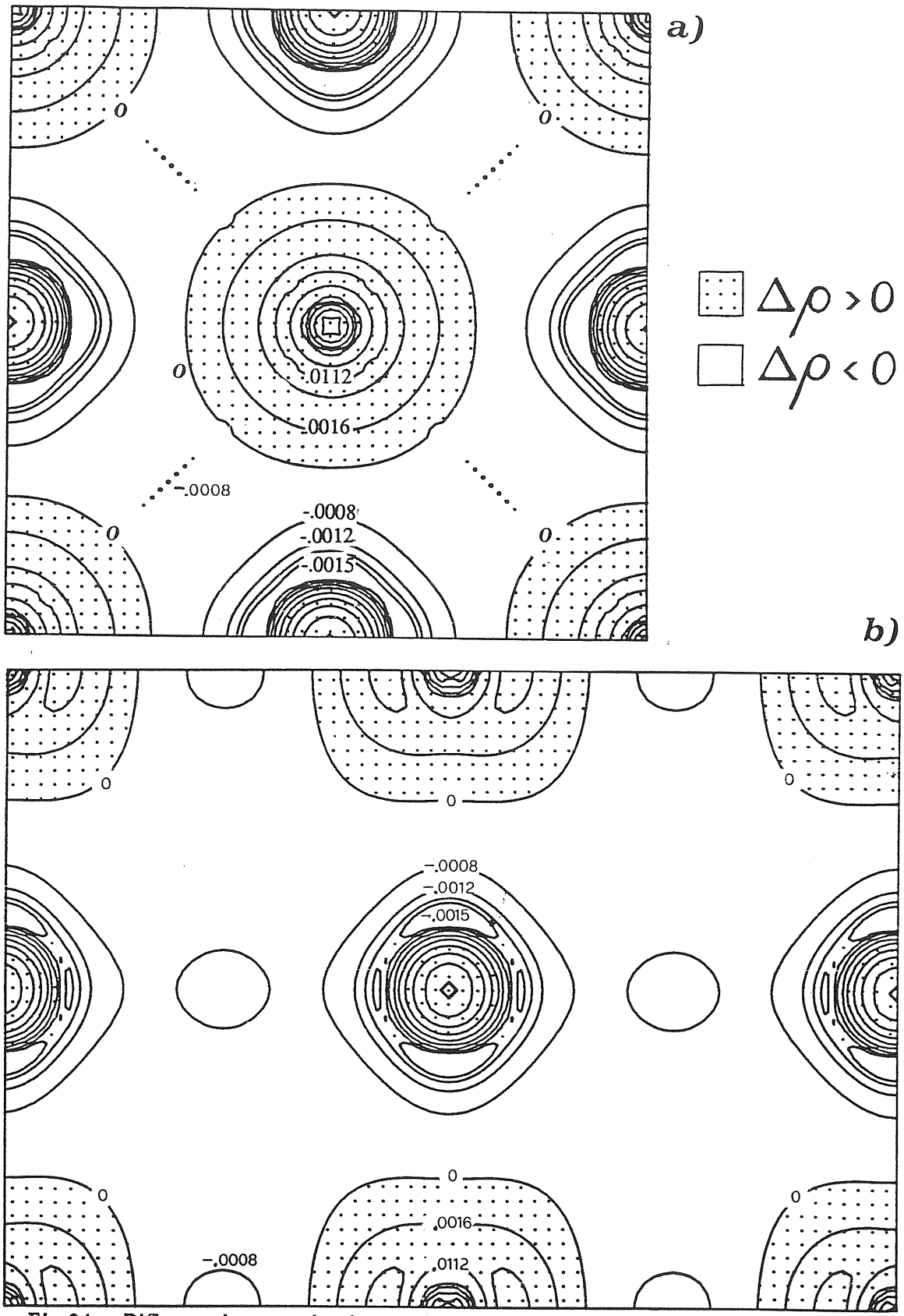

Fig.24: Difference between the electron density calculated within the present tight–binding scheme and in within the free–ion approximation in the (001) plane (a) and in the (011) plane (b). Chlorine ions are at the corners. The lowest level corresponds to $-.0015 \cdot 10^{-3}$ electrons/a.u.^{3}, and the interval between the i–level and the $(i-1)$–level is 10^{-4} electrons/a.u.^{3}.

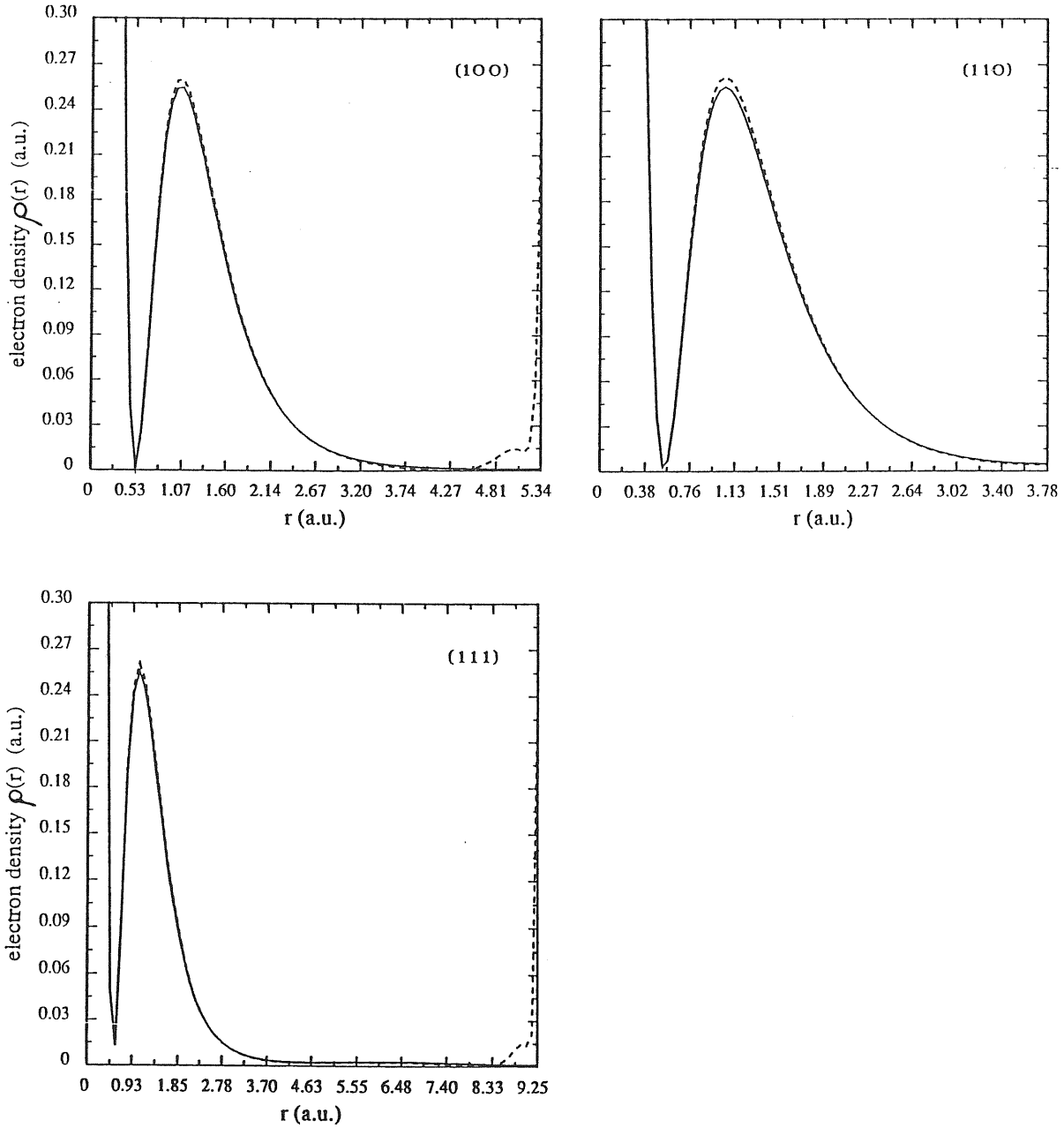

Fig.25: Valence electron density profile along (100), (110), and (111) directions calculated within the free–ion approximation (solid line) and within the present tight–binding approach (dashed line), as a function of the distance from the chlorine site.

Deviations from sphericity

If we look at the charge density plots in the free–ion approximation we recognize that the crystal charge density is spherical to a high degree around a lattice site; deviations from the spherical shape are evident in the interstitial regions and arise from the overlapping of the rigid ions put together to form the crystal.

The sphericity of the localized charge distributions constituting the crystal is not substantially modified in the present calculations; from the differential plot of the charge density we see that anisotropic effects due to the overlaps are very small. As suggested by physical intuition, the anion–anion overlap, which is dominant, causes a shrinkage of the valence electron density principally along the (110) direction, and the anion–cation overlap along the direction of the chemical bonding; in Fig. 24 we recognize a "hole" of electron density between two NN anions. We compare in Fig. 26 the valence electron density profiles around a Cl^- site along the three directions (100), (110) and (111).

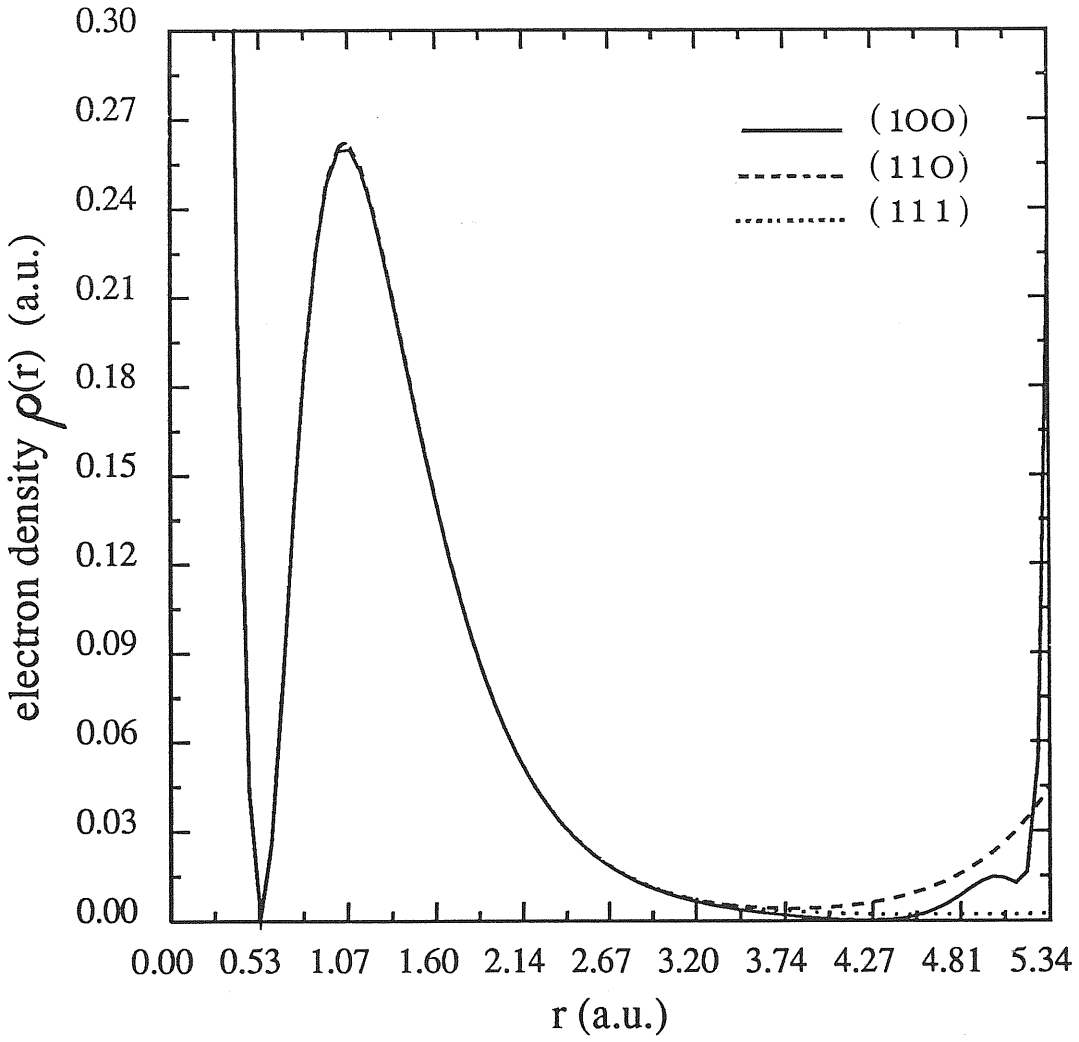

Fig.26: Valence electron density calculated within the present tight-binding approach along the directions (100), (110), and (111).

4.2
DEFINITION OF "PSEUDOION" AND "ORTHOGONALITY" CHARGE

a) Translational symmetry of the charge density

Localized charges

The periodicity of the crystal is taken into account in the tight-binding approach to the charge density through the Bloch functions. With this approach we are able to describe the charge density over the whole crystal, but it is not evident the relationship with its constituents. Since the charge density has itself the periodicity of the crystal, it should be written as a sum of charge densities – which are no longer the spherical ionic charge densities, of course – centered on the lattice sites $\mathbf{R}_n$:

$$\rho(\mathbf{r}) = \sum_{\mathbf{R}_n} \tilde{\rho}(\mathbf{r} - \mathbf{R}_n) \tag{4.2.1}$$

The advantage of this description is that one can directly compare these new-defined charges $\tilde{\rho}$ with the charge density of a single free ion, trying to understand how the ions modify from the free state when they are put together to form the crystal. Our purpose now is not doing a new complete numerical calculation, but trying an analytic approach to the problem to describe qualitatively the physical mechanism.

With a small effort we can manipulate the formulas already used and express the crystal charge density in terms of the ionic orbitals. We must remember the expression of the charge density:

$$\rho(\mathbf{r}) = 2\frac{\Omega}{(2\pi)^3} \sum_{\mathbf{k}} \sum_{\mu\nu,\mu'\nu'} \Psi^*_{\mu\nu}(\mathbf{k},\mathbf{r}) \left(O^{-1}(\mathbf{k})\right)_{\mu\nu,\mu'\nu'} \Psi_{\mu'\nu'}(\mathbf{k},\mathbf{r}) \tag{4.2.2}$$

and of the Bloch sums with the correct phase factors:

$$\Psi_{\mu\nu}(\mathbf{k},\mathbf{r}) = i^{l_\nu} \sum_{\mathbf{R}_n} e^{i\mathbf{k}\cdot(\mathbf{d}_\mu + \mathbf{R}_n)} \varphi_{\mu\nu}(\mathbf{r} - \mathbf{d}_\mu - \mathbf{R}_n) \tag{4.2.3}$$

From the equations (4.2.1), (4.2.2), (4.2.3) one obtains:

$$\tilde{\rho}(\mathrm{r}) = 2\frac{\Omega}{(2\pi)^3}\sum_{\mathrm{k}}\sum_{\mu\nu,\mu'\nu'} i^{l_{\nu'}-l_\nu} e^{i\mathrm{k}\cdot(\mathrm{d}_{\mu'}-\mathrm{d}_\mu)} \left(O^{-1}(\mathrm{k})\right)_{\mu\nu,\mu'\nu'} \cdot$$

$$\cdot\varphi_{\mu\nu}(\mathrm{r}-\mathrm{d}_\mu)\sum_{\mathrm{R}_n} e^{i\mathrm{k}\cdot\mathrm{R}_n}\varphi_{\mu\nu'}(\mathrm{r}-\mathrm{d}_{\mu'}-\mathrm{R}_n) \qquad (4.2.4)$$

Definition of pseudoion and orthogonality charge

If we consider the orthogonalization also with respect to the cation, in the complicated expression written before one can easily recognize three types of terms, which contain respectively products of Cl^- orbitals only, of Na^+ orbitals only, and mixed products of Cl^- and Na^+ orbitals. The sum $\sum_{\mu\nu,\mu'\nu'}$ over the orbitals can be separated into three sums:

$$\sum_{\mu\nu,\mu'\nu'} = \sum_{\substack{\nu,\nu' \\ \mu=\mu'=Cl^-}} + \sum_{\substack{\nu,\nu' \\ \mu=\mu'=Na^+}} + \sum_{\substack{\mu\nu,\mu'\nu' \\ \mu\neq\mu'}}$$

and the same holds for the charge density $\tilde{\rho}(\mathrm{r})$.

One can look at the first two terms involving orbitals of the same ion as a redefinition of the charge density of the ion, whereas the term with mixed products of orbitals can be seen as a certain orthogonality charge. In conclusion one can describe the crystal charge density as a sum of some "pseudoions" and of new "orthogonality" charges:

$$\rho(\mathrm{r}) = \sum_{\mathrm{R}_n}[\tilde{\rho}_{Cl^-}(\mathrm{r}-\mathrm{d}_{Cl^-}-\mathrm{R}_n) + \tilde{\rho}_{Na^+}(\mathrm{r}-\mathrm{d}_{Na^+}-\mathrm{R}_n) + \tilde{\rho}_{OC}(\mathrm{r}-\mathrm{R}_n)] \qquad (4.2.5)$$

Although we have used a well defined criterion to distinguish in such a way the localized charge densities, the definition of pseudoions and orthogonality charge depends on our choice and it is not unique. It could be convenient, for instance, to include also the mixed terms in the definition of the pseudoions.

b) The pseudoion

Total valence charge of the pseudoion

According to our previous choice, the charge density of the pseudoion μ is given by:

$$\tilde{\rho}_\mu(\mathrm{r}) = 2\frac{\Omega}{(2\pi)^3}\sum_{\mathrm{k}}\sum_{\nu,\nu'} i^{l_{\nu'}-l_\nu}\left(O^{-1}(\mathrm{k})\right)_{\mu\nu,\mu\nu'}\varphi_{\mu\nu}(\mathrm{r})\sum_{\mathrm{R}_n} e^{i\mathrm{k}\cdot\mathrm{R}_n}\varphi_{\mu\nu'}(\mathrm{r}-\mathrm{R}_n) \tag{4.2.7}$$

We ask ourselves which is the difference with respect to the free ion charge density $\rho_\mu(\mathrm{r})$, and in particular we try to investigate analytically the deviations from the spherical shape and to calculate the net amount of charge of this pseudoion.

The last point requires a minimum effort. In fact if we integrate over the whole space the pseudocharge $\tilde{\rho}_\mu(\mathrm{r})$, it is easy to recognize that:

$$i^{l_{\nu'}-l_\nu}\sum_{\mathrm{R}_n} e^{i\mathrm{k}\cdot\mathrm{R}_n}\int_{space}\varphi_{\mu\nu}(\mathrm{r})\varphi_{\mu\nu'}(\mathrm{r}-\mathrm{R}_n)d\mathrm{r} \;=\; O_{\mu\nu,\mu\nu'}(\mathrm{k}) \tag{4.2.8}$$

so that the total charge of the pseudoion is simply given by:

$$\int_{space}\tilde{\rho}_\mu(\mathrm{r})d\mathrm{r} \;=\; 2\frac{\Omega}{(2\pi)^3}\sum_{\mathrm{k}}\sum_{\nu,\nu'}\left(O^{-1}(\mathrm{k})\right)_{\mu\nu,\mu\nu'}O_{\mu\nu,\mu\nu'}(\mathrm{k}) \tag{4.2.9}$$

In the following table we report the total number of valence electrons of the pseudo Cl^- and of the pseudo Na^+ in the different approximations.

	Cl^-	Na^+
Γ	8.0176	.0176
L	8.0406	.0406
Γ, X, L	8.0388	.0388
B	8.0430	.0430
C_1, C_2	8.0419	.0419
$Cl^- - Cl^-$ only	8.0000	.0000
free ion	8.0000	.0000

Tab.12: Total number of valence electrons of the "pseudoions" using different approximations. The first four rows are referred to the present tight-binding calculations, including the effect of both the anion-anion and anion-cation overlaps; there are also reported for comparison the values obtained when only Cl^--Cl^- overlaps are included, and within the free-ion approximation.

In this picture we have a net amount of $-1.04\ |e|$ on Cl^- and of $+.96\ |e|$ on Na^+: this is different from the effective charge picture, according to which the overlapping charges of opposite sign partly neutralize with a significative reduction of the effective charge. The neutrality of the system in our picture is assured by the orthogonality charge, which is something of the order of $+.08\ |e|$ per unit cell.

Notice that neglecting the Cl^-–Na^+ overlaps one looses the essential features of this picture, i.e. the variation of the charge tranfer with respect the picture of perfectly ionized ions and the introduction of the concept of orthogonality charge. Taking into account just the anion-anion overlap, the effect of a redistribution of the charge density different from the rigid and perfectly spherical one in the free ion is however recovered.

Charge density of the pseudoion at the Γ point

We try now to investigate the redistribution of the pseudoion charge: since we are interested in a qualitative description of the effect, we study the situation at the Γ point, where:

$$\tilde{\rho}_\mu(\Gamma,\mathrm{r}) = 2\sum_{\nu,\nu'} i^{l_{\nu'}-l_\nu}\left(O^{-1}(\Gamma)\right)_{\mu\nu,\mu\nu'}\varphi_{\mu\nu}(\mathrm{r})\sum_{\mathrm{R}_n}\varphi_{\mu\nu'}(\mathrm{r}-\mathrm{R}_n) \qquad (4.2.10)$$

At Γ the situation is very simplified, since the Bloch sums constructed from ionic orbitals with different quantum numbers l and m belong to different representations or different rows and are thus orthogonal. In our case the index ν runs from 1 to 4 for each ion, and indicates s, p_x, p_y, p_z orbitals respectively. The overlap matrix and its inverse are thus diagonal with respect to ν:

$$O_{\mu\nu,\mu'\nu'}(\Gamma) = \delta_{\nu\nu'}O_{\mu\nu,\mu'\nu}(\Gamma) \qquad (4.2.11)$$

$$\left(O^{-1}(\Gamma)\right)_{\mu\nu,\mu'\nu'} = \delta_{\nu\nu'}\left(O^{-1}(\Gamma)\right)_{\mu\nu,\mu'\nu} \qquad (4.2.12)$$

In the expression of the pseudoion charge $\tilde{\rho}_{ion}$ at Γ there are not mixed products of orbitals of different kinds; we can finally write the extremely simple formula:

$$\tilde{\rho}_{ion}(\Gamma,\mathrm{r}) = 2\sum_{\nu}\left(O^{-1}(\Gamma)\right)_{\nu\nu}\varphi_\nu(\mathrm{r})\sum_{\mathrm{R}_n}\varphi_\nu(\mathrm{r}-\mathrm{R}_n) \qquad (4.2.13)$$

where the index μ of the ion is understood.

We now compare it with the free ion charge density:

$$\rho_{ion}(\mathrm{r}) = 2\sum_{\nu}|\varphi_\nu(\mathrm{r})|^2 \qquad (4.2.14)$$

A first difference is already evident from the terms $|\varphi_\nu(\mathrm{r})|^2$, which enter in $\tilde{\rho}_{ion}$ with a renormalization factor $\left(O^{-1}(\Gamma)\right)_{\nu\nu}$ which takes into account the orthogonalization effects with all the ions of the crystal.

Looking at the matrix $\mathrm{O}^{-1}(\Gamma)$ one recognizes that in Cl^- the reduction of the s orbital is largely compensated by the weighting factor for the p states, increased by 24% : this is due to the fact that the $(pp\sigma)$ overlap, which is dominant at the nn distance, is negative. This mechanism can partially explain the localization of the electron charge density around the anion.

With the terms containing only orbitals centered on the same site the spherical shape is retained, since the matrix elements $\mathrm{O}^{-1}(\Gamma)$ are the same for $\nu = p_x, p_y, p_z$. Anisotropic deformations arise from products between orbitals centered on different sites and are consequently smaller.

c) The orthogonality charge

Total orthogonality charge over the unit cell

The expression of the orthogonality charge is something more complicated than the pseudoion charges. We have:

$$\tilde{\rho}_{OC}(\mathrm{r}) = 2\frac{\Omega}{(2\pi)^3}\sum_{\mathrm{k}}\sum_{\substack{\mu\nu,\mu'\nu' \\ \mu\neq\mu'}} i^{l_{\nu'}-l_\nu} e^{i\mathrm{k}\cdot(\mathrm{d}_{\mu'}-\mathrm{d}_\mu)} \left(O^{-1}(\mathrm{k})\right)_{\mu\nu,\mu'\nu'} \cdot$$

$$\cdot\varphi_{\mu\nu}(\mathrm{r}-\mathrm{d}_\mu)\sum_{\mathrm{R}_n} e^{i\mathrm{k}\cdot\mathrm{R}_n}\varphi_{\mu'\nu'}(\mathrm{r}-\mathrm{d}_{\mu'}-\mathrm{R}_n) \qquad (4.2.15)$$

The sum $\sum_{\substack{\mu\nu,\mu'\nu' \\ \mu\neq\mu'}}$ contains for each term $(\mu\nu,\mu'\nu')$ its complex conjugate, so that we have a sum over distinct couples $(\mu\nu,\mu'\nu')$ of orbitals:

$$\tilde{\rho}_{OC}(\mathrm{r}) = 2\frac{\Omega}{(2\pi)^3}\sum_{\mathrm{k}}\sum_{\substack{\text{distinct couples} \\ (\mu\nu,\mu'\nu')}} \left[i^{l_{\nu'}-l_\nu} e^{i\mathrm{k}\cdot(\mathrm{d}_{\mu'}-\mathrm{d}_\mu)} \left(O^{-1}(\mathrm{k})\right)_{\mu\nu,\mu'\nu'} \cdot\right]$$

$$\left[\cdot\varphi_{\mu\nu}(\mathrm{r}-\mathrm{d}_\mu)\sum_{\mathrm{R}_n} e^{i\mathrm{k}\cdot\mathrm{R}_n}\varphi_{\mu'\nu'}(\mathrm{r}-\mathrm{d}_{\mu'}-\mathrm{R}_n) + \textit{ complex conjugate}\right] \qquad (4.2.16)$$

It appears now clear that the orthogonality charge is real:

$$\tilde{\rho}_{OC}(\mathrm{r}) = 4\frac{\Omega}{(2\pi)^3}\sum_{\mathrm{k}}\sum_{\substack{\text{distinct couples}\\(\mu\nu,\mu'\nu')}}\left(O^{-1}(\mathrm{k})\right)_{\mu\nu,\mu'\nu'}\cdot$$

$$\cdot\varphi_{\mu\nu}(\mathrm{r}-\mathrm{d}_\mu)\sum_{\mathrm{R}_n}\cos\left[\frac{\pi}{2}(l_{\nu'}-l_\nu)+\mathrm{k}\cdot(\mathrm{d}_{\mu'}-\mathrm{d}_\mu)+\mathrm{k}\cdot\mathrm{R}_n\right]\varphi_{\mu'\nu'}(\mathrm{r}-\mathrm{d}_{\mu'}-\mathrm{R}_n) \tag{4.2.17}$$

It is evident the structure of the orthogonality charge: we have products of the orbitals of one ion μ at a reference site with all those of the ions μ' of the other kind centered on all the sublattice sites and the same for the other ion μ'. Since we can distinguish in $\tilde{\rho}_{OC}$ two parts, we have a criterion to give a new definition of the pseudoions including also the orthogonality charge, if it would be convenient.

However, let us examine it entirely; first of all we can give the amount over a unit cell, as reported in the following Tab. 13:

	orthogonality charge
Γ	$-.0352$
Γ, X, L	$-.0776$
B	$-.0860$
C_1, C_2	$-.0838$

Tab.13: Total amount of orthogonality charge per unit cell, as obtained in the present tight–binding calculations at different levels of approximation.

Distribution of the orthogonality charge at the Γ point

Let us study $\tilde{\rho}_{OC}$ at Γ. The formula is simplified:

$$\tilde{\rho}_{OC}(\Gamma,\mathrm{r}) = 4\sum_{\substack{\text{distinct couples}\\(\mu\nu,\mu'\nu')}}\cos\left[\frac{\pi}{2}(l_{\nu'}-l_\nu)\right]\left(O^{-1}(\Gamma)\right)_{\mu\nu,\mu'\nu'}\cdot$$

$$\cdot\varphi_{\mu\nu}(\mathrm{r}-\mathrm{d}_\mu)\sum_{\mathrm{R}_n}\varphi_{\mu'\nu'}(\mathrm{r}-\mathrm{d}_{\mu'}-\mathrm{R}_n) \tag{4.2.18}$$

Notice that there are not present mixed products of orbitals s and p_x, or p_x and p_y ..., because the corresponding elements of the inverse of the overlap matrix are zero, as already explained in the analysis of the pseudoion charge. The expression of the orthogonality charge at Γ is thus further reduced; in

conclusion expliciting the sum over the two kinds of ions and taking into account the symmetry of $\mathbf{O}^{-1}$, we write:

$$\tilde{\rho}_{OC}(\Gamma,\mathbf{r}) = 4\sum_{\nu}\left(O^{-1}(\Gamma)\right)_{\mu\nu,\mu'\nu}\cdot$$

$$\cdot\left[\varphi_{\mu\nu}(\mathbf{r}-\mathbf{d}_{\mu})\sum_{\mathbf{R}_n}\varphi_{\mu'\nu}(\mathbf{r}-\mathbf{d}_{\mu'}-\mathbf{R}_n)+\varphi_{\mu'\nu}(\mathbf{r}-\mathbf{d}_{\mu'})\sum_{\mathbf{R}_n}\varphi_{\mu\nu}(\mathbf{r}-\mathbf{d}_{\mu}-\mathbf{R}_n)\right] \tag{4.2.19}$$

where the index ν indicates the orbitals of the same kind (i.e. $2s$ for Na^+ with $3s$ for Cl^-, etc. ...). This orthogonality charge is not localized, but it is sum of quantities centered on anionic and cationic sites.

4.3
A "CLUSTER" APPROACH WITH THE USE OF SYMMETRY

a) Various approaches to the charge density

We remember the starting point for our calculations of the charge density in the crystal:

$$\rho(\mathrm{r}) = 2\frac{\Omega}{(2\pi)^3}\sum_{\mathrm{k}}\sum_{\mu\nu,\mu'\nu'}\Psi^*_{\mu\nu}(\mathrm{k},\mathrm{r})\left(O^{-1}(\mathrm{k})\right)_{\mu\nu,\mu'\nu'}\Psi_{\mu'\nu'}(\mathrm{k},\mathrm{r}) \qquad (4.3.1)$$

where $\Psi_{\mu\nu}$ are the Bloch sums and O(k) is the corresponding overlap matrix as defined in this work .

According to a general result of Lowdin[34] for closed-shell systems the charge density can also be written as:

$$\rho(\mathrm{r}) = 2\sum_{\mu\nu,\mu'\nu'}\sum_{\mathrm{R}_m,\mathrm{R}_n}\varphi_{\mu\nu}(\mathrm{r}-\mathrm{d}_\mu-\mathrm{R}_m)\left(o^{-1}\right)_{\mu\nu,\mathrm{R}_m;\mu'\nu',\mathrm{R}_n}\varphi_{\mu'\nu'}(\mathrm{r}-\mathrm{d}_{\mu'}-\mathrm{R}_n) \qquad (4.3.2)$$

where now the overlap matrix is between ionic orbitals:

$$o_{\mu\nu,\mathrm{R}_m;\mu'\nu',\mathrm{R}_n} = <\varphi_{\mu\nu}(\mathrm{r}-\mathrm{d}_\mu-\mathrm{R}_m)\mid\varphi_{\mu'\nu'}(\mathrm{r}-\mathrm{d}_{\mu'}-\mathrm{R}_n)>_{space} \qquad (4.3.3)$$

and has in principle an infinite rank.

We have already developed the eq. (4.3.1) and expressed the charge density in terms of the ionic orbitals:

$$\rho(\mathrm{r}) = 2\frac{\Omega}{(2\pi)^3}\sum_{\mathrm{k}}\sum_{\mu\nu,\mu'\nu'} i^{l_{\nu'}-l_\nu}e^{i\mathrm{k}\cdot(\mathrm{d}_{\mu'}-\mathrm{d}_\mu)}\left(O^{-1}(\mathrm{k})\right)_{\mu\nu,\mu'\nu'}\cdot$$

$$\cdot\sum_{\mathrm{R}_m,\mathrm{R}_n}e^{i\mathrm{k}\cdot(\mathrm{R}_n-\mathrm{R}_m)}\varphi_{\mu\nu}(\mathrm{r}-\mathrm{d}_\mu-\mathrm{R}_m)\varphi_{\mu'\nu'}(\mathrm{r}-\mathrm{d}_{\mu'}-\mathrm{R}_n) \qquad (4.3.4)$$

Comparing eq. (4.3.1) with eq. (4.3.3) we can establish the relationship between the elements of the two overlap matrices:

$$\left(o^{-1}\right)_{\mu\nu,\mathrm{R}_m;\mu'\nu',\mathrm{R}_n} = \frac{\Omega}{(2\pi)^3}\sum_{\mathrm{k}} i^{l_{\nu'}-l_\nu}e^{i\mathrm{k}\cdot(\mathrm{d}_{\mu'}+\mathrm{R}_n-\mathrm{d}_\mu-\mathrm{R}_m)}\left(O^{-1}(\mathrm{k})\right)_{\mu\nu,\mu'\nu'} \qquad (4.3.5)$$

i.e. we can tranform one into the other with a 3–dimensional Fourier transform.

If one want to approach the problem of the crystal charge density from the localized charge densities of the pseudoions and from the orthogonality charge, the Lowdin formula seems to be more convenient than that one we have used: but a heavy numerical effort is required to calculate and invert the infinite order overlap matrix.

It must be possible however to do some semplifications. Using the translational properties of the system, the localized charge density is, following the Lowdin approach:

$$\tilde{\rho}(\mathbf{r}) = 2 \sum_{\mu\nu,\mu'\nu'} \varphi_{\mu\nu}(\mathbf{r}-\mathbf{d}_\mu) \sum_{\mathbf{R}_n} \left(o^{-1}\right)_{\mu\nu,0;\mu'\nu',\mathbf{R}_n} \varphi_{\mu'\nu'}(\mathbf{r}-\mathbf{d}_{\mu'}-\mathbf{R}_n) \quad (4.3.6)$$

This localized charge density must have the complete cubic symmetry Γ_1^+ of the crystal, and for this reason it must be written as a sum of products whose factors have the same symmetry . It follows that, if I group the lattice vectors into shells, and write:

$$\tilde{\rho}(\mathbf{r}) = 2 \sum_{\mu\nu,\mu'} \varphi_{\mu\nu}(\mathbf{r}-\mathbf{d}_\mu) \sum_{\substack{n \\ shells}} \left[\sum_{\substack{\mathbf{R}_n \\ \in shell}} \sum_{\nu'} \left(o^{-1}\right)_{\mu\nu,0;\mu'\nu',\mathbf{R}_n} \varphi_{\mu'\nu'}(\mathbf{r}-\mathbf{d}_{\mu'}-\mathbf{R}_n) \right] \quad (4.3.7)$$

the object within square brakets must have the same symmetry of $\varphi_{\mu\nu}(\mathbf{r}-\mathbf{d}_\mu)$, since the contributions of the various shells are independent, being not mixed by the operations of the punctual cubic group O_h; one could thus consider within each shell only some particular linear combinations of atomic orbitals.

At this point it is more convenient to face the problem from the beginning. Let us define a sort of "shell symmetrized orbitals" $\Phi_n^{(\alpha)}(\mathbf{r})$, where α indicates the symmetry species, and n is related to the shell and to the type of orbitals considered (for each shell we can found more than one independent linear combination of orbitals with symmetry Γ_α). This is a sort of "cluster" approach, in which the ion at the center of the cluster plays an essential role; for our purposes we shall thus consider the cluster around Cl^- and that one around Na^+. The "shell symmetrized orbitals" depend explicitly on the center of the cluster, that we should specify with another index: we do not worry about it for the moment, not to confuse with a lot of indices.

The contribution to the localized charge density arisig from the symmetrized orbital $\Phi_1^{(\alpha)}(\mathbf{r})$, which is just a real ionic orbital centered at the origin of the cluster, is given by:

$$\tilde{\rho}^{(\alpha)}(\mathbf{r}) = 2\Phi_1^{(\alpha)}(\mathbf{r}) \sum_n \left(\mathrm{O}^{-1}\right)_{1,\alpha;n,\alpha} \Phi_n^{(\alpha)}(\mathbf{r}) \quad (4.3.8)$$

where O is the overlap matrix, as usual, between the functions of this new basis set:

$$\mathbf{O}_{n,\alpha;n',\alpha'} = < \Phi_n^{(\alpha)}(\mathbf{r}) \mid \Phi_{n'}^{(\alpha')}(\mathbf{r}) > \tag{4.3.9}$$

The important point is that since functions of different symmetry do not mix, this overlap matrix is block–diagonal:

$$\mathbf{O}_{n,\alpha;n',\alpha'} = \delta_{\alpha\alpha'}\mathbf{O}_{n,\alpha;n',\alpha} = \delta_{\alpha\alpha'}\mathbf{O}_{nn'}(\alpha) \tag{4.3.10}$$

It becomes evident now the advantage of this cluster approach; infact the inverse of a block–diagonal matrix is itself block–diagonal, and precisely each bloch can be separately inverted:

$$\begin{pmatrix} A & \emptyset & \dots & \emptyset \\ \emptyset & B & \dots & \emptyset \\ \vdots & \vdots & \ddots & \vdots \\ \emptyset & \emptyset & \dots & C \end{pmatrix}^{-1} = \begin{pmatrix} A^{-1} & \emptyset & \dots & \emptyset \\ \emptyset & B^{-1} & \dots & \emptyset \\ \vdots & \vdots & \ddots & \vdots \\ \emptyset & \emptyset & \dots & C^{-1} \end{pmatrix} \tag{4.3.11}$$

We have thus to invert more than one matrix, as many as the number of the irreducible representations Γ_α corresponding to the orbitals of a single ion; the dimension of each matrix is determined by the number of neighbour shells we want to include, and by the number of linear combinations – with that symmetry – of orbitals belonging to each shell. A similar approach was used in Ref. 61, confined to s–states, for the determination of the density matrix of LiH and in Ref. 62 for the density matrix arising from π bands in graphite and hexagonal BN.

We will see in the following section how many and which linear combinations of orbitals we must consider. Since we are interested in an analytic study, we stop to the NNN ions: the calculation requires a patient work, since we have s and p orbitals.

b) Symmetrized orbitals

Method to construct symmetrized orbitals

We point out that each shell can be considered separately, since there is no operation of the cubic punctual group transforming a vector of a given shell into one of another shell; furthermore, for each shell one can consider separately the sets of s and p orbitals since there is no operation of that group tranforming a s–like orbital into a p–like or viceversa.

We must solve the following general problem: for a given shell with N sites and n orbitals centered on each site, how many symmetrized orbitals can be constructed, and of which symmetry species ?

We can answer precisely to these questions using few simple concepts of the group theory. We start writing the character table for the class of the $n \times N$ ionic orbitals under the transformation of the cubic punctual group : each character is the sum of the characters of the single ionic orbital, each one considered at the proper lattice site. Once we have the character table we can decompose the class of the $n \times N$ orbitals into irreducible representations; according to a well–known theorem of the group theory this decomposition is uniquely defined and the coefficients $n_{\Gamma_{irr.}}$ are given by solving the linear system of equations:

$$\sum_{\Gamma_{irr.}} n_{\Gamma_{irr.}} \chi_{\Gamma_{irr.}}(i) = \chi_{\substack{class\ of \\ orbitals}}(i) \qquad (4.3.12)$$

where χ are the character tables and the index i indicates a particular row.

In Tab. 14 is reported the character table for the irreducible representations of the group O_h.

	E	$8C_3$	$3C_2$	$6C_4$	$6C_2'$	J	$8JC_3$	$3JC_2$	$6JC_4$	$6JC_2'$
Γ_1^+	+1	+1	+1	+1	+1	+1	+1	+1	+1	1
Γ_2^+	+1	+1	+1	−1	−1	+1	+1	+1	−1	−1
Γ_3^+	+2	−1	+2	+0	+0	+2	−1	+2	+0	0
Γ_4^+	+3	+0	−1	+1	−1	+3	+0	−1	+1	−1
Γ_5^+	+3	+0	−1	−1	+1	+3	+0	−1	−1	1
Γ_1^-	+1	+1	+1	+1	+1	−1	−1	−1	−1	−1
Γ_2^-	+1	+1	+1	−1	−1	−1	−1	−1	+1	1
Γ_3^-	+2	−1	+2	+0	+0	−2	+1	−2	+0	0
Γ_4^-	+3	+0	−1	+1	−1	−3	+0	+1	−1	1
Γ_5^-	+3	+0	−1	−1	+1	−3	+0	+1	+1	−1

Tab.14: Character table for the group O_h (from Ref. 51).

Since we are interested in calculating more accurately the valence crystal charge density, we consider here the s and p orbitals of the outer shell of both Na^+ and Cl^-. Taking into account the ion at the center of the cluster and the NN and NNN ions we have six classes of orbitals:

$$
\begin{aligned}
&(1)\ class = shell\ \emptyset\ ,\ 1\ orbital\ s\\
&(2)\ class = shell\ \emptyset\ ,\ 3\ orbitals\ p\\
&(3)\ class = shell\ NN\ ,\ 6\ orbitals\ s\\
&(4)\ class = shell\ NN\ ,\ 18\ orbitals\ p\\
&(5)\ class = shell\ NNN,\ 12\ orbitals\ s\\
&(6)\ class = shell\ NNN,\ 36\ orbitals\ p
\end{aligned}
$$

It is evident that the orbital s at the center of the cluster has symmetry Γ_1^+ and the orbitals p_x, p_y, p_z belong to the different rows of the 3–dimensional irreducible representation Γ_4^- , whereas the calculation of the character tables for the remaining classes of orbitals require more attention; results are presented in the following Tab. 15.

		E	$8C_3$	$3C_2$	$6C_4$	$6C_2'$	JE	$8JC_3$	$3JC_2$	$6JC_4$	$6JC_2'$
s orbital	0	1	1	1	1	1	1	1	1	1	1
p orbitals	0	3	0	−1	1	−1	−3	0	1	−1	1
s orbitals	NN	6	0	2	2	0	0	0	4	0	2
p orbitals	NN	18	0	−2	2	0	0	0	4	0	2
s orbitals	NNN	12	0	0	0	2	0	0	4	0	2
p orbitals	NNN	36	0	0	0	−2	0	0	4	0	2

Tab.15: Character table for the six classes of s and p orbitals centered on a given lattice site and on its NN and NNN sites.

Using the eq. (4.3.12) we have calculated the coefficients of the decomposition into irreducible representations. The results are summarized in Tab. 16; the letters A, B indicate the two different ionic species.

ion	*orbitals*	*shell*	*decomposition*
A	s	$\emptyset$	Γ_1^+
A	p	$\emptyset$	Γ_4^-
B	s	NN	$\Gamma_1^+ + \Gamma_3^+ + \Gamma_4^-$
B	p	NN	$\Gamma_1^+ + \Gamma_3^+ + \Gamma_4^+ + 2\Gamma_4^- + \Gamma_5^+ + \Gamma_5^-$
A	s	NNN	$\Gamma_1^+ + \Gamma_3^+ + \Gamma_4^- + \Gamma_5^+ + \Gamma_5^-$
A	p	NNN	$\Gamma_1^+ + \Gamma_2^+ + \Gamma_2^- + 2\Gamma_3^+ + \Gamma_3^- + 2\Gamma_4^+ + 3\Gamma_4^- + 2\Gamma_5^+ + 2\Gamma_5^-$

Tab.16: Decomposition in terms of irreducible representations of the six classes of s and p orbitals in the cluster with two neighbour shells described in this chapter.

For each of the two cluster (one with $A{\equiv}Cl^-$ and $B{\equiv}Na^+$, the other with $A{\equiv}Na^+$ and $B{\equiv}Cl^-$) we thus can construct 5 symmetrized orbitals with symmetry Γ_1^+ and 24 with symmetry Γ_4^- (8 for each row of the 3–D irreducible representation Γ_4^-); each of them is a linear combination of some ionic orbitals centered on particular lattice sites and taken with a proper sign. Tab.17 summarizes the kind of ionic orbitals involved in the construction of each symmetrized orbital. In Fig. 27 and 28 the particular ionic orbitals chosen here to construct the symmetrized orbitals are shown in detail, each one with its proper sign considered in the linear combination.

Γ_1^+ symmetrized orbitals			
$\Phi_1^{\Gamma_1^+}$	*orbitals* s,	*shell* $\emptyset$,	*ion* A
$\Phi_2^{\Gamma_1^+}$	*orbitals* s,	*shell* NN,	*ion* B
$\Phi_3^{\Gamma_1^+}$	*orbitals* p,	*shell* NN,	*ion* B
$\Phi_4^{\Gamma_1^+}$	*orbitals* s,	*shell* NNN,	*ion* A
$\Phi_5^{\Gamma_1^+}$	*orbitals* p,	*shell* NNN,	*ion* A

Tab.17a

$\Gamma^-_{4,i}$	symmetrized orbitals	
$\Phi_1^{\Gamma_4^-}$	*orbitals* p,	*shell* $\emptyset$, *ion* A
$\Phi_2^{\Gamma_4^-}$	*orbitals* s,	*shell* NN, *ion* B
$\Phi_3^{\Gamma_4^-}$	*orbitals* p,	*shell* NN, *ion* B
$\Phi_4^{\Gamma_4^-}$	*orbitals* p,	*shell* NN, *ion* B
$\Phi_5^{\Gamma_4^-}$	*orbitals* s,	*shell* NNN, *ion* A
$\Phi_6^{\Gamma_4^-}$	*orbitals* p,	*shell* NNN, *ion* A
$\Phi_7^{\Gamma_4^-}$	*orbitals* p,	*shell* NNN, *ion* A
$\Phi_8^{\Gamma_4^-}$	*orbitals* p,	*shell* NNN, *ion* A

Tab.17b

Tab.17: List of symmetrized orbitals with Γ_1^+ and Γ_4^- (one row) symmetry constructed with the s and p orbitals of the cluster described in the present chapter.

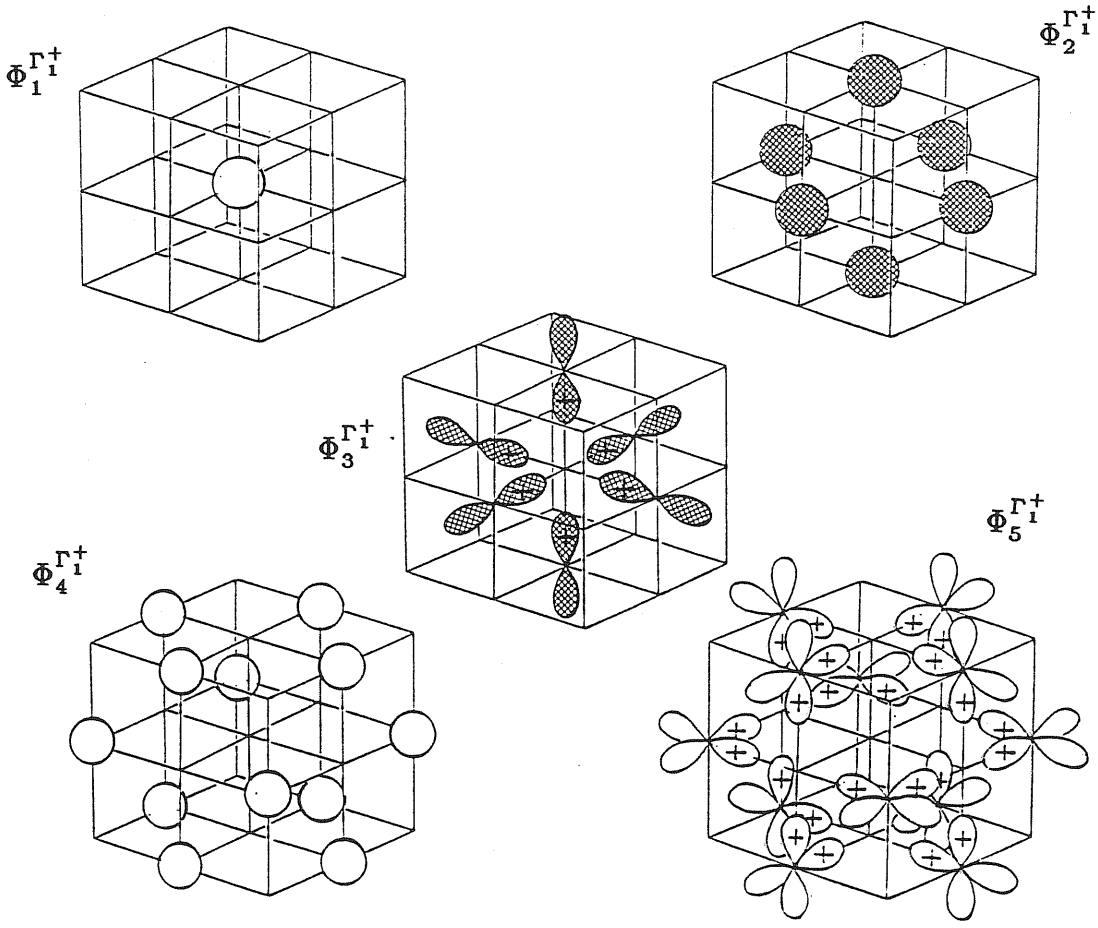

Fig.27: Ionic orbitals constituting the Γ_1^+ symmetrized cluster orbitals, each one with the proper sign considered in the linear combination.

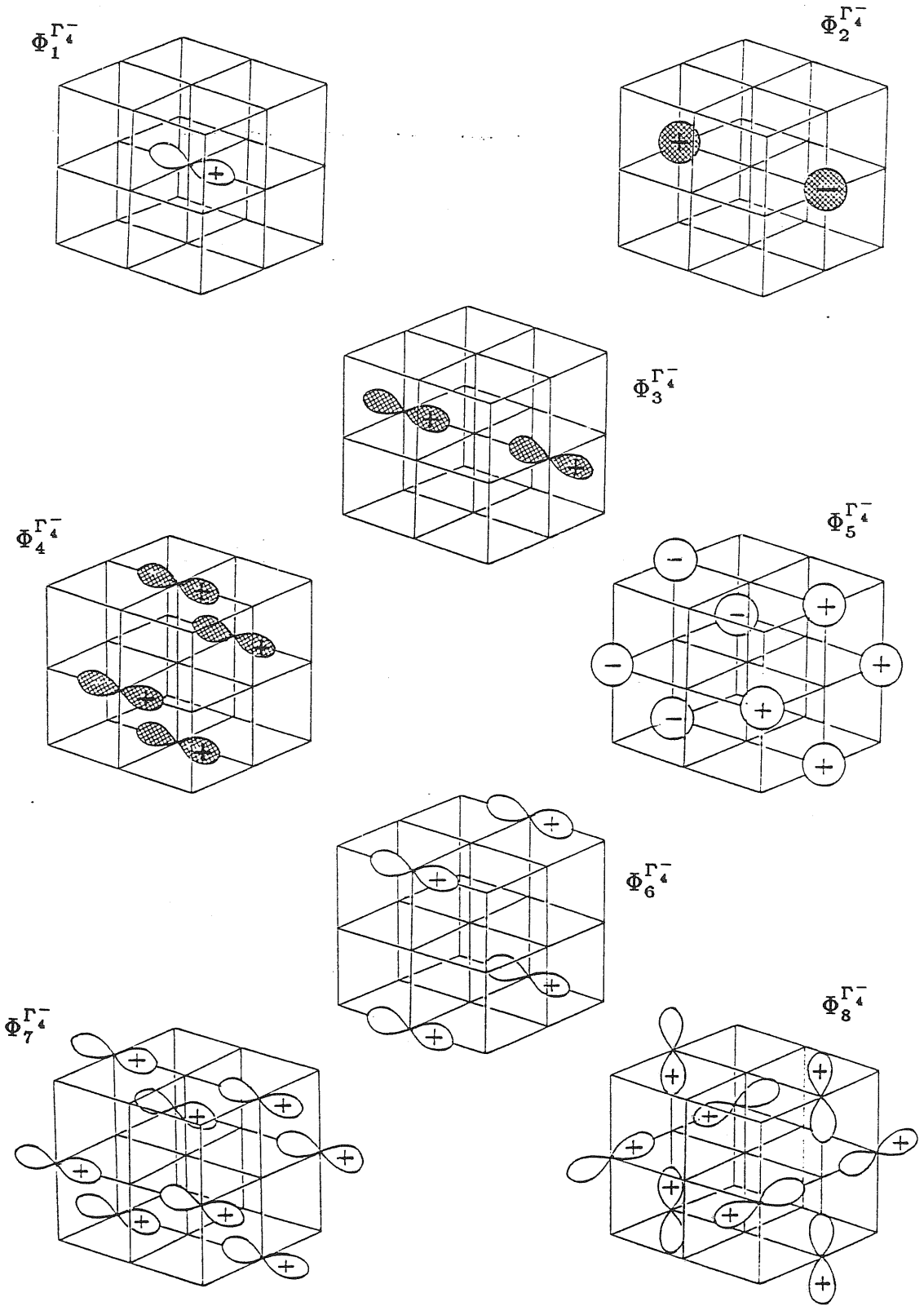

Fig.28: Ionic orbitals constituting the Γ_4^- symmetrized cluster orbitals, each one with the proper sign considered in the linear combination.

Overlap matrices

We have to compute now the overlap matrices $\mathbf{O}(\Gamma_1^+)$ and $\mathbf{O}(\Gamma_4^-)$, which are respectively a 5×5 and 8×8 real symmetric matrices. The calculation of their elements requires a patient work but can be carried out analytically; taking into account the overlaps between NN ions of different kind and nn ions of the same kind, we can express all the elements in terms of the usual few independent overlap integrals:

$$\begin{array}{ccccc} (s_A s_A \sigma), & (s_A p_A \sigma), & (p_A p_A \sigma), & (p_A p_A \pi), & \\ (s_B s_B \sigma), & (s_B p_B \sigma), & (p_B p_B \sigma), & (p_B p_B \pi), & (4.3.13) \\ (s_A s_B \sigma), & (s_A p_B \sigma), & (s_B p_A \sigma), & (p_A p_B \sigma), & (p_A p_B \pi) \end{array}$$

We report in Tables 18 and 19 the results, listing for semplicity only the non-zero elements.

Matrix elements of $\mathbf{O}(\Gamma_1^+)$

$$O_{11} = 1$$
$$O_{12} = 6(s_A s_B \sigma)_{NN}$$
$$O_{13} = 6(s_A p_B \sigma)_{NN}$$
$$O_{14} = 12(s_A s_A \sigma)_{nn}$$
$$O_{15} = 12\sqrt{2}(s_A p_A \sigma)_{nn}$$
$$O_{22} = 6\,[1 + 4(s_B s_B \sigma)_{nn}]$$
$$O_{23} = 12\sqrt{2}(s_B p_B \sigma)_{nn}$$
$$O_{24} = 24(s_A s_B \sigma)_{NN}$$
$$O_{25} = 24(s_B p_A \sigma)_{NN}$$
$$O_{33} = 6\,[1 - 2(p_B p_B \sigma)_{nn} + 2(p_B p_B \pi)_{nn}]$$
$$O_{35} = 24(p_A p_B \pi)_{nn}$$
$$O_{44} = 12\,[1 + 4(s_A s_A \sigma)_{nn}]$$
$$O_{45} = 24\sqrt{2}(s_A p_A \sigma)_{nn}$$
$$O_{55} = 24\,[1 - (p_A p_A \sigma)_{nn} + 3(p_A p_A \pi)_{nn}]$$

Tab.18: The non-zero independent matrix elements between Γ_1^+ symmetrized cluster orbitals. The indices are referred to the symmetrized orbitals as indicated in Fig.27.

Matrix elements of $O(\Gamma^-_{4,\alpha})$

$$O_{11} = 1$$
$$O_{12} = -2(s_B p_A \sigma)_{NN}$$
$$O_{13} = 2(p_A p_B \sigma)_{NN}$$
$$O_{14} = 4(p_A p_B \pi)_{NN}$$
$$O_{15} = -4\sqrt{2}(s_A p_A \sigma)_{nn}$$
$$O_{16} = 4(p_A p_A \pi)_{nn}$$
$$O_{17} = 4\left[(p_A p_A \sigma)_{nn} + (p_A p_A \pi)_{nn}\right]$$
$$O_{18} = 4\left[(p_A p_A \sigma)_{nn} - (p_A p_A \pi)_{nn}\right]$$
$$O_{22} = 2$$
$$O_{24} = -4\sqrt{2}(s_B p_B \sigma)_{nn}$$
$$O_{25} = 8(s_A s_B \sigma)_{NN}$$
$$O_{28} = 8(s_B p_A \sigma)_{NN}$$
$$O_{33} = 2$$
$$O_{34} = 4\left[(p_B p_B \sigma)_{nn} + (p_B p_B \pi)_{nn}\right]$$
$$O_{37} = 8(p_A p_B \pi)_{NN}$$
$$O_{44} = 4\left[1 + 2(p_B p_B \pi)_{nn}\right]$$
$$O_{45} = 8(s_A p_B \sigma)_{NN}$$
$$O_{46} = 8(p_A p_B \pi)_{NN}$$
$$O_{47} = 8(p_A p_B \sigma)_{NN}$$
$$O_{55} = 8\left[1 + 2(s_A s_A \sigma)_{nn}\right]$$
$$O_{56} = -8\sqrt{2}(s_A p_A \sigma)_{nn}$$
$$O_{58} = 8\sqrt{2}(s_A p_A \sigma)_{nn}$$
$$O_{66} = 4$$
$$O_{67} = 8\left[(p_A p_A \sigma)_{nn} + (p_A p_A \pi)_{nn}\right]$$
$$O_{77} = 8\left[1 + 2(p_A p_A \pi)_{nn}\right]$$
$$O_{88} = 8\left[1 - (p_A p_A \sigma)_{nn} + (p_A p_A \pi)_{nn}\right]$$

Tab.19: The non–zero independent overlap matrix elements between Γ^-_4 symmetrized cluster orbitals. The indices are referred to the symmetrized orbitals as indicated in Fig.28.

Substituting the independent integrals with their values, we have explicitly computed $O(\Gamma_1^+)$ and $O(\Gamma_4^-)$ both for Cl^- and Na^+ at the center of the cluster; also in this calculation we have neglected the overlap integral between cations. The inversion of the overlap matrices has also been performed. Results are in Tab. 20–23.

Overlap matrix $O(\Gamma_1^+)$, Cl^- ion at the center

	$\Phi_1^{\Gamma_1^+}$	$\Phi_2^{\Gamma_1^+}$	$\Phi_3^{\Gamma_1^+}$	$\Phi_4^{\Gamma_1^+}$	$\Phi_5^{\Gamma_1^+}$
$\Phi_1^{\Gamma_1^+}$	1.000	−0.049	−0.075	0.058	0.542
$\Phi_2^{\Gamma_1^+}$	−0.049	6.000	0.000	−0.197	−1.101
$\Phi_3^{\Gamma_1^+}$	−0.075	0.000	6.000	0.000	0.230
$\Phi_4^{\Gamma_1^+}$	0.058	−0.197	0.000	12.231	1.085
$\Phi_5^{\Gamma_1^+}$	0.542	−1.101	0.230	1.085	27.014

Tab.20

Overlap matrix $O(\Gamma_{4,x}^-)$, Cl^- ion at the center

	$\Phi_1^{\Gamma_4^-}$	$\Phi_2^{\Gamma_4^-}$	$\Phi_3^{\Gamma_4^-}$	$\Phi_4^{\Gamma_4^-}$	$\Phi_5^{\Gamma_4^-}$	$\Phi_6^{\Gamma_4^-}$	$\Phi_7^{\Gamma_4^-}$	$\Phi_8^{\Gamma_4^-}$
$\Phi_1^{\Gamma_4^-}$	1.000	0.092	−0.074	0.038	−0.181	0.071	−0.218	−0.360
$\Phi_2^{\Gamma_4^-}$	0.092	2.000	0.000	0.000	−0.066	0.000	−0.367	0.000
$\Phi_3^{\Gamma_4^-}$	−0.074	0.000	2.000	0.000	0.000	0.000	0.077	0.000
$\Phi_4^{\Gamma_4^-}$	0.038	0.000	0.000	8.000	0.100	0.077	−0.296	0.000
$\Phi_5^{\Gamma_4^-}$	−0.181	−0.066	0.000	0.100	8.077	−0.362	0.000	0.362
$\Phi_6^{\Gamma_4^-}$	0.071	0.000	0.000	0.077	−0.362	4.000	−0.436	0.000
$\Phi_7^{\Gamma_4^-}$	−0.218	−0.367	0.077	−0.296	0.000	−0.436	8.284	0.000
$\Phi_8^{\Gamma_4^-}$	−0.360	0.000	0.000	0.000	0.362	0.000	0.000	8.721

Tab.21

Overlap matrix $O(\Gamma_1^+)$, Na^+ ion at the center

	$\Phi_1^{\Gamma_1^+}$	$\Phi_2^{\Gamma_1^+}$	$\Phi_3^{\Gamma_1^+}$	$\Phi_4^{\Gamma_1^+}$	$\Phi_5^{\Gamma_1^+}$
$\Phi_1^{\Gamma_1^+}$	1.000	−0.049	0.275	0.000	0.000
$\Phi_2^{\Gamma_1^+}$	−0.049	6.117	0.542	−0.197	0.301
$\Phi_3^{\Gamma_1^+}$	0.275	0.542	7.081	0.000	0.230
$\Phi_4^{\Gamma_1^+}$	0.000	−0.197	0.000	12.000	0.000
$\Phi_5^{\Gamma_1^+}$	0.000	0.301	0.230	0.000	24.000

Tab.22

Overlap matrix $O(\Gamma_{4,x}^-)$, Na^+ ion at the center

	$\Phi_1^{\Gamma_4^-}$	$\Phi_2^{\Gamma_4^-}$	$\Phi_3^{\Gamma_4^-}$	$\Phi_4^{\Gamma_4^-}$	$\Phi_5^{\Gamma_4^-}$	$\Phi_6^{\Gamma_4^-}$	$\Phi_7^{\Gamma_4^-}$	$\Phi_8^{\Gamma_4^-}$
$\Phi_1^{\Gamma_4^-}$	1.000	−0.025	−0.074	0.038	0.000	0.000	0.000	0.000
$\Phi_2^{\Gamma_4^-}$	−0.025	2.000	0.000	−0.181	−0.066	0.000	0.100	0.000
$\Phi_3^{\Gamma_4^-}$	−0.074	0.000	2.000	−0.218	0.000	0.000	0.077	0.000
$\Phi_4^{\Gamma_4^-}$	0.038	−0.181	−0.218	8.284	−0.367	0.077	−0.296	0.000
$\Phi_5^{\Gamma_4^-}$	0.000	−0.066	0.000	−0.367	8.000	0.000	0.000	0.000
$\Phi_6^{\Gamma_4^-}$	0.000	0.000	0.000	0.077	0.000	4.000	0.000	0.000
$\Phi_7^{\Gamma_4^-}$	0.000	0.100	0.077	−0.296	0.000	0.000	8.000	0.000
$\Phi_8^{\Gamma_4^-}$	0.000	0.000	0.000	0.000	0.000	0.000	0.000	8.000

Tab.23

Tab.20–23: Overlap matrix elements between the symmetrized orbitals considered in the present chapter and shown in Fig.27–28.

c) Pseudoion and orthogonality charge in terms of symmetrized orbitals

The charge density from the symmetrized orbitals

It is necessary now to introduce a new label for the symmetrized orbitals to specify also the type of ion at the center of the cluster; we will write $\Phi_n^{\Gamma_\alpha,ion}(\mathrm{r})$. We have seen that the contribution to the localized charge density arising from the symmetrized orbital $\Phi_1^{\Gamma_\alpha,ion}(\mathrm{r})$ is:

$$\tilde{\rho}^{\Gamma_\alpha,ion}(\mathrm{r}) = 2\Phi_1^{\Gamma_\alpha,ion}(\mathrm{r}) \sum_n \left(\mathrm{O}^{-1}(\Gamma_\alpha, ion)\right)_{1,n} \Phi_n^{\Gamma_\alpha,ion}(\mathrm{r}) \qquad (4.3.14)$$

and hence the total charge localized on the site of an ion, for instance, will be:

$$\begin{aligned}\tilde{\rho}^{ion}(\mathrm{r}) &= \sum_{\Gamma_\alpha} \tilde{\rho}^{\Gamma_\alpha,ion}(\mathrm{r}) \\ &= 2\sum_{\Gamma_\alpha} \Phi_1^{\Gamma_\alpha,ion}(\mathrm{r}) \sum_n \left(\mathrm{O}^{-1}(\Gamma_\alpha, ion)\right)_{1,n} \Phi_n^{\Gamma_\alpha,ion}(\mathrm{r}) \qquad (4.3.15)\end{aligned}$$

where the sum $\sum_{\Gamma_\alpha}$ runs over all the irreducible representations involved and all their rows, in particular over the three rows of the Γ_4^- representation.

Up to now we have considered the symmetrized orbitals for one of these rows; what about the others ? A proper or improper rotation T of the cubic axes transform all the symmetrized orbitals (remember that functions with Γ_4^- symmetry transform like a vector) but leave the overlap matrix and its inverse unchanged; in particular this holds for those operations which transform a x–like function into a y–like or a z–like function or, in other words, which change one row of Γ_4^- with another one. Formally we have thus:

$$\begin{aligned}\Phi_n^{T\Gamma_{4,i}^-}(\mathrm{r}) &= \Phi_n^{\Gamma_{4,i}^-}(T^{-1}\mathrm{r}) \\ O(\Gamma_{4,i}^-) &= O(\Gamma_{4,j}^-) \equiv O(\Gamma_4^-) \qquad \textit{also for } i \neq j \\ O^{-1}(\Gamma_{4,i}^-) &= O^{-1}(\Gamma_{4,j}^-) \equiv O^{-1}(\Gamma_4^-) \qquad \textit{also for } i \neq j \qquad (4.3.16)\end{aligned}$$

The resulting effect on the contribution to the localized charge density is:

$$\tilde{\rho}^{T\Gamma_{4,i}^-}(\mathrm{r}) = \tilde{\rho}^{\Gamma_{4,i}^-}(\mathrm{r}) \qquad (4.3.17)$$

The localized charge density, explicitly written, is:

$$\begin{aligned}\tilde{\rho}^{ion}(\mathrm{r}) = 2\Bigg[&\Phi_1^{\Gamma_1^+,ion}(\mathrm{r}) \sum_{n=1}^{5} \left(\mathrm{O}^{-1}(\Gamma_1^+, ion)\right)_{1,n} \Phi_n^{\Gamma_1^+,ion}(\mathrm{r}) \\ &+ \sum_{i=1}^{3} \Phi_1^{\Gamma_4^-,ion}(T_i\mathrm{r}) \sum_{n=1}^{8} \left(\mathrm{O}^{-1}(\Gamma_4^-, ion)\right)_{1,n} \Phi_n^{\Gamma_4^-,ion}(T_i\mathrm{r})\Bigg] \qquad (4.3.18)\end{aligned}$$

where now Γ_4^- means one particular row of the Γ_4^- representation and $T_1 = E, T_2$ and T_3 transform this row into the others.

We can give a definition of pseudoion and of orthogonality charge also in terms of these symmetrized orbitals. According to the definitions used in Ch. 4.2 we can consider for the pseudoion the terms which are products of symmetrized orbitals only arising from atomic orbitals of that ion; looking at the Tab. 17 of the symmetrized orbitals we have – notice the difference with $\tilde{\rho}^{ion}$ which indicates the total charge density localized at that ion site – :

$$\tilde{\rho}_{\substack{pseudo \\ ion}}(\mathrm{r}) = 2\Bigg[\Phi_1^{\Gamma_1^+,ion}(\mathrm{r}) \sum_{n=1;4;5} \left(\mathrm{O}^{-1}(\Gamma_1^+,ion)\right)_{1,n} \Phi_n^{\Gamma_1^+,ion}(\mathrm{r})$$

$$+\sum_{i=1}^{3} \Phi_1^{\Gamma_4^-,ion}(T_i\mathrm{r}) \sum_{n=1;5,8} \left(\mathrm{O}^{-1}(\Gamma_4^-,ion)\right)_{1,n} \Phi_n^{\Gamma_4^-,ion}(T_i\mathrm{r})\Bigg] \qquad (4.3.19)$$

With the orbitals we have used, this is exactly the valence charge density if the ion considered is Cl^-, whereas for Na^+ we must subtract, as already pointed out, the external core charge density.

For the orthogonality charge we have to sum the contributions arising from the cluster centered on the anion and that one centered on the cation:

$$\tilde{\rho}_{OC}(\mathrm{r}) = 2 \sum_{ion=A,B} \Bigg[\Phi_1^{\Gamma_1^+,ion}(\mathrm{r}) \sum_{n=2;3} \left(\mathrm{O}^{-1}(\Gamma_1^+,ion)\right)_{1,n} \Phi_n^{\Gamma_1^+,ion}(\mathrm{r})$$

$$+\sum_{i=1}^{3} \Phi_1^{\Gamma_4^-,ion}(T_i\mathrm{r}) \sum_{n=2,4} \left(\mathrm{O}^{-1}(\Gamma_4^-,ion)\right)_{1,n} \Phi_n^{\Gamma_4^-,ion}(T_i\mathrm{r})\Bigg] \qquad (4.3.20)$$

Comparison with the free ion

In terms of symmetrized orbitals the free ion charge is:

$$\rho_{ion}(\mathrm{r}) = 2\left[|\Phi_1^{\Gamma_1^+,ion}(\mathrm{r})|^2 + \sum_{i=1}^{3} |\Phi_1^{\Gamma_4^-,ion}(T_i\mathrm{r})|^2\right] \qquad (4.3.21)$$

It easy to recognize the renormalization of the terms products of orbitals on the same site; one immediately recognizes that such terms give a spherical contribution to the ion, since $\left(\mathrm{O}^{-1}(\Gamma_4^-,ion)\right)$ is identically the same for each row of Γ_4^-. Deviations from spherical symmetry are due to the terms which are mixed products of orbitals belonging to different shells.

Also in this scheme we have evaluated the total valence charge density for the pseudoion and the total orthogonality charge per unit cell. The results, expressed in number of electrons, are:

$$\begin{aligned} \rho_{pseudo\ Cl^-} &= 8.0433 \\ \rho_{pseudo\ Na^+} &= 0.0423 \\ \rho_{OC} &= -.0856 \end{aligned} \tag{4.3.22}$$

very close to those obtained with the tight-binding approach.

Chapter 5
CONCLUSIONS

It is convenient now to summarize the results obtained in this thesis, and to sketch some lines for a future work. The results can be summarized in the following points.

• Our first purpose was to explain the validity of the Vegard law for the lattice parameters for the alkali halide solid solutions. To this goal we have first developed a simple model based on the virtual crystal approximation and on the Born–Mayer model for the evaluation of the lattice energy. The resulting theoretical predictions are very poor: the predicted lattice parameter $a(x)$ deviates considerably from both Vegard and Retgers laws, too much with respect to the experimental data. These simple computations however allow us to understand the importance of anharmonic forces in alkali halide solid solutions. Separating the lattice energy into harmonic and anharmonic terms we have evaluated how much each one contributes to the small deviations of $a(x)$ from Vegard law. Harmonic terms alone give the wrong sign for the deviations, (i.e. a sub-linear behaviour), and only with the inclusion of the anharmonic terms one obtains the experimentally observed positive bowing. Including anharmonic terms, positive deviations from Vegard law are predicted for all alkali halide solid solutions.

We have then proposed a model allowing internal distorsions of the lattice. Although the distribution of A and B ions in the homogeneous $A_{1-x}B_xC$ solid solution is random, we have simulated the alloy with a periodically repeated supercell. Since the macroscopic symmetry of the real alloy is cubic, we have chosen a cubic supercell and distributed anions and cations in it according to cubic symmetry. With these criteria a given cell allows only for particular compositions x and symmetry-restricted atomic displacements from the ideal sites of the rocksalt virtual crystal. Using the smallest cubic supercell allowing internal distorsions, i.e. the FCC cell with 16 ions, we have evaluated the lattice energy which depends on the lattice parameter and one distorsion parameter, and we have obtained the equilibrium structure by minimizing the lattice energy simultaneously with respect to both parameters.

We have seen that the atomic–scale rearrangement of the crystalline structure allows for a considerable reduction of the average ionic volume, and this favours the additivity of distances rather than the additivity of volumes. Appreciable results are obtained within the supercell method: positive deviations from Vegard law are still predicted, but very close to the experimental data. The calculations are performed both including and neglecting polarization effects: the agreement with the experimental data is improved when including polarization effects, in particular when the negative ion is polarized.

• Another purpose of this work was to explain the bimodal distribution

of the NN anion–cation distances. It was evident that the crystal structure of an alloy cannot be at equilibrium if the ions occupy the virtual crystal lattice sites, because of the different intensities of the repulsive forces for different ion pairs. The supercell model can explain the experimental data: after weighted average of the several NN distances present at equilibrium in the supercell, we have obtained A–C and B–C distances which are closer to the respective distances in the pure AC and BC compounds than to the virtual crystal NN distance, in accordance with EXAFS data. Also for this lengths, the inclusion of the polarization effects improves the agreement with the experimental data.

• Further improvements of these results could be obtained by applying the simple model developed here to bigger supercells, in which more distortions are allowed. Using the small FCC supercell, it has been possible to deal only with average A-C and B-C distances, but with bigger supercells we could also study the distribution of A-C and B-C distances around their average value. A great supercell could also allow for more configurations for each given composition x: we could determine the lowest energy configuration and examine its dependence on the degree of order in the crystal.

• A larger part of the thesis has been reserved to some quantum mechanical calculations for an accurate description of the alkali halide electron density. We have chosen NaCl as a prototype. Using Hartree–Fock ionic wave functions we have performed tight–binding calculations for the charge density, taking into account the overlap between the ions in the crystal. The result is a clear shrinkage of the valence charge around the anions, the effect being essentially determined by the anion–anion overlap, in particular between P orbitals. The effect is of the order of few percent on the charge density: we are going to examine its relevance on the lattice Coulomb energy (this calculation is in progress now).

The electronic distribution in the pure alkali halides is not a new source of investigation, whereas —as far as I know— the same quantity in the alkali halide solid solutions has still to be examined. This constitutes the other purpose of our next work. We would like to extend the techniques acquired and developed here for the charge distribution of the pure alkali halide compounds to study their solid solutions. We have implemented very general programs to calculate overlap integrals between ionic orbitals as well as Bloch sums, and the application to new systems can be easily done.

We would also like to go fully through the cluster–symmetrized–orbitals approach, a technique which has so far only outlined, but which seems to be very convenient.

References

1) H. Witte and E. Wolfel, *Z. Phys. Chem.* **3**, 296 (1955).
2) R. Yoder and R. Colella, *Phys. Rev.* B**25**, 2545 (1982).
3) J. Kondo and J. Yamashita, *J. Phys. Chem. Solids* **10**, 245 (1959).
4) E. G. Wikner, W. E. Blumberg, and E. L. Hahn, *Phys. Rev.* **118**, 631 (1961).
5) The subject has recently been reviewed by V. Hari Babu and U. V. Subba Rao, *Prog. Crystal Growth and Charact.* **8**, 189 (1984).
6) A. V. Tobolski *J. Chem. Phys.* **10**, 187 (1942).
7) D. L. Fancher and G. R. Barsch, *J. Phys. Chem. Solids* **30**, 2503 (1969) and cited references.
8) W. E. Wallace, *J. Chem. Phys.* **17**, 1095 (1949).
9) H. H. Landolt and R. Boernstein, *Numerical Data and Functional Relationships in Science and Technology*, edited by K. H. Hellewege (Springer-Verlag, Berlin-Heidelberg-New York 1973), group III, **7**a.
10) O. D. Slagle and H. A. McKinstry, *Acta Cryst.* **21**, 1013 (1966).
11) I. R. Nair and C. T. Walker, *Phys. Rev.* B**7**, 2740 (1973).
12) L. Vegard, Z. Physik **5**, 17 (1921).
13) H. G. Grimm and K. F. Herzfeld, *Z. Physik* **16**, 77 (1923).
14) J. B. Boyce and J. C. Mikkelsen, in *EXAFS and Near Edge Structure III*, edited by K. O. Hodgson, B. Hedman and J. E. Penner-Hahn (Springer-Verlag, Berlin, 1984), p.426.
15) T. Murata, in *EXAFS and Near Edge Structure III*, edited by K. O. Hodgson, B. Hedman and J. E. Penner-Hahn (Springer-Verlag, Berlin, 1984), p.432.
16) J. B. Boyce and J. C. Mikkelsen, *Phys. Rev.* B**31**, 6903 (1985).
17) M. P. Tosi in *Solid State Physics*, edited by F.Seitz and D. Turnbull (Academic Press, New York, 1964), **16**, p.1 .
18) A. Zunger and A. J. Freeman, *Phys. Rev.* B**16**, 2901 (1977).
19) G. Bobel, P. Cortona, C. Sommers, and F. G. Fumi, *Acta Cryst.* A**39**, 400 (1983).
20) W. Andreoni, K. Maschke, and M. Schluter, *Phys. Rev.* B**26**, 2314 (1982).
21) S. Froyen and M. L. Cohen, *Phys. Rev.* B**29**, 3770 (1984).
22) F. Gygi, K. Maschke, and W. Andreoni, *Sol. State Commun.* **49**, 437 (1984).
23) H. J. F. Jansen and A. J. Freeman, *Phys. Rev.* B**33**, 8629 (1986).

24) C. K. Shih, W. E. Spicer, W. A. Harrison, and A. Sher, *Phys. Rev.* B**31**, 1139 (1985).
25) J. R. Hardy, *J. Phys. Chem. Solids* **15**, 39 (1960).
26) Y. Fukay, *J. Phys. Soc. of Japan* **18**, 1413 (1963); *J. Phys. Soc. of Japan* **18**, 1580 (1963).
27) B. G. Dick and T. P. Das, *Phys. Rev.* **127**, 1053 (1962).
28) F. Hess, *J. Phys. Chem. Solids* **46**, 1463 (1985).
29) G. S. Durham and J. A. Hawkins, *J. Chem. Phys.* **19**, 149 (1951).
30) J. Shanker, S. C. Sharma, and M. Kumar, *Phys. Stat. Sol. (b)* **141**, 409 (1987).
31) A. Cox and M. J. L. Sangster, *J. Phys.* C**18**, L1123 (1985).
32) C. V. Krishnamurthy and Y. V. G. S. Murti, *Phys. Rev.* B**34**, 8922 (1986).
33) M. P. Tosi and F. G. Fumi, *J. Phys. Chem. Solids* **23**, 359 (1962); M. P. Tosi, *J. Phys. Chem. Solids* **24**, 1067 (1963).
34) P. O. Lowdin, *Adv. in Phys.* **5**, 1 (1956).
35) a review on DF-LDA is for instance: J. Callaway and N. H. March in *Solid State Physics*, edited by H. Ehrenreich, D. Turnbull and F. Seitz (Academic Press, Orlando, 1984), **38**, p. 136.
36) R. G. Gordon and Y. S. Kim, *J. Chem. Phys.* **56**, 3122 (1972).
37) W. A. Harrison, *Phys. Rev.* B**23**, 5230 (1981); *Phys. Rev.* B**31**, 2787 (1986); *Phys. Rev.* B**34**, 2121 (1985).
38) U. Shrœder, *Solid State Commun.* **4**, 347 (1966).
39) A. N. Basu, D. Roy, and S. Sengupta, *Phys. Stat. Sol. (a)* **23**, 11 (1974).
40) J. C. Mikkelsen and J. B. Boyce, *Proc. 17th Int. Conf. on the Physics of Semiconductors* (Springer-Verlag, New York, 1985), p.933.
41) A. Balzarotti, M. Czyzyk, A. Kisiel, N. Motta, M. Podgorny, and M. Zimnal-Starnawska, *Phys. Rev.* B**30**, 2295 (1984); *Phys. Rev.* B**31**, 7526 (1985); *Proc. 17th Int. Conf. on the Physics of Semiconductors* (Springer-Verlag, New York, 1985), p.807.
42) N. Motta, A. Balzarotti, P. Letardi, A. Kisiel, M. J. Czyzyk, M. Zimnal-Starnawska, and M. Podgorny, *Solid State Commun.* **53**, 509 (1985); *Solid State Commun.* **55**, 413 (1985).
43) W. B. Pearson, *The Crystal Chemistry and Physics of Metals and Alloys*, (Wiley, Interscience), ch.IV and cited references.
44) T. Fukuy, *Jpn. J. Appl. Phys.* **23**, L208 (1984); *J. Appl. Phys.* **57**, 5188 (1985).
45) P. Boguslawski and A. Baldereschi, *Proc. 17th Int. Conf. on the Physics of Semiconductors* (Springer-Verlag, New York, 1985), p.939.
46) G. P. Srivastava, J. L. Martins, and A. Zunger, *Phys. Rev.* B**31**, 2561 (1985) and references therein.

47) J. R. Hardy and A. M. Karo, *The Lattice Dynamics and Statics of Alkali-Halide Crystals* (Plenum, New York, 1979).
48) F. W. de Wette, W. Kress, and U. Schroeder, *Phys. Rev.* B**32**, 4143 (1985) and cited references.
49) M. P. Tosi and M. Doyama, *Phys. Rev.* **160**, 716 (1967) and cited references.
50) J. R. Tessman, A. K. Kahn, and W. Shockley, *Phys. Rev.* **92**, 890 (1953).
51) see for instance S. Knox and A. Gold, *Symmetry in the Solid State* (Benjamin, New York, 1974).
52) E. Clementi and C. Roetti, *Atomic data and Nuclear data Tables* **14**, 177 (Academic Press, New Work, 1974).
53) J. C. Slater and G. F. Koster, *Phys. Rev.* **94**, 1498 (1954).
54) D. M. Silver and K. Ruedenberg, *J. Chem. Phys.* **49**, 4301 (1968).
55) see for instance F. Bassani and G. Pastori Parravicini, *Electronic States and Optical Transitions in Solids* (Pergamon Press, Oxford, 1975), ch. III.
56) see for instance W. A. Harrison, *Electronic structure and the properties of solids; the physics of the chemical bond* (Freeman, San Francisco, 1980).
57) L. Kleinmann and J. C. Phillips, *Phys. Rev.* **116**, 880 (1959).
58) A. Baldereschi, *Phys. Rev.* B**7**, 5212 (1973).
59) D. J. Chadi and M. L. Cohen, *Phys. Rev.* B8, 5747 (1973).
60) H. Monkhorst and J. D. Pack, *Phys. Rev.* B**13**, 5188 (1976).
61) G. Grosso, G. Pastori Parravicini, and R. Resta, *Phys. Stat. Sol. (b)* **73**, 371 (1976).
62) W. Andreoni, G. Grosso, and G. Pastori Parravicini, *Solid State Commun.* **23**, 923 (1977).
63) M. Peressi and A. Baldereschi, *Solid State Commun.* **63**, 91 (1987).